NON DESTRUCTIVE EVALUATION
OF
CERAMIC BEARINGS

FEBRUARY 4, 1994

Sponsored By

Advanced Research Projects Agency (DOD)

Defense Small Business Innovation Research Program

ARPA ORDER NO. 5916

Issued By U.S. Army Missile Command Under

Contract #DAAH01-93-C-R116

Name of Contractor:	Quatro Corporation	Principal Investigator:	Dr. George W. Rhodes
Business Address:	4209 Balloon Pk Rd., NE Albuquerque, N.M. 87109	Phone Number:	(505)345-0444
		Short Title of Work:	Non Destructive Evaluation of Ceramic Bearings

Effective Date of Contract: December 12, 1992

Contract Expiration Date: June 30, 1994

Reporting Period: December 21, 1992 through May 4, 1994

DISCLAIMER

REPORT DOCUMENTATION PAGE

Form Approved
OMB No. 0704-0188

1. AGENCY USE ONLY *(Leave blank,*	2. REPORT DATE	REPORT
	FEB 4, 1994	

4. TITLE AND SUBTITLE
NON DESTRUCTIVE EVALUATION OF CERAMIC BEARINGS

5. FUNDING NUMBERS

RHODES, GEORGE W.

7. PERFORMING ORGANIZATION NAME(S) AND ADDRESS(ES)

QUATRO CORPORATION
4209 BALLOON PK RD, NE
ALBUQUERQUE, N.M. 87109

8. PERFORMING ORGANIZATION REPORT NUMBER
DSRS U 34110

9. SPONSORING/MONITORING AGENCY NAME(S) AND ADDRESS(ES)

ADVANCE RESEARCH PROJECT AGENCY
3701 FAIRFAX DRIVE
ARLINGTON, VA 2203

10. SPONSORING/MONITORING AGENCY REPORT NUMBER
DAAH0193CR116

11. SUPPLEMENTARY NOTES

12a. DISTRIBUTION/AVAILABILITY STATEMENT
OPEN PUBLICATION

12b. DISTRIBUTION CODE

13. ABSTRACT *(Maximum 200 words)*

14. SUBJECT TERMS
CERAMIC BEARING
ULTRASOUND SPECTROSCOPY

15. NUMBER OF PAGES

16. PRICE CODE

17. SECURITY CLASSIFICATION OF REPORT	18. SECURITY CLASSIFICATION OF THIS PAGE	19. SECURITY CLASSIFICATION OF ABSTRACT	20. LIMITATION OF ABSTRACT
SAR			SAR

TABLE OF CONTENTS

EXECUTIVE SUMMARY

for the

ARPA/U.S. ARMY/MICOM

CERAMIC BEARING NON-DESTRUCTIVE INSPECTION PROJECT

using

RESONANT ULTRASOUND SPECTROSCOPY (RUS)

by: Quatro Corporation

BACKGROUND

Through a phase II SBIR, MICOM funded Quatro to evaluate the Resonant Ultrasound Spectroscopy (RUS) techniques to ceramic bearings, specifically those made with Si_3N_4. The light weight, high temperature and hardness attributes of this material are well known, but a concern exists regarding their manufacturability, quality and failure mechanisms. The determination of surface and near surface flaws is an operational problem which has hindered the acceptance of this material into widespread commercial applications. Before RUS no non-destructive inspection technique was able to rapidly and reliably find all the manufacturing flaws which could be present in this material and their location relative to the surface.

The use of mechanical resonances to test the properties of materials is as old as the industrial revolution. The earliest attempts to use resonances included documented cases of engineers tapping the wheels of a train and listening to the response to qualitatively assess the integrity of the new high performance alloys. This is not altogether different from the acoustic tests now employed by industry. While many attempts were made to mathematically understand the resonances of solids, based on their shape and composition, the problem resisted attack for several years. In the 1960's, Holland, Anderson and Demarest, at Bell Labs developed new numerical methods that enabled the computation of the resonances of homogeneous anisotropic objects of any simple geometric shape. However the electronics and transducers, required for accuracy, were crude and intruded upon the measurement. The ability to compute the elastic properties from the resonances (the inverse problem) remained largely unsolved. Due to their work on superconductivity, Los Alamos National Laboratory invented a technique capable of examining the resonance phenomena at a signal to noise level not seen before. This technique is called Resonant Ultrasound Spectroscopy and has been exclusively licensed to Quatro Corporation.

The resonances of a solid are affected by its elastic moduli, shape, size, material and density. Any deviation (crack, inclusion, scratch, dimensional change...) changes the resonance spectrum. If we apply continuous sound to a solid sample, the object will resonate, or ring just like a bell, provided the applied sound frequency matches one of the samples natural vibrational frequencies. We measure the frequency of a resonance by driving the sample continuously with ultrasound and changing the frequency of the sound until the sample begins to resonate. The resonating sample behaves as if it were a natural amplifier and greatly increases the amplitude of the vibrations. At that point we need only to measure the frequency and analyze the results. Each solid exhibits numerous frequencies which increase in number by the cube of the longest dimension. We need only to select a few of these as diagnostics of the measurements we are addressing. The key is to choose the right ones for analysis. Recognition of these effects allows a microprocessor/controller to select or reject manufactured items. The basic process is most amenable to automation. We have designed an industrial process by which Si_3N_4 spheres, of any diameter in excess of 1/4 inch, can be sorted according to their quality.

APPROACH

To establish the requirements for a production ceramic bearing ball sorter it was necessary to identify resonances of the object which related to specific flaws. Our early work could find all the bulk flaws, but couldn't discern those which were resident in surface regions vs flaws existing deeper into the structure. The recognition that higher order resonances can exhibit Surface Acoustic Wave (SAW) properties led to this capability. In addition, we learned that the wavelength of our resonant SAW modes provided an examination of a region extending from the surface to a defined region deeper in the sphere. This became valuable in describing the location of the flaw.

These criteria were used with process rates, materials handling techniques, power conditioning, and safety requirements to establish the system design requirements for a fully automated Si_3N_4 bearing ball sorter capable of handling 13.5 million parts per year.

SUMMARY

Quatro has developed a process to sort Silicon Nitride bearing balls on a commercial scale and consistent with industrial standards. This report will examine the technology and the system design for the Resonant Ultrasound Spectrometer ceramic ball sorter.

I INTRODUCTION

Through a phase II SBIR, MICOM funded Quatro to evaluate the Resonant Ultrasound Inspection (RUS) techniques on ceramic bearings, specifically those made with Si_3N_4. The light weight, high temperature, corrosive resistance and hardness attributes of this material have been well characterized, but concerns regarding their manufacturability, quality and failure mechanisms exist. The determination of surface/near surface flaws are an operational problem which has hindered the acceptance of this material into widespread commercial applications. Recent tribological data has shown that the critical wear failures of Si_3N_4 balls are a direct function of the surface/near surface region. Before RUS no non-destructive inspection technique was able to rapidly and reliably find all the manufacturing flaws which could be present in this material and their location relative to the surface.

Laboratory concepts and experiments may achieve some degree of success in the measurement of meaningful physical parameters. The conversion of such procedures remain a curiosity until a process can be developed which can achieve similar results on a commercial scale. This report will provide the data to support the Quatro design which can be built into a reliable industrial machine which can sort Silicon Nitride spheres at a cost and scale which is acceptable to the industry.

II BACKGROUND

The use of mechanical resonances to test the properties of materials is as old as the industrial revolution. The earliest attempts to use resonances included documented cases of engineers tapping the wheels of a train and listening to the response to qualitatively assess the integrity of the new high performance alloys. While many attempts were made to mathematically understand the resonances of solids, based on their shape and composition, the problem resisted attack for several years. In the 1960's, Holland, Anderson and Demarest, at Bell Labs, developed new numerical methods that enabled the computation of the resonances of homogeneous anisotropic objects of any simple geometric shape. However, the electronics and transducers required for accuracy were crude and intruded upon the measurement. The ability to compute the elastic properties from the resonances (the inverse problem) remained largely unsolved. Due to their work on superconductivity, Los Alamos National Laboratory invented a technique capable of examining the resonance phenomena at a signal to noise level not seen before. This technique is called Resonant Ultrasound Spectroscopy (RUS) and has been exclusively licensed to Quatro Corporation. Our commercial unit is designated as the Quatro NDI (nondestructive inspection) system.

The resonances of a solid are affected by its elastic moduli, shape, size, material and density. Any deviation (crack, inclusion, scratch, dimensional change...) changes the resonance spectrum. If we apply continuous sound to a solid sample, the object will

resonate, or ring just like a bell, provided the applied sound frequency matches one of the samples natural vibrational frequencies. We measure the frequency of a resonance by driving the sample continuously with ultrasound and changing the frequency of the sound until the sample begins to resonate. The resonating sample behaves as if it were a natural amplifier and greatly increases the amplitude of the vibrations. At that point, we need only to measure the frequency and analyze the results. Each solid exhibits numerous frequencies which increase in number by the cube of the longest dimension. We need only to select a few of these as diagnostics of the measurements we are addressing. The key is to choose the right one for analysis. Recognition of these effects allows a microprocessor/controller to select or reject manufactured items. The basic process is most amenable to automation.

The use of RUS for the testing of ball bearings such as those of interest here is particularly advantageous because these are objects whose geometry is sufficiently simple that their shape is easily described by a few simple functions. For such shapes, new methods developed at LANL can be used to compute directly the mechanical resonant frequencies dramatically faster than finite element methods. This is important because for such very high precision computable objects, the measurements using RUS are more accurate than reasonably meshed finite element codes can calculate. This is why we were forced to revisit a seemingly solved computational problem. The new computational approach is based on a Lagrangian minimization method where the usual volume integral can be converted to surface integral. Thus where a finite element code must make a number of computations dependent on the cube of the length of the object, our code must only make a number of computations dependent on the square of the length of the object.

With this method, we are able to greatly improve on any finite element method in both speed and accuracy, and at the same time determine elastic moduli (even anisotropic ones) to the highest accuracy achieved for any routine materials diagnostic modulus measurement system. For example, our code will compute the first 100 modes of a sphere in less than 1.0s on a Cray to 14 digits, or less than 30s on a 50MHz 486 PC to 7 digits. This performance enables the computation to exceed the measurement in accuracy. Because of the very high accuracy and the structure of the computation, we can also compute the effects of small perturbations, and thus generate a procedure for determining whether a ball is truly spherical. Cracks (including subsurface ones), roundness errors, texturing, and internal strain all break spherical symmetry, and so RUS can be used to test bearings at the levels required for good performance for all possible flaws and with very high resolution.

For a perfect sphere, the lowest resonant mode is 5-fold degenerate. That is, there are 5 different modes all with the same frequency, but with different displacement orientations on the sphere. If the sphere is deformed (that is, one of the above mentioned flaws is present), the 5 modes no longer have the same frequency and the resonance splits into 3 or 5 peaks. Using the computation, we can quantify the breaking

of spherical symmetry caused by the flaw. Thus the frequency splitting of one resonance peak can be translated into an effective dimensional error in an elastically isotropic perfect sphere, or a quantitative flaw detector otherwise. Typically, our measurement limit is about 1ppm for spheres, and the measurement takes only a few seconds using dry contact and our patented transducers. No particular precision or care is required to load the sphere into the measurement system, and essentially perfect reproducability is achieved upon remounting. This measurement limit is also comparable to the required production accuracy as well. Thus our RUS technique achieves in one or two seconds what optical scanning techniques take on the order of one hour to do. In addition, there is no other NDI technique at all that can detect a micron size subsurface crack or inclusion in a ball bearing or similar component, or that can detect elastic anisotropies associated with internal strain or texture. The only competing possibilities are pulse-echo ultrasound and eddy current inspection. Pulse echo(including SAW waves) on a curved surface cannot detect anything very small, and eddy current inspection can only see a crack very close to the surface in a conducting material.

np=10 Table I

n	f_r	f_m	% error	k	i	mode
1	.775706	.775707	-.000138	1	1	1T2
2				6	1	
3				4	1	
4				4	2	
5				7	1	
6	.819567	.819983	-.050778	5	1	1S2
7				3	1	
8				5	2	
9				8	1	
10				2	1	
11	1.075664	1.075399	.024614	1	2	1S1
12				7	2	
13				6	2	
14	1.198616	1.198505	.009239	5	3	1T3
15				2	2	
16				3	2	
17				8	2	
18				3	3	
19				8	3	
20				2	3	
21	1.217375	1.217850	-.039042	1	3	1S3
22				6	3	
23				7	3	
24				1	4	
25				6	4	
26				7	4	
27				4	3	

Chi Square(%)= .0124
Shear Modulus(GPa)= 123.74
Poisson Ratio= .2703
Density(gm/cc)= 3.2325 Mass(gm)= .43337 diameter(cm)= .63500

In table I we show the measurement (f_m) and computation (f_r) for an unflawed NBD-100 silicon nitride ball for a few of the lowest modes. The first column is the resonance number. Gaps in the second and third columns are left to indicate the degeneracy. For example, the first 5 modes all have the same frequency. The fourth column indicates the difference in percent between computation and measurement while the fifth and sixth columns indicate the symmetry type and order of the mode. At the bottom of Table I we also show the measured elastic moduli for this batch of silicon nitride and this particular ball. These data for moduli are the most accurate ever obtained in a modulus measurement system designed for routine materials testing. Assume that we have a perfectly spherical bearing at room temperature, as determined optically, with no cracks anywhere, and with perfectly homogeneous material. We have tested several groups of

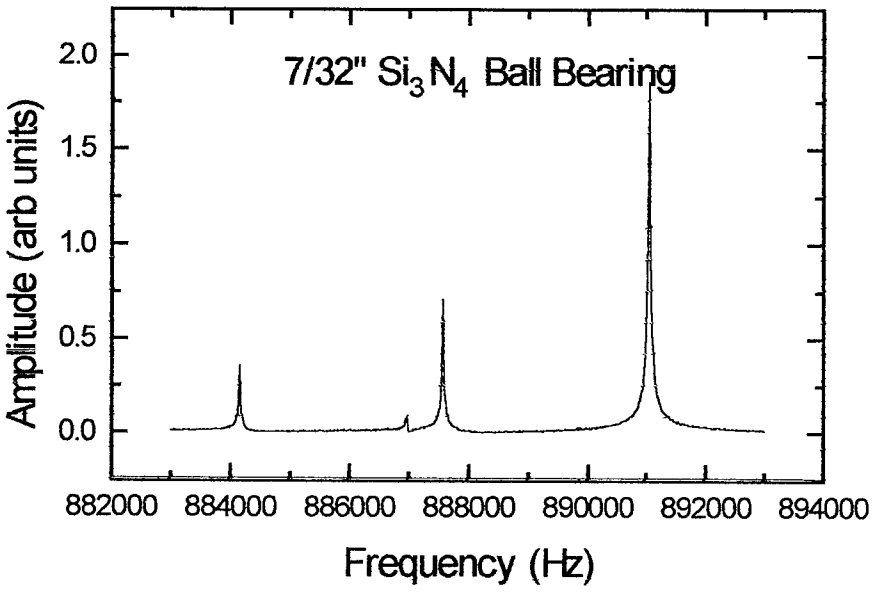

Figure 1

such ostensibly perfect Si_3N_4 bearings and find resonance splittings, shown in fig.1, commensurate with spherical symmetry errors of 1000ppm or more. Because Si_3N_4 ceramic is composed of a material that has hexagonal symmetry, we know that the basic material has two thermal expansion coefficients, α_1 and α_2, and five elastic moduli c_{ij} exhibiting strong anisotropy. If we realize that considerable strain often occurs in preparation of the ceramic prior to final finishing, and that this strain can easily produce texturing, then it is clear that what we observe is most likely a result of both. That is, internal strain and texturing together break the spherical symmetry by generating anisotropic bearing STIFFNESS and anisotropic thermal expansion.

We can do a very accurate determination of the elastic anisotropy associated with the

texture that induces the frequency splitting. Part of this procedure involves fitting the peak shapes to multiple resonances as shown in Fig. 2 where the solid line is a fit of three Lorentzian peaks to the actual data (circle), with the following values:

f_1= 232.6151kHz Width= 0.0299kHz
f_2= 232.6383kHz Width= 0.0111kHz
f_3= 232.6544kHz Width= 0.0138kHz

In this case, we have used data from a nearly perfect 0.8" Si_3N_4 ball just to illustrate how well a separation can be made for nearly overlapping peaks. The numerical results that follow are, however, for the more badly split (and easier to separate) resonances of the 7/32" ball. Once the actual resonances of overlapping modes are determined, we can use a complex fitting algorithm to find the elastic moduli. To do this, we assume that the sphere is transversely isotropic so that it has 5 independent moduli. Using the measured resonances and the full anisotropic theory developed by LANL, we can compute c_{11} , c_{33}, c_{44}, c_{66}, c_{23} (which is one of several equivalent representations of

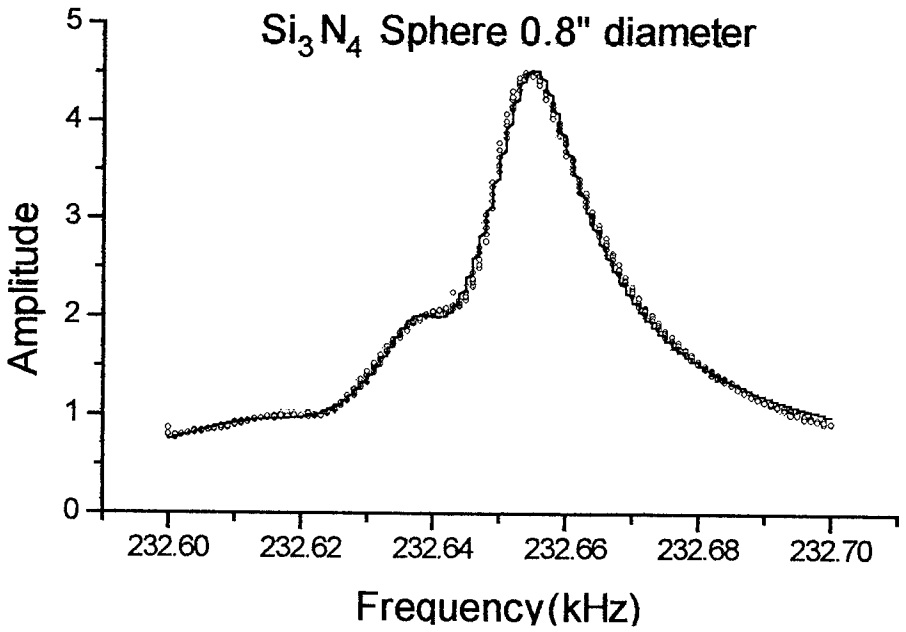

Figure 2

the elastic responses of such a material). As a guide to what these moduli mean, consider that for an elastically isotropic material,

$c_{11}=c_{33}=c_{12}+2c_{44}$
$c_{12}=c_{23}$
$c_{44}=c_{66}=\mu$=shear modulus
$K=c_{12}+2c_{44}/3$=bulk modulus
$\sigma=(3K-2c_{44})/(6K+2c_{44})$ =Poisson ratio.
$E=9Kc_{44}/(3K+c_{44})$=Young's Modulus

The output of the computation for elastic anisotropy is shown in Table II, where n is the mode number, f_{ex} is the measured mode frequency, f_r is the best fitted frequency determined by adjusting elastic moduli and their anisotropy, %err is the deviation between computed and measured frequency, wt is the weight given the mode in the fit, k and i are mode type indices, and d33, d23, d12, d44 and d66 are the relative dependencies of the mode frequency on the appropriate elastic constant and where ρ= 3.2761 gm/cm^3 at 290.00 K for a sphere of diameter 0.5525 cm and where the moduli are subject to the constraint that $(c_{11}-c_{12})/2=c_{66}$.

Table II

n	f_{ex}	f_r	%err	wt	k	i	d33	d23	d12	d44	d66
1	0.884200	0.886405	0.25	1.0	4	1	0.02	-0.01	0.01	0.18	0.31
2	0.886800	0.886405	-0.04	1.0	6	1	0.02	-0.01	0.01	0.18	0.31
3	0.887500	0.888641	0.13	1.0	4	2	0.00	0.00	0.00	0.47	0.03
4	0.891000	0.890499	-0.06	1.0	7	1	0.24	-0.17	0.09	0.09	0.25
5	0.000000	0.890499	0.00	0.0	1	1	0.24	-0.17	0.09	0.09	0.25
6	0.933300	0.934178	0.09	1.0	5	1	0.02	0.00	0.00	0.02	0.46
7	0.933600	0.934178	0.06	1.0	3	1	0.02	0.00	0.00	0.02	0.46
8	0.934300	0.939578	0.56	1.0	2	1	0.00	0.00	0.01	0.47	0.02
9	0.945300	0.939578	-0.61	1.0	8	1	0.00	0.00	0.01	0.47	0.02
10	0.945400	0.946603	0.13	1.0	5	2	0.48	-0.34	0.19	0.01	0.16
11	1.229300	1.225169	-0.34	1.0	7	2	0.13	0.02	0.01	0.11	0.24
12	1.233500	1.225169	-0.68	1.0	1	2	0.13	0.02	0.01	0.11	0.24
13	1.256000	1.249278	-0.54	1.0	6	2	0.05	-0.09	0.15	0.25	0.13
14	1.370100	1.371008	0.07	1.0	8	2	0.02	-0.02	0.01	0.25	0.23
15	1.371100	1.371008	-0.01	1.0	2	2	0.02	-0.02	0.01	0.25	0.23
16	1.371600	1.371728	0.01	1.0	3	2	0.00	0.00	0.00	0.37	0.13
17	1.373200	1.373037	-0.01	1.0	8	3	0.09	-0.06	0.03	0.24	0.20
18	1.373300	1.373037	-0.02	1.0	2	3	0.09	-0.06	0.03	0.24	0.20
19	1.373600	1.374918	0.10	1.0	5	3	0.24	-0.17	0.09	0.02	0.31
20	1.373700	1.374918	0.09	1.0	3	3	0.24	-0.17	0.09	0.02	0.31
21	1.386900	1.387299	0.03	1.0	7	3	0.03	0.00	0.00	0.01	0.46
22	1.388700	1.387299	-0.10	1.0	1	3	0.03	0.00	0.00	0.01	0.46
23	1.393000	1.393054	0.00	1.0	4	3	0.01	0.00	0.01	0.32	0.16
24	1.393100	1.393054	0.00	1.0	6	3	0.01	0.00	0.01	0.32	0.16
25	0.000000	1.400020	0.00	0.0	7	4	0.18	-0.13	0.08	0.26	0.10
26	0.000000	1.400020	0.00	0.0	1	4	0.18	-0.13	0.08	0.26	0.10
27	1.404000	1.403630	-0.03	1.0	6	4	0.31	-0.23	0.14	0.15	0.13
28	1.650700	1.656882	0.37	1.0	5	4	0.11	0.12	0.13	0.02	0.13
29	1.743100	1.742418	-0.04	1.0	3	4	0.07	0.02	0.02	0.03	0.36
30	1.743600	1.742418	-0.07	1.0	5	5	0.07	0.02	0.02	0.03	0.36
31	1.744400	1.751966	0.43	1.0	2	4	0.05	0.02	0.04	0.32	0.08
32	1.756800	1.751966	-0.28	1.0	8	4	0.05	0.02	0.04	0.32	0.08
33	0.000000	1.763267	0.00	0.0	5	6	0.29	-0.18	0.16	0.08	0.15
34	1.775900	1.776125	0.01	1.0	3	5	0.03	0.01	0.00	0.01	0.46
35	1.776600	1.776125	-0.03	1.0	5	7	0.03	0.01	0.00	0.01	0.46
36	1.777500	1.781580	0.23	1.0	8	5	0.01	0.01	0.01	0.24	0.23
37	1.780600	1.781580	0.06	1.0	2	5	0.01	0.01	0.01	0.24	0.23
38	1.787000	1.788129	0.06	1.0	5	8	0.10	-0.06	0.05	0.28	0.14
39	0.000000	1.788129	0.00	0.0	3	6	0.10	-0.06	0.05	0.28	0.14
40	0.000000	1.793531	0.00	0.0	2	6	0.19	-0.14	0.10	0.24	0.11
41	0.000000	1.793531	0.00	0.0	8	6	0.19	-0.14	0.10	0.24	0.11
42	1.797300	1.796312	-0.05	1.0	5	9	0.26	-0.20	0.14	0.18	0.13
43	1.807500	1.807545	0.00	1.0	4	4	0.00	0.00	0.00	0.33	0.17
44	1.807700	1.808280	0.03	1.0	6	5	0.03	-0.02	0.01	0.30	0.18
45	1.808200	1.808280	0.00	1.0	4	5	0.03	-0.02	0.01	0.30	0.18
46	1.808600	1.808578	0.00	1.0	7	5	0.05	-0.03	0.02	0.26	0.20
47	1.808900	1.808578	-0.02	1.0	1	5	0.05	-0.03	0.02	0.26	0.20
48	1.809900	1.810870	0.05	1.0	6	6	0.16	-0.11	0.06	0.12	0.27
49	1.810400	1.810870	0.03	1.0	4	6	0.16	-0.11	0.06	0.12	0.27
50	1.810700	1.812075	0.08	1.0	7	6	0.22	-0.15	0.08	0.05	0.30

This fit produces the following values for the moduli (in GPa), with a chi square of 0.02%:
c_{11}=407.041+0.8% ; c_{33}=82.671+0.5% ; c_{23}=142.739+0.92% ;
c_{44}=124.677+0.04% ;c_{66}=123.427+0.08%

Note that optical measurements at room temperature on this NC132 ball, supplied by Dr. Mike Gardos of Hughes Aircraft, indicate surface sphericity to be accurate to better than 1ppm. It is clear that the textured sphere is a worse approximation to the mathematical model than the perfect sphere of Table I, because the chi square is larger. This is most likely because the texturing and internal strain must have some variation inside the ball, making it weakly inhomogeneous.

Having determined that the sphere has a transversely isotropic texture, we can compute the two extreme values of Young's Modulus. They are:

$$E_c=(c_{11}-c_{12})\left[c_{33}(c_{11}+c_{12})-2c_{13}^2\right] / \left[c_{11}c_{33}+c_{13}^2\right]$$
and
$$E_a=\left[c_{33}(c_{11}+c_{12})-2c_{12}^2\right] /(c_{11}+c_{12}) ,$$

recalling the constraint that $c_{12}=c_{11}-2c_{66}$.

We can now use the experimentally determined (as best fit by the code) values for the moduli to obtain:

E_a=321.5GPa
E_c=310.8GPa

for a 3.44% anisotropy in Young's modulus. Using a 300lb load on our 7/32" ball gives a stress of 100MPa by approximating the sphere as a cylinder of equal height and volume. With E=315GPa, we obtain a deformation strain of

$\Delta D/D$= (.1GPa)/(315GPa)=317ppm=1.8μm

But the variation in loaded diameter must also be 3.44%, about 11ppm or 0.061μm. Thus the loaded ball will behave as if it were 0.061μm out of round.

In addition, if the sphere is operated at elevated temperatures, it will expand anisotropically. For Si_3N_4 ceramic, both the stiffness of the parent single-crystal material and its thermal expansion differ by about 20% between the two key directions in the hexagonal system, that is down the c-axis and in the a-plane. Thus we expect that the sphere will not expand uniformly by about an amount:

$\Delta R/R=\Delta E/E \times \Delta T \times \alpha$

where α is the average thermal expansion coefficient, E is Young's modulus, ΔE the anisotropy in Young's modulus and ΔT the difference in absolute temperature between the operating conditions and the testing conditions. We can estimate this error at an operating temperature of 800°C by noting that:

$\Delta E/E = .077$
$\Delta T = 500°C$
$\alpha = 3 \times 10^{-6}/C$

Then $\Delta R/R = 110$ppm from thermal expansion, or about 0.61μm out of round, an error far above the reject limit of a ball.

If the ball has the typical 2ppm errors in sphericity that many high-quality bearings exhibit, and if, as is probable, the small diameter aligns with the soft modulus direction (because of the way balls are ground), then the manufacturing errors, the 11ppm errors in sphericity arising from modulus anisotropy under load, and 110ppm errors from thermal expansion anisotropy combine to act as if the ball were 135ppm, or 0.67μm out of round under load at operating temperature. Such effects are very large, and, if known, may change the way ceramic and other bearings are tested. More importantly, with such a rapid and inexpensive testing procedure as provided by RUS, manufacturers may be able to change both materials and fabrication processes to prevent disastrous bearing failures in critical applications.

In particular, we point out that some of these effects remain even if the parent compound is cubic (isotropic thermal expansion). For an unstrained cubic material, no matter what the texture, thermal expansion is isotropic, thus removing 90% of the above roundness error. However if internal strain exists, both the thermal expansion and elastic stiffness are anisotropic, but not as anisotropic as a non-cubic material. Thus such ceramics as SiC and other cubic systems may prove to be much better choices for high temperature/high load ceramic bearings if processing problems can be solved. RUS would clearly seem to be the only diagnostic capable of providing rapid information to be used for process and materials improvements.

The principle of this particular RUS method is to examine degenerate resonances. These are resonate states which have identical eigenvalues and eigenvectors. In a perfect homogeneous isotropic material, these degenerate resonances will appear as single peaks. When a flaw is introduced, the symmetry is broken and the eigenstates become different. The peaks then split into multiple components and the separation between the split peaks is a quantitative measurement of the defect present.

We were able to employ our Sphere model to predict the high lying modes of a Si_3N_4 sphere of a given diameter and weight. In performing this operation, we also measured both the shear modulus and Poisson's ratio. We focussed our attentions on doubly

degenerate modes for easy analysis. We were pleased to find that a large number of near surface shear resonances exist which satisfied our criteria.

III APPROACH

We would examine hundreds of bearing balls from two manufacturers, Cerbec and Toshiba. For brevity only a small sets of data on 10 Toshiba 13/16" and 7 Cerbec 7/8" NBD-200 balls will be reported on in this report. If any reader desires additional data or reports, they should contact Quatro directly. The range of sphere diameters included 1/4" to 15/16". We were to record resonance data from the lowest lying shear and spherical modes as well as higher resonances to look for surface effects which might be different from bulk information. We would then draw conclusions regarding their patterns and meanings. These data would then be used to construct plausible criteria by which balls could be categorized as to their overall and surface quality. Measurements as to the reliability and repeatability of RUS had to be made. We must confirm whether or not all quantifiable flaws could be determined from a single RUS measurement or if multiple ball/transducer orientations must be employed to achieve the requisite standard. A single transmitter with two receivers was selected as the baseline experimental setup. The transducer stage provided a three point contact on which to set the ball being tested.

Confident that we had selected the minimum number of resonances which would represent a complete diagnostic of the sphere, we would then turn our full attentions to the design of the sorting system. The data acquisition requirements would then be included with the materials handling portion to form the full system requirements. Minimal tradeoff studies on materials handling were to be avoided because we were concerned that vast resources could be consumed on a subject that would have little impact on the efficacy of the process. In the examination of the Quatro software decision algorithms, a decision was made to design the system to sort a part every 1.5 seconds. In addition, we can run two test heads per cpu which would result in a process which could examine 6.75 million parts per year. Since most industrial processes demand a throughput of a 10million parts minimum, we adopted a strategy of making the system doubly redundant. 13,500,000 parts per year was established as the design point. This was to prove to be prudent in cost efficiency. We also decided to select a mechanical materials handling system for ease of design and integration, vs. robotics, or so we thought. We were able to obtain equipment design specification requirements from several industrial sources. These were compiled to ensure a preliminary design which would be acceptable to the most demanding industry.

The "user manual" was to become the definitive design document. It would include 5 major subsections as is explained below. The introduction shall include the theory and operation of RUS, the applicable documents and software listings as well as the system

specifications. Section 2 shall define the installation instructions. The issues to be defined here include those which will allow the proper placement of all hardware and the establishment of the control settings. Section 3 shall present the system hardware diagrams, locations and schematics. The operations of all hardware and software shall be presented in section 4 and maintenance and troubleshooting in section 5.

Once the system requirements were established, we would design and cost each subsystem. A schedule for procuring the piece parts and labor forecasts would also be made. The aggregate of these design activities would give us a preliminary design by which Quatro could build a commercial Silicon Nitride ball sorter and deliver the system with minimal business risk.

IV RESULTS

The evaluation of the lowest lying modes revealed that the $^1S_1$ mode produced the most reliable result. The lowest lying torsional mode ($^1T_2$), while valuable for measuring the shear modulus, often became perturbed (on heavy samples) by the transducer contact forces and produced an artificial splitting. The same was true for the next spherical mode the $^1S_2$. However the third mode ($^1S_1$) exhibited all the required attributes i.e., the mode represents a whole body combination of torsion and radial motion while showing no effects of contact perturbations.

Similarly, several high lying modes were found which exhibited the desired surface/near surface only characteristics. These were confirmed by placing a 1mg spot of typewriter correction material (snowpake) on an otherwise perfect sphere and observing the split which occurred as a result. Later a microscopic nick was placed on a surface to perform a destructive test. We examined the 10 samples of the Toshiba 13/16 Si_3N_4 balls provided to us by Pratt & Whitney. As a group, these are the best quality samples that we tested. Sample # 3 was chosen as the part for which the elastic moduli were measured. We obtained the values of 118.6 Gpa for the shear modulus and .278 for Poisson's ratio. These values are about 1% higher than the previously examined samples of this size. The processing must have created a difference, with the earlier samples, if the raw samples were identical.
These spectra are presented in appendix A. The following summary restates the spectral data in table 3:

sample #	bulk rating 314kHz	200 micron level 787 kHz	65 micron level 1780 kHz	32 micron level 3115 kHz
1	2	3	2	3
2	2	2	3	2
3	1	1	1	1
4	1	2	3	3
5	2	3	3	4
6	2	1	1	1
7	3	2	4	2
8	2	2	1	2
9	2	2	3	2
10	2	2	3	2

Table 3

Some samples show internal defects while others indicate surface or near surface problems. The resonances between 2 and 4 Mhz appear to be well suited for the near surface examination of these samples. By directing the transducer at an oblique angle, to the surface, one observes an amplitude increase in these modes. This is the opposite effect that is noticed for bulk phenomena where the transducer prefers to be in a perpendicular orientation. The surface/near surface evaluation appears to be extremely valuable when inclusions are suspected to be present.

The shear modulus of sample #3 was determined to be $1.1862*10^{12}$ dynes/cm^2 and the Poisson ratio is .2777. These data are included in our standard format and can be found on page 1 of appendix A.

Pratt & Whitney was able completely corroborate these results with their xray data. In fact, it was our work on previous batches which showed significant flaws in these materials. Their data showed that only two samples were of acceptable surface quality. Samples 3 and 6 were the best samples as determined by RUS. They were completely unaware of these defects until our analysis was made. This collaboration proved to be invaluable in expanding the RUI capabilities. In addition, we have performed the following analysis to suggest the depth to which this surface accoustic wave (SAW) phenomenon can interrogate beneath the surface. It is important to recognize that solutions to the wave equation, for a sphere, include many resonances well below the normally accepted frequencies of 10s of mHz values.

The 3115 Mhz line represents a resonance in excess of the 100th mode. This corresponds to about 314 (π* mode #) full wavelengths or 628 1/2 wavelengths around the sphere. For a 2.0584 in. diameter sphere, we estimate this SAW wave to penetrate to about 32 microns. The reader will note that the spectra indicate that only samples 1 and 7 have flaws in this region. Applying the same procedure to the 1780 Khz mode suggests that the surface to 65 microns is being examined. Only parts 3,6 and 8 pass this screen. This would suggest that the flaws contained in the other parts are in this region. The 787 Khz resonance is the 16th mode which may represent up to 200 μ in depth. At this depth only parts 3 and 6 pass. Whereas these data are consistent with SAW penetration, we would have to extensively examine the model to confirm their character. At this time I can't confidently identify a mode which allows the examination down to 800μ, which is a wish of the aerospace industry.

None of these parts exhibit over a 75ppm total volumetric defect as can be deduced from the 325 Khz scan and only parts 3 & 4 show no defect. The errors in the 200 μ band approach 200 ppm, 100 ppm in the 65 μ and 200 ppm in the 32 μ bands respectively. The volumetric measurements are as follows: The volume of each band is calculated from $V= 4/3\pi r^3$ and V2..Vi subtracted from V1. The volume fractions are then calculated and when multiplied by the weight of the object yield the weight of the band.

The ppm as determined from the spectra (the δf/f is written in % and must be divided by 100 to yield ppm) is multiplied by the band weight to reveal the defect size in grams which when divided by the density expresses the defect volume in μ. The following table 4 applies for a 100 ppm flaw indication:

Band	sphere	200 μ	65 μ	32 μ
volume M^3	$4.57E^{-6}$	$2.62E^{-7}$	$8.55E^{-8}$	$4.25E^{-8}$
vol fract (vf)		$5.73E^{-2}$	$1.87E^{-2}$	$9.30E^{-3}$
vf* wt (band wt)	14.798	848mg	277mg	137mg
band wt*ppm (defect wt) for 100ppm flaw indication	1.1mg	.17mg	.06mg	.03mg
defect wt*ρ (Flaw volume) cm^3	$3.4E^{-4}$	$5.25E^{-5}$	$1.85E^{-5}$	$9.2E^{-6}$

Table 4

Similiar results were obtained with 60 7/8" NBD-200 balls supplied by GE Aircraft Engines. These samples had been through the ARPA sponsored wear tests. We were fortunate in that earlier samples of the identical material had been sent to us from Pratt & Whitney. In appendix B the spectra are shown which record data for the perfect sphere (spectra numbered at bottom right as 1 and 2) and progressing to a part which had two spall locations. We have hand written remarks on the spectra for reference.

It was confirmed that all needed data could be collected by transmitting at a single location and receiving at two other locations. While a split can be "missed" by a single receiver, it is unlikely that both receivers will be blind to the flaw. Work on this issue will continue, at Quatro, following the conclusion of the ARPA effort. The only case which has presented us difficulty, is that where a small surface flaw is place in contact with the transmitting transducer. Our workarround is to switch the transmitter with a receiver location during the data acquisition cycle. This has not proven to be a requirement and is not included in this baseline design.

Appendix C, the Users Manual, describes the full bearing ball sorting system. It is written as a "stand alone" document for a potential user. Multiple appendices will be appended to it to fufill the documents promised its table of contents. One of these addendums deals with the system software and algorithms required for flexible part sorting. We have been employing similar selection algorithms on different parts for the past 6 months. This development is well beyond the scope, and monies available to, the ARPA program. In addition, we discovered late into the project, that robotic vacuum pick and place materials handling units were not as complex as we had been led to believe. We would probably incorporate such a technique into the next production unit design.

V SUMMARY

Quatro has applied Resonant Ultrasound Spectroscopy to silicon nitride balls to identify flaws which might hinder their successful operation. We have been able to identify diagnostic resonances which examine the bulk object as well as some which isolate the surface/near surface regions. The flaw signatures have been incorporated into software which is capable of making pass/fail decisions on a reliable and repeatable basis. The software will have to be tailored for a specific client and part size based on their requirements. Around rigorous system requirements we have completely designed a ball sorter capable of providing 100% inspection for up to 13,500,000 parts annually. The "Users Manual" incorporated as Appendix C, in this document, is a complete treatment of the design.

APPENDIX A

np= 10 TOSHIBA XX3

i	fr	fm	df(%)	k	i
1	.234006	.234000	.002770	6	1
2				4	1
3				1	1
4				7	1
5				4	2
6	.247322	.247130	.077789	8	1
7				2	1
8				3	1
9				5	1
10				5	2
11	.325949	.325950	-.000192	6	2
12				1	2
13				7	2
14	.361581	.361610	-.007978	3	2
15				2	2
16				2	3
17				3	3
18				8	2
19				8	3
20				5	3
21	.367532	.367170	.098611	7	3
22				1	3
23				4	3
24				6	3
25				1	4
26				7	4
27				6	4
28	.442209	.442200	.002143	5	4
29	.462630	.462810	-.038851	5	5
30				3	4
31				2	4
32				8	4
33				5	6
34	.470611	.470270	.072471	5	7
35				5	8
36				3	5
37				2	5
38				5	9
39				8	5
40				2	6
41				8	6
42				3	6
43	.476651	.476740	-.018601	1	5
44				6	5
45				4	4
46				4	5
47				7	5
48				4	6
49				6	6
50				1	6
51				7	6

sigma(%)= .0216459
diameter(cm)= 2.0584000
Shear Modulus(10**12 dynes/cm**2)= 1.1862000
Poisson Ratio= .2777000
Density(gm/cc)= 3.2405230 Mass(gm)=14.7980000
s(gm)=14.7980000

01/06/94 10:53am Filename: <tos00001.BDT>
Frequency 325.500000 - 326.500000 kHz, Amplitude 0.100000 volt
Data point density: 1000 Stepwidth: 1.001001 Hz.

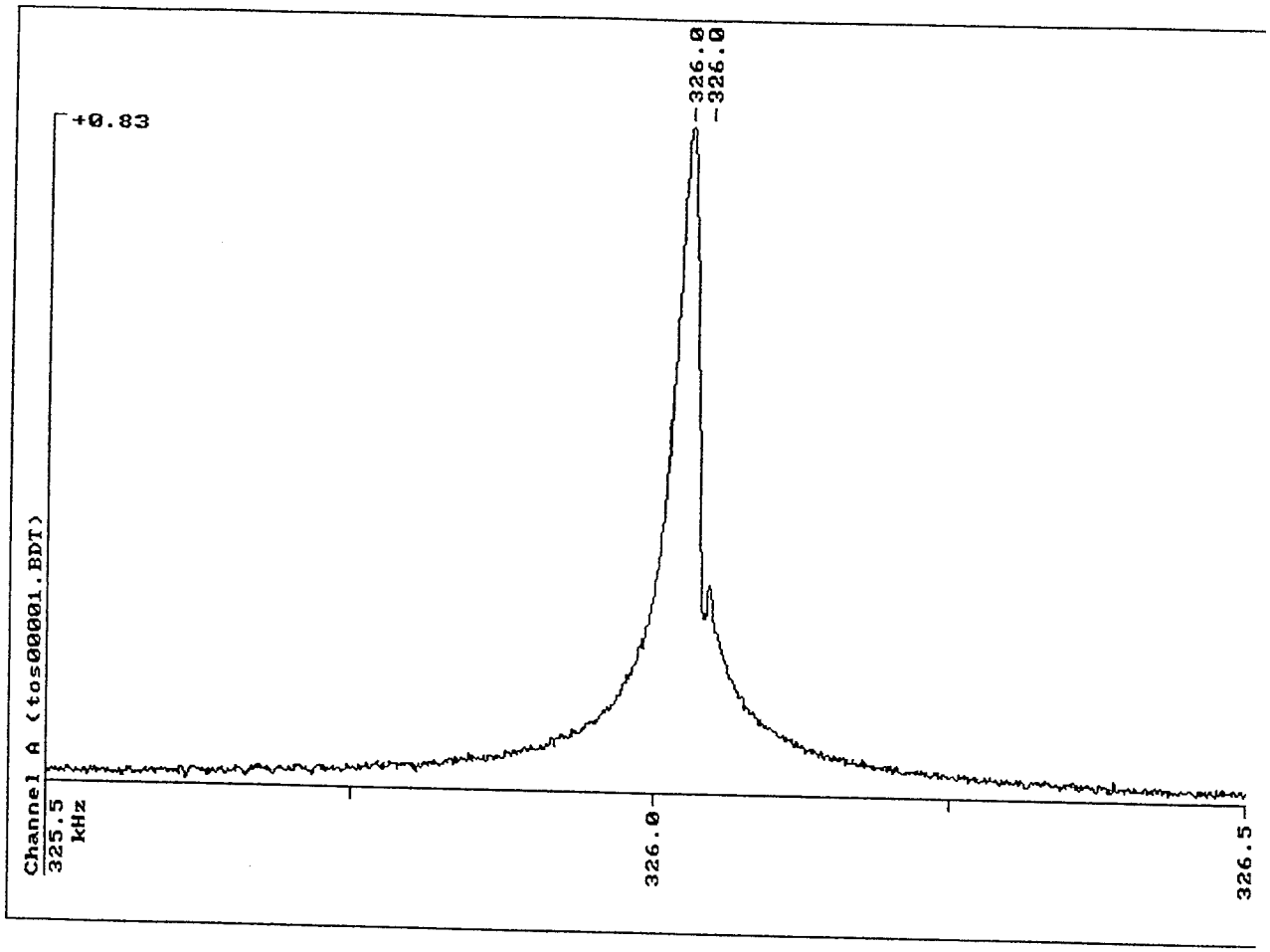

01/06/94 10:57am Filename: <tos00002.BDT>
Frequency 325.500000 - 326.500000 kHz, Amplitude 0.200000 volt
Data point density: 1000 Stepwidth: 1.001001 Hz.

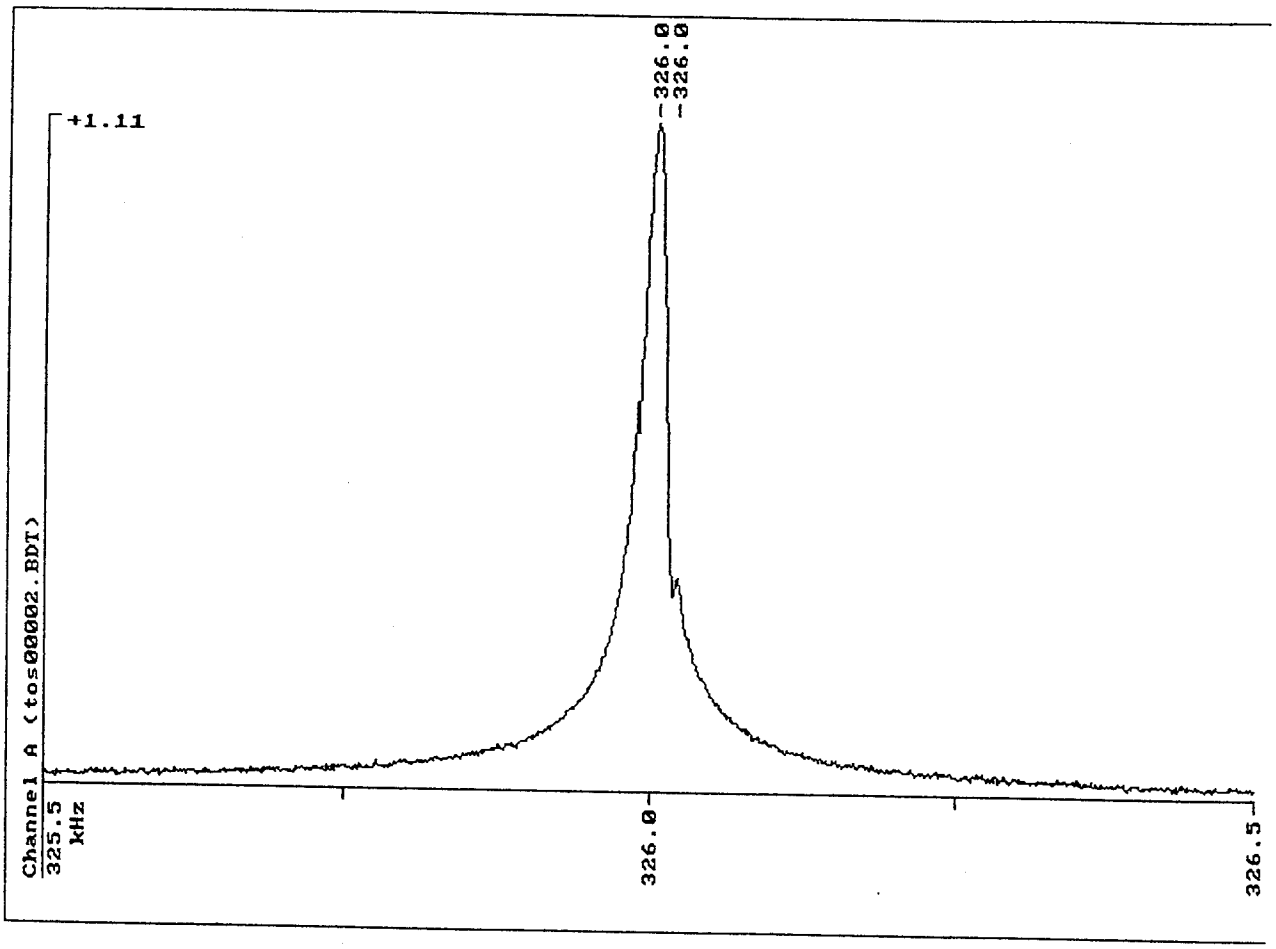

01/06/94 10:50am Filename: <tos00003.BDT>
Frequency 325.500000 - 326.500000 kHz, Amplitude 0.100000 volt
Data point density: 1000 Stepwidth: 1.001001 Hz.

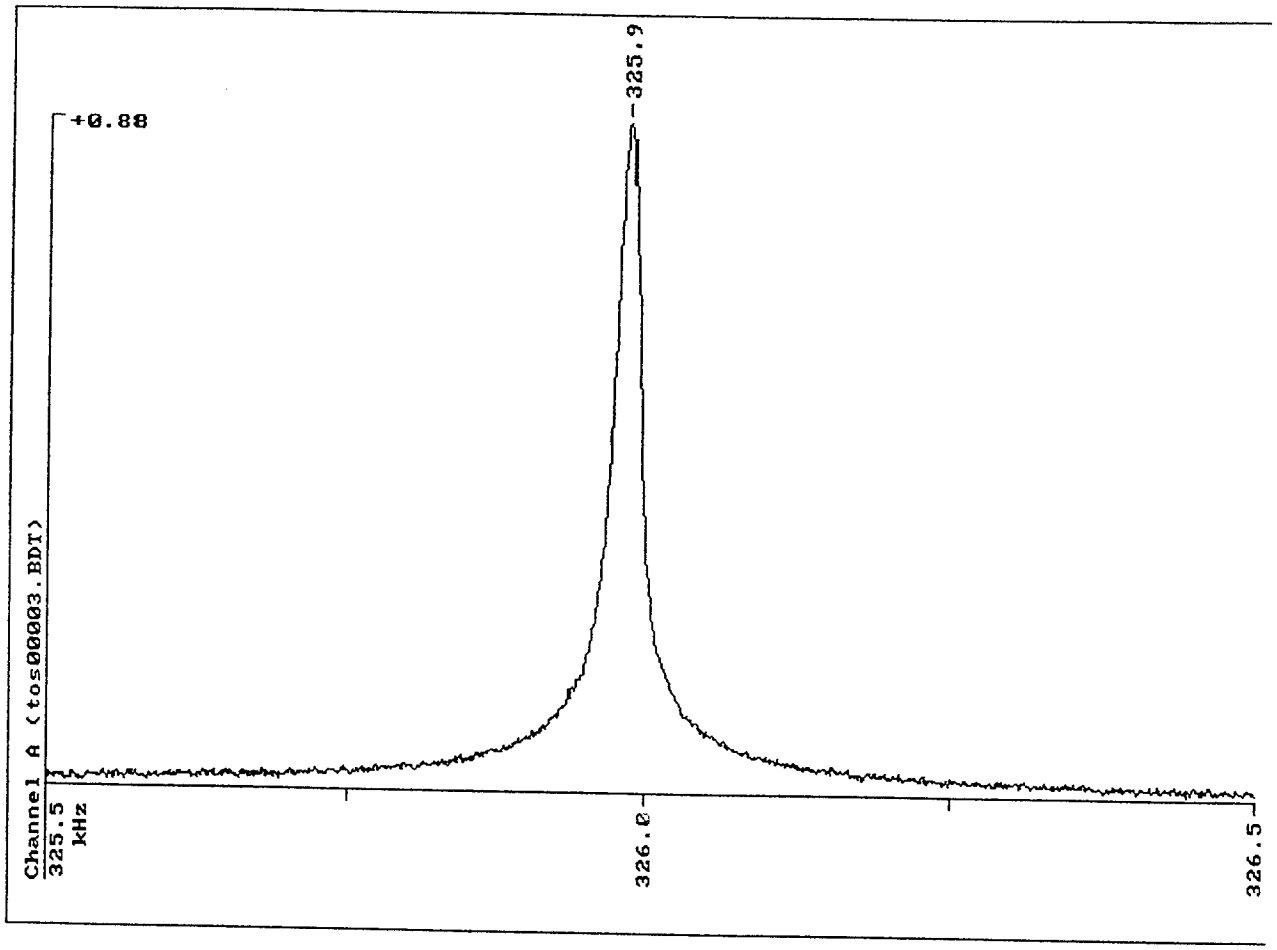

01/06/94 10:59am Filename: <tos00004.BDT>
Frequency 325.500000 - 326.500000 kHz, Amplitude 0.200000 volt
Data point density: 1000 Stepwidth: 1.001001 Hz.

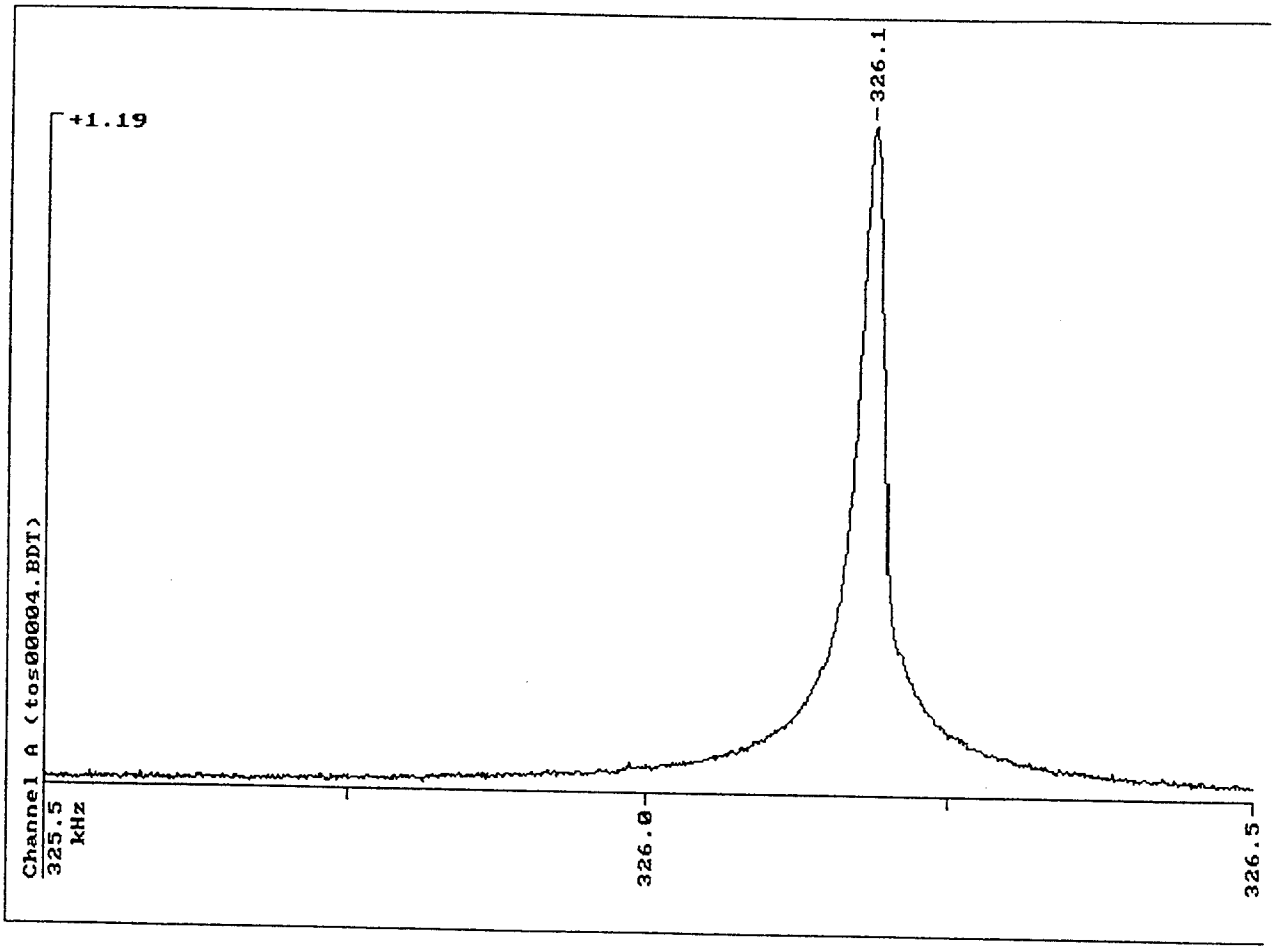

01/06/94 11:01am Filename: <tos00005.BDT>
Frequency 325.500000 - 326.500000 kHz, Amplitude 0.200000 volt
Data point density: 1000 Stepwidth: 1.001001 Hz.

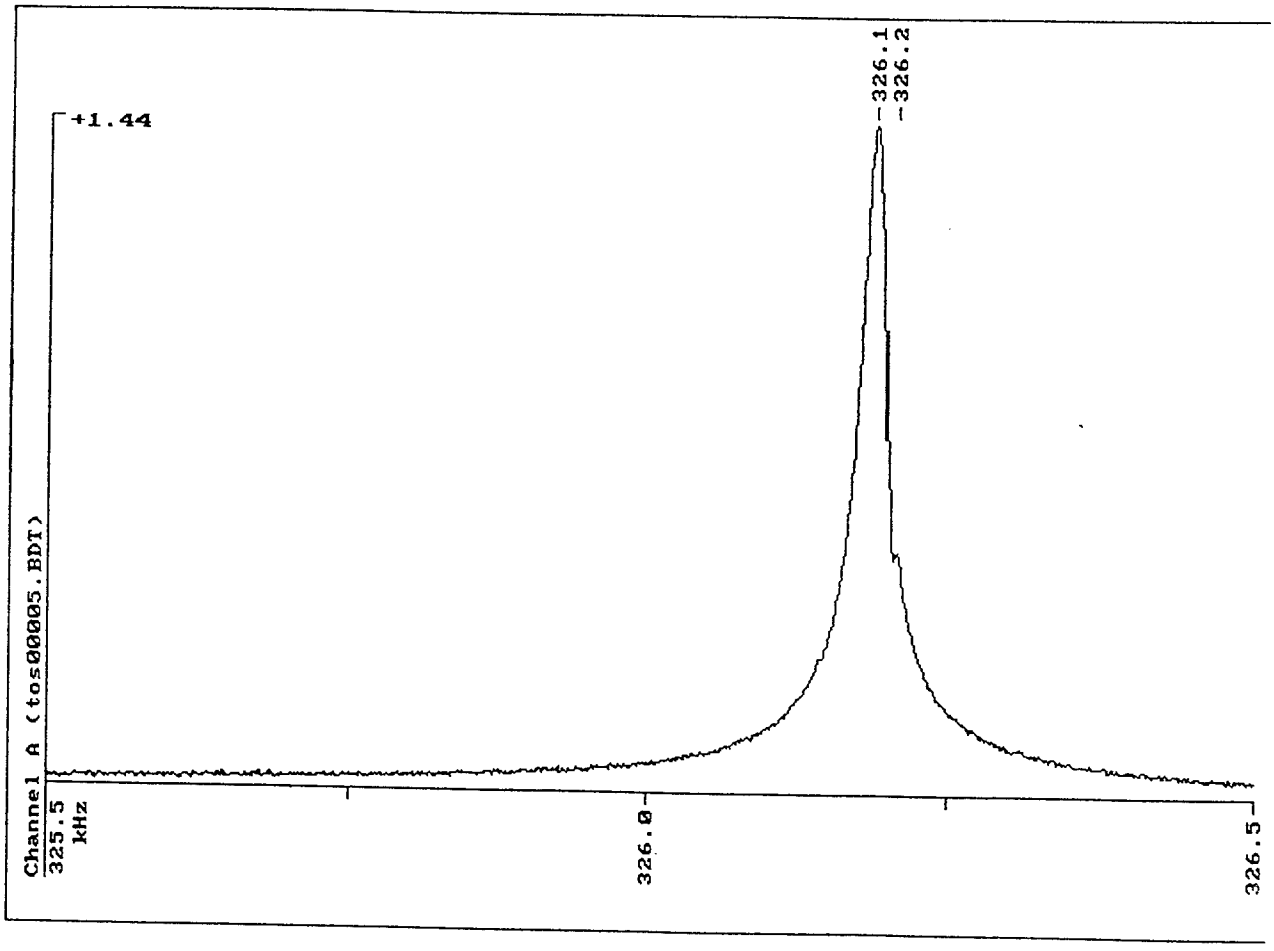

01/06/94 11:03am Filename: <tos00006.BDT>
Frequency 325.500000 - 326.500000 kHz, Amplitude 0.200000 volt
Data point density: 1000 Stepwidth: 1.001001 Hz.

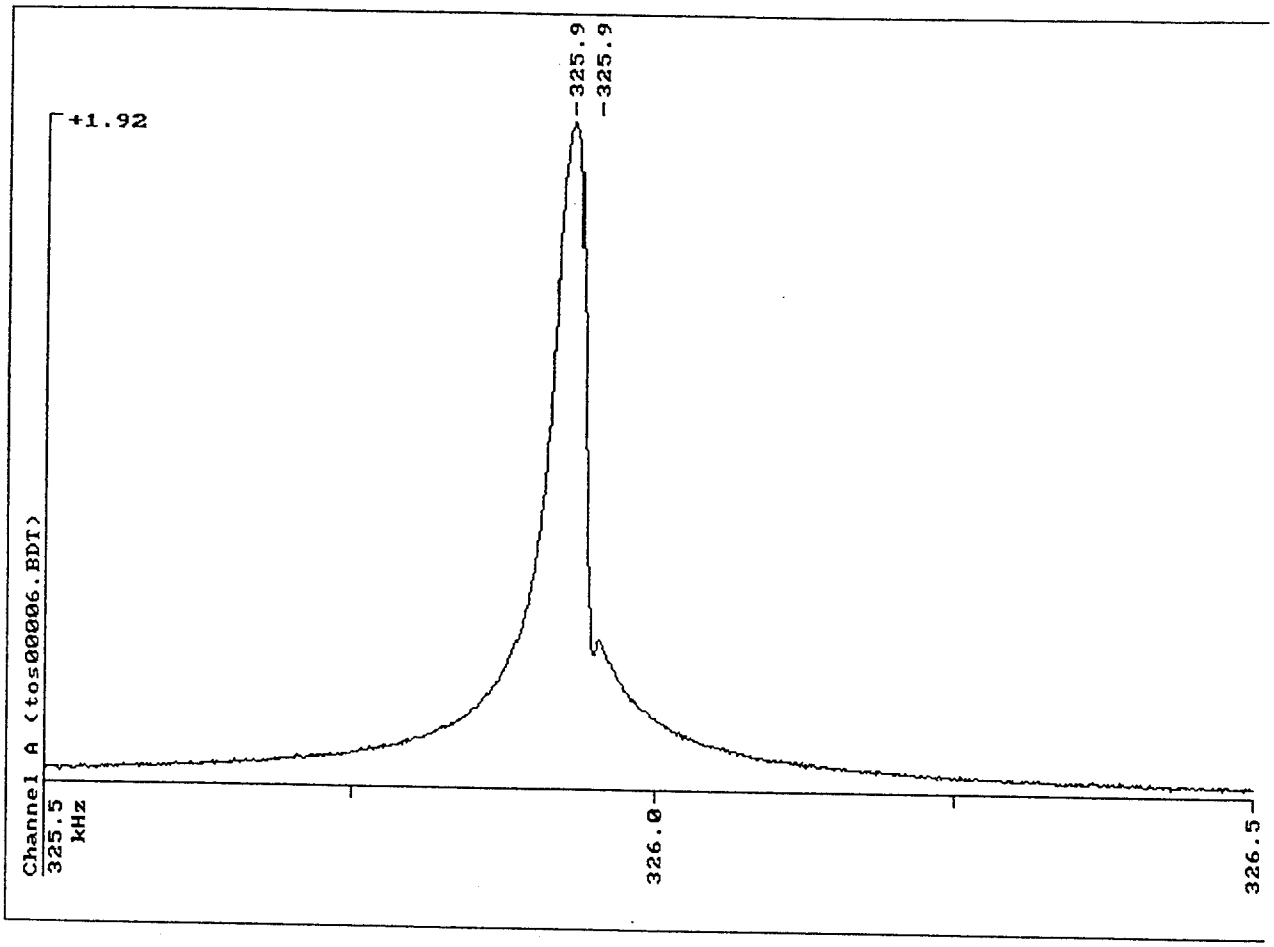

01/06/94 11:04am Filename: <tos00007.BDT>
Frequency 325.500000 - 326.500000 kHz, Amplitude 0.200000 volt
Data point density: 1000 Stepwidth: 1.001001 Hz.

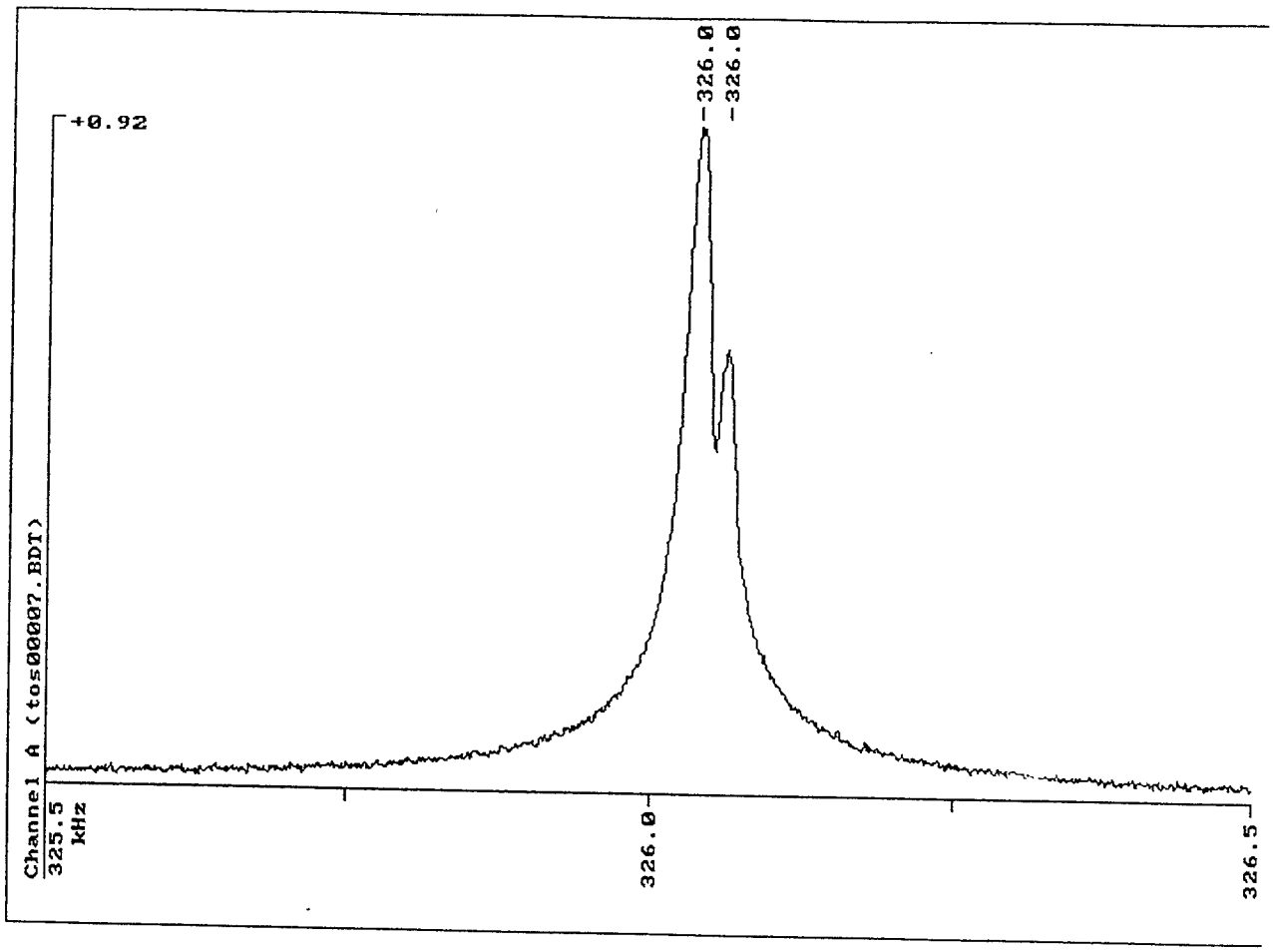

01/06/94 11:06am Filename: <tos00008.BDT>
Frequency 325.500000 - 326.500000 kHz, Amplitude 0.200000 volt
Data point density: 1000 Stepwidth: 1.001001 Hz.

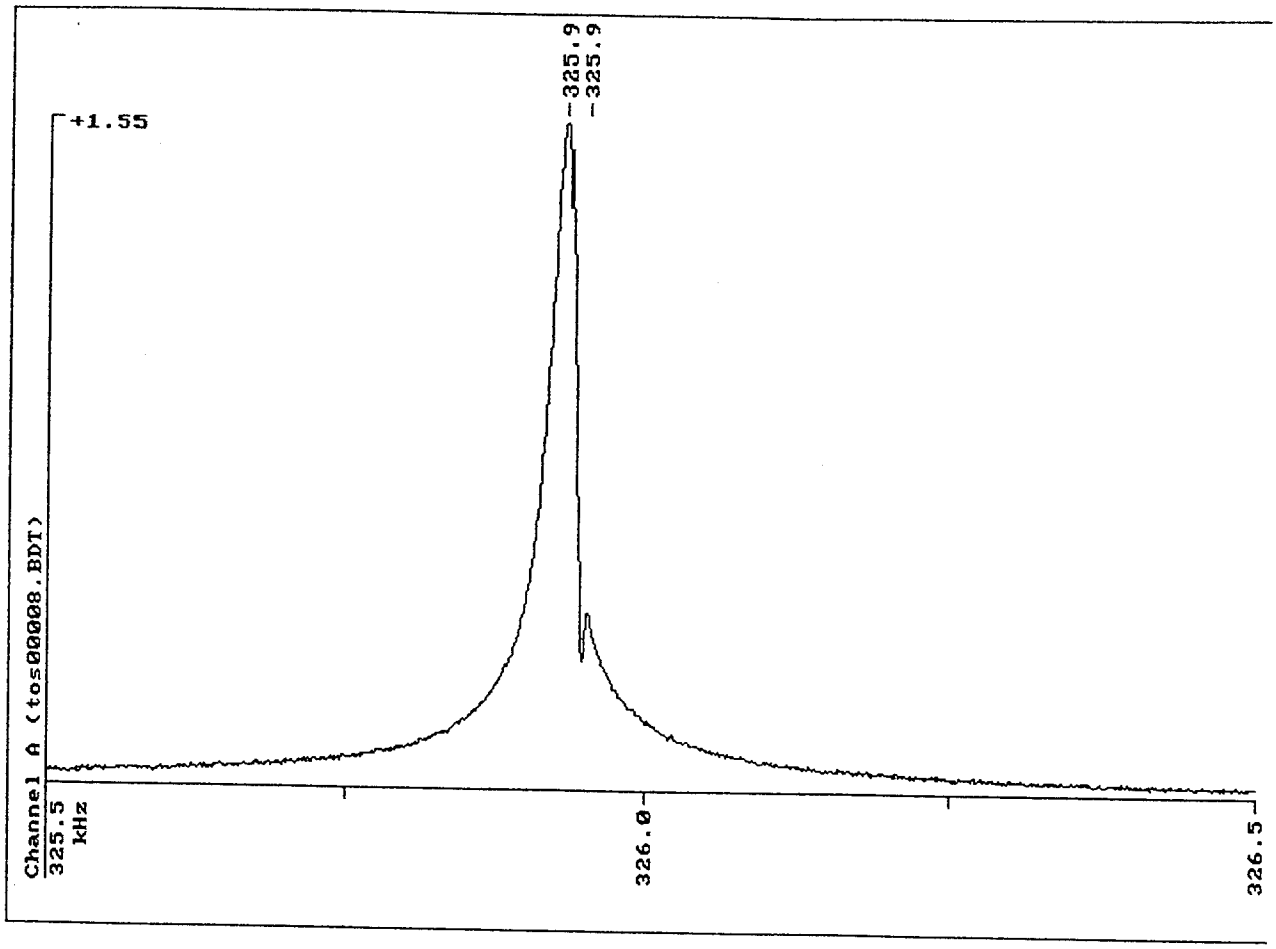

01/06/94 11:08am Filename: <tos00009.BDT>
Frequency 325.500000 - 326.500000 kHz, Amplitude 0.200000 volt
Data point density: 1000 Stepwidth: 1.001001 Hz.

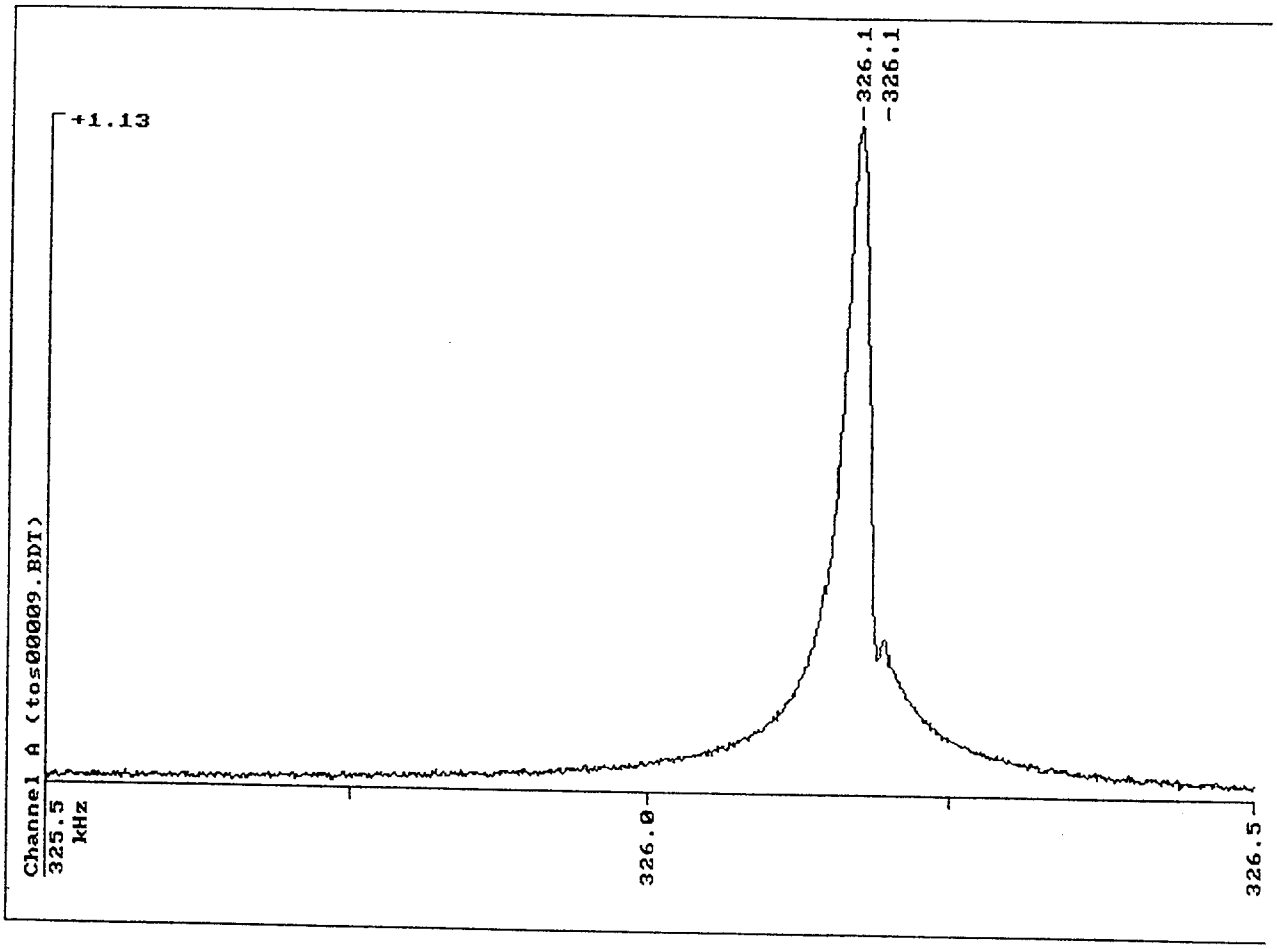

64 ppm

01/06/94 11:07am Filename: <tos00010.BDT>
Frequency 325.500000 - 326.500000 kHz, Amplitude 0.200000 volt
Data point density: 1000 Stepwidth: 1.001001 Hz.

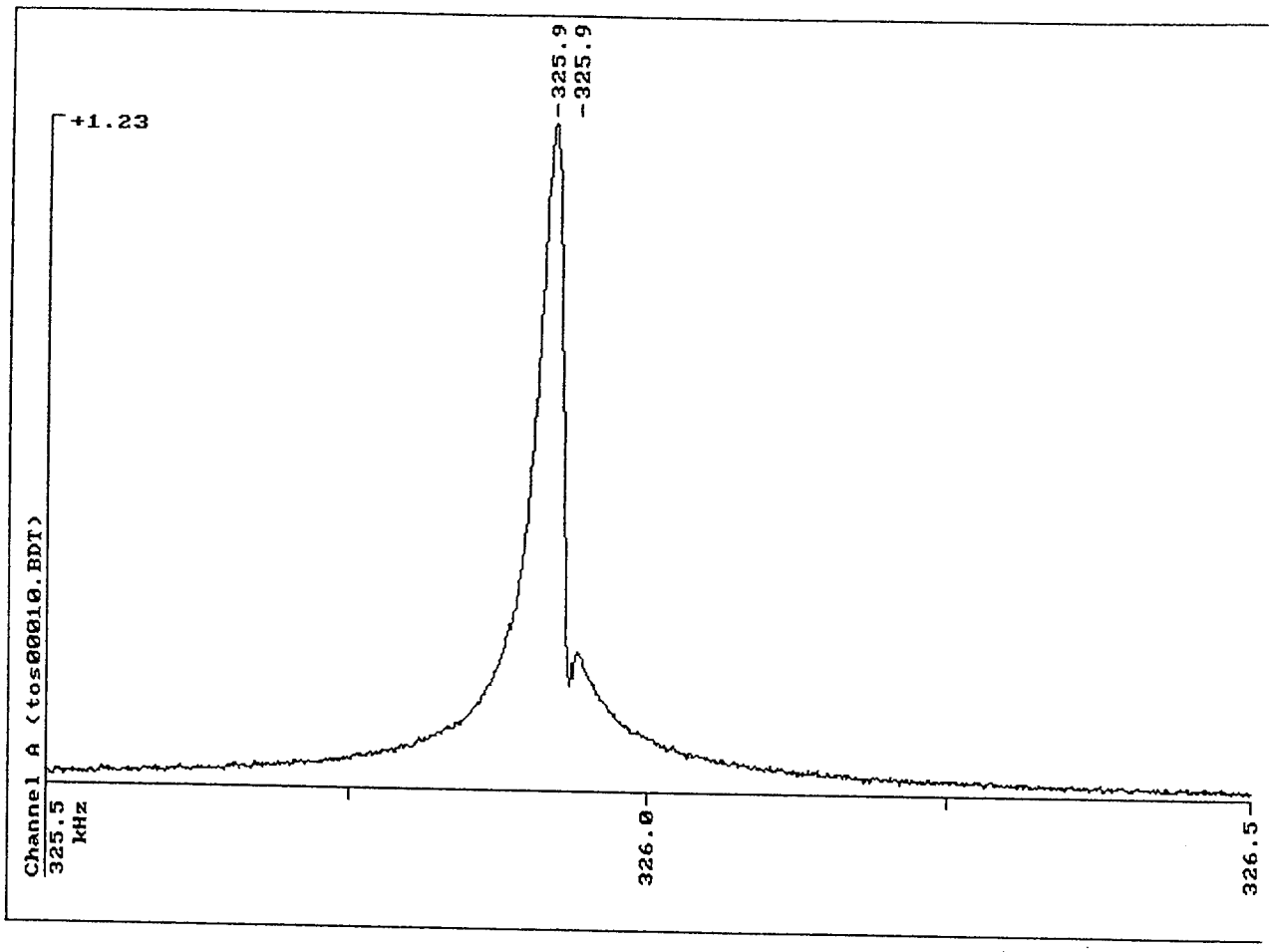

01/06/94 11:53am Filename: <TOS00001.BDT>
Frequency 1780.000000 - 1790.000000 kHz, Amplitude 1.000000 volt
Data point density: 400 Stepwidth: 25.062657 Hz.

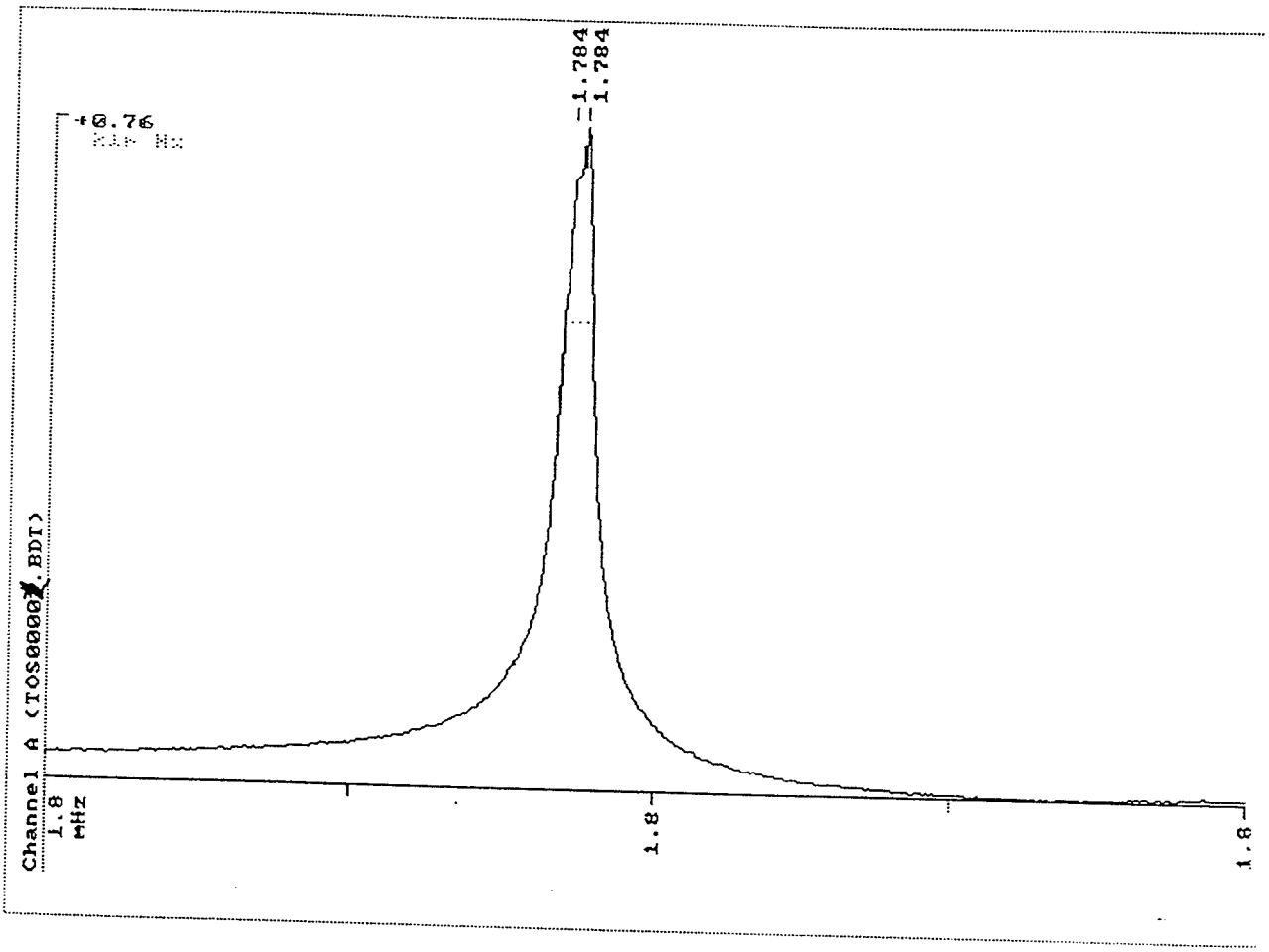

$\delta f / f = .0045$

01/06/94 11:56am Filename: <TOS00002.BDT>
Frequency 1780.000000 - 1790.000000 kHz, Amplitude 1.000000 volt
Data point density: 400 Stepwidth: 25.062657 Hz.

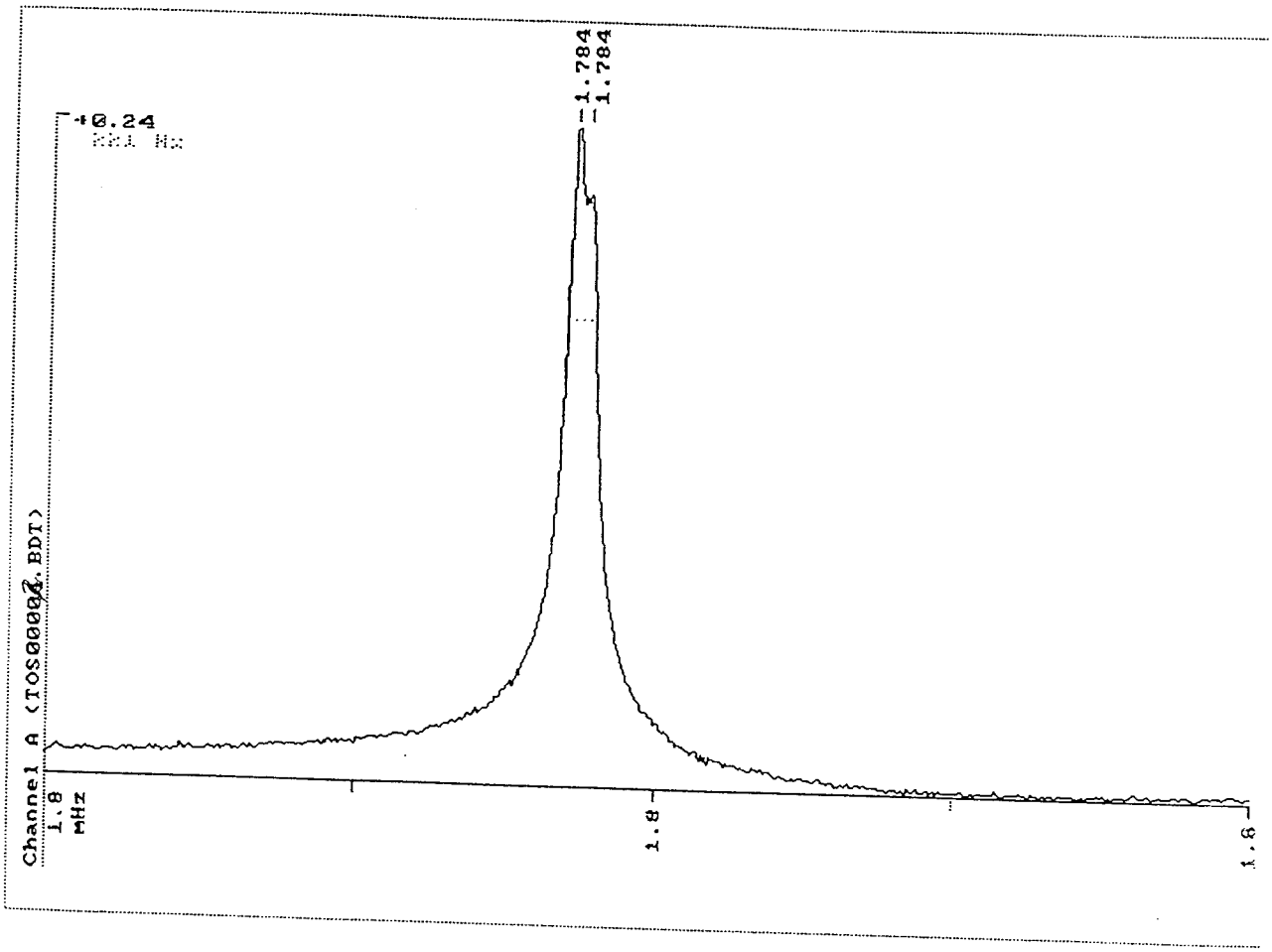

$\delta f/f = .0064$

01/06/94 11:58am Filename: <TOS00002.BDT>
Frequency 1783.000000 - 1785.000000 kHz, Amplitude 1.000000 volt
Data point density: 400 Stepwidth: 5.012531 Hz.

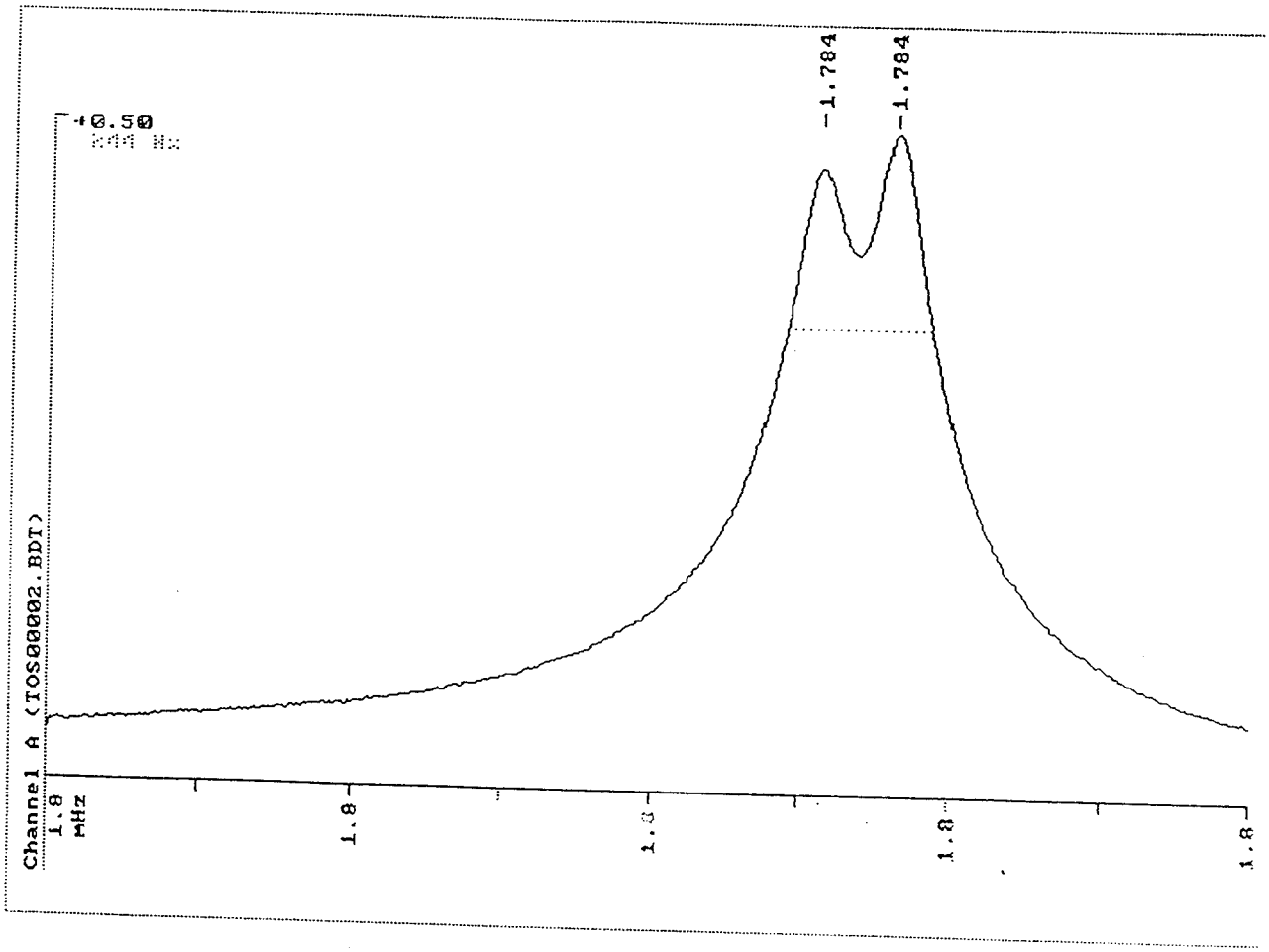

$\delta f/f = .0010$

01/04/94 11:06am Filename: <TOS00003.BDT>
Frequency 1780.000000 - 1790.000000 kHz, Amplitude 1.000000 volt
Data point density: 400 Stepwidth: 25.062657 Hz.

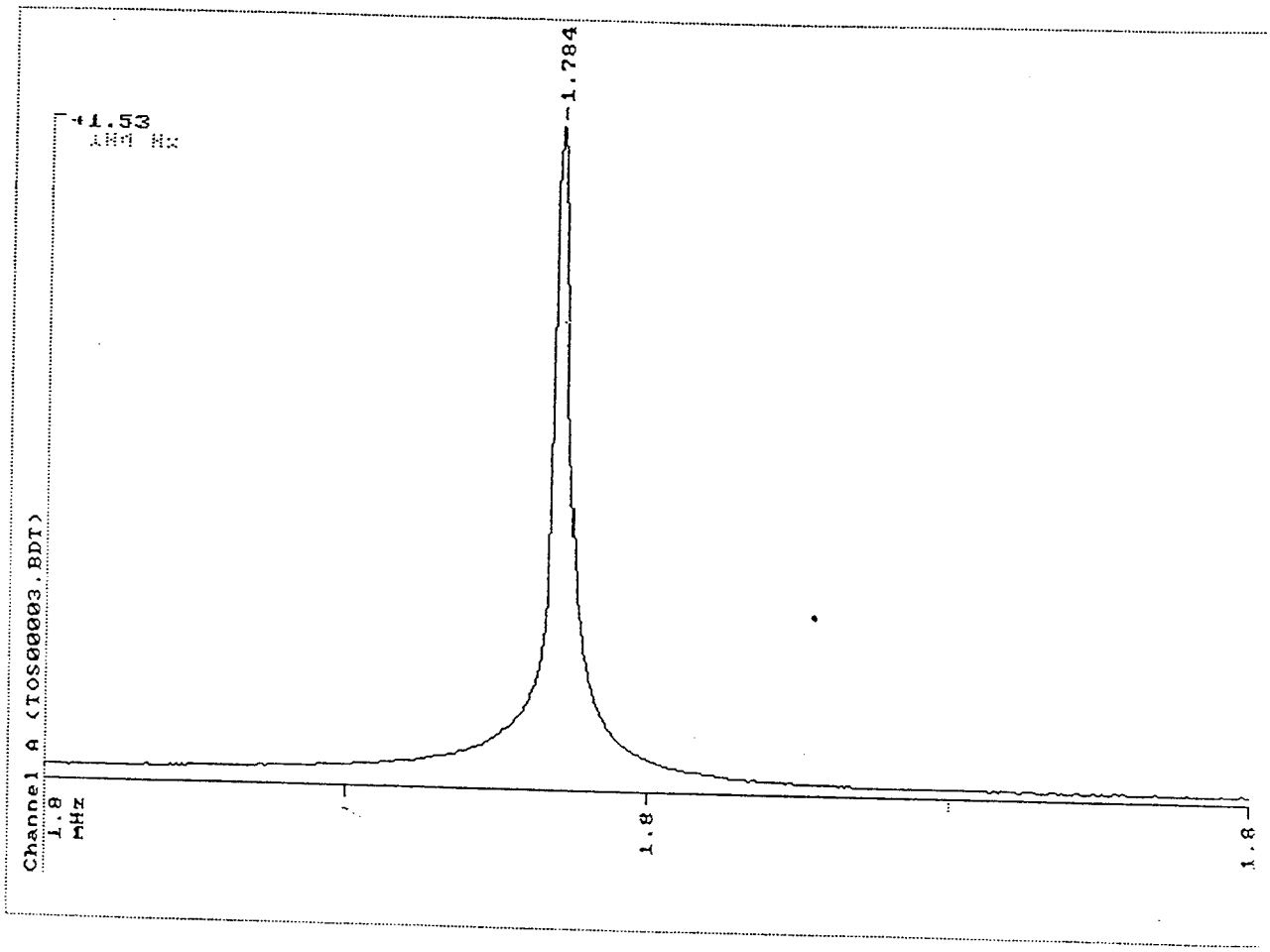

01/06/94 12:01pm Filename: <TOS00003.BDT>
Frequency 1783.000000 - 1785.000000 kHz, Amplitude 1.000000 volt
Data point density: 400 Stepwidth: 5.012531 Hz.

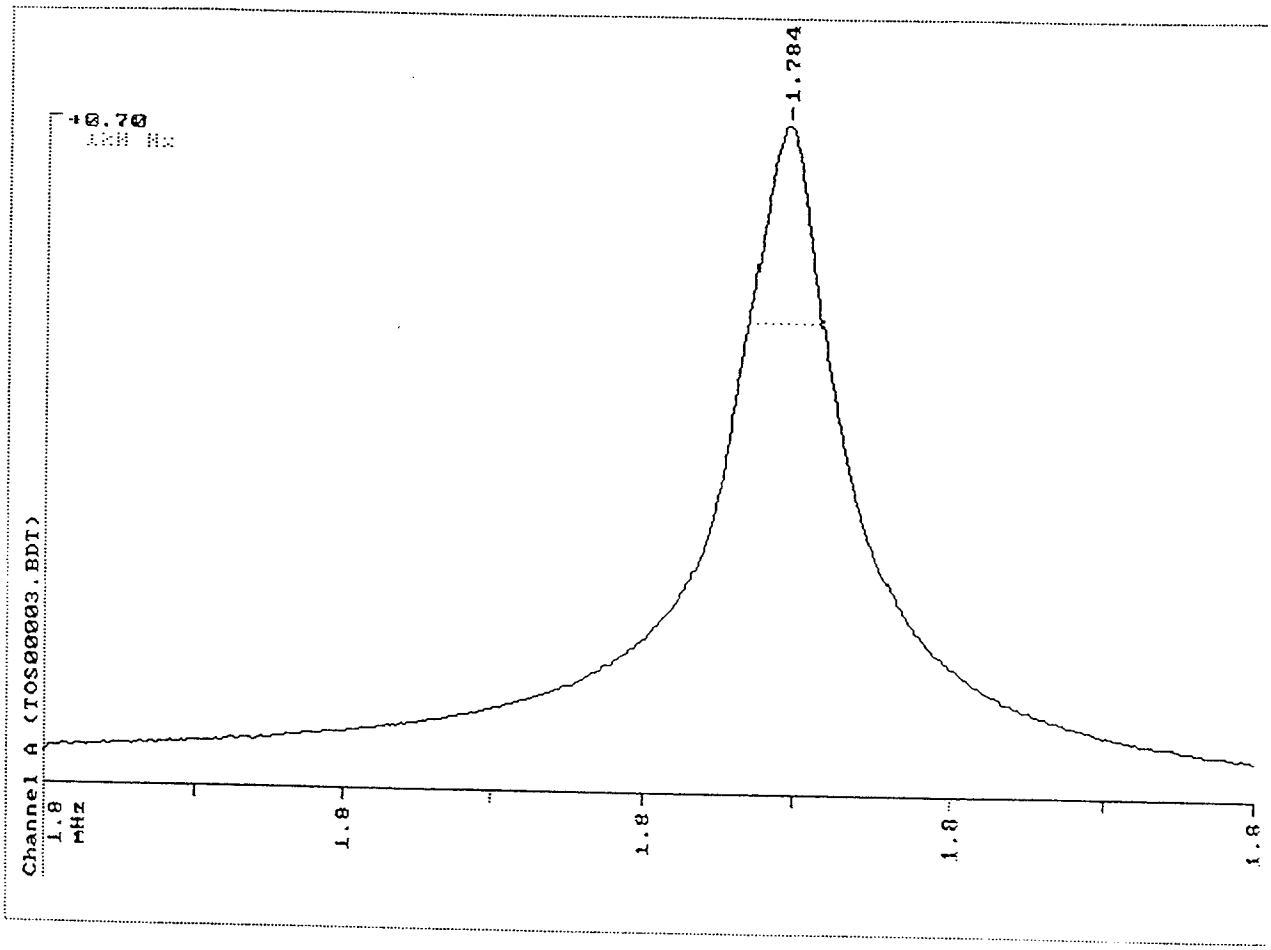

01/04/94 10:51am Filename: <TOS00004.BDT>
Frequency 1780.000000 - 1790.000000 kHz, Amplitude 1.000000 volt
Data point density: 400 Stepwidth: 25.062657 Hz.

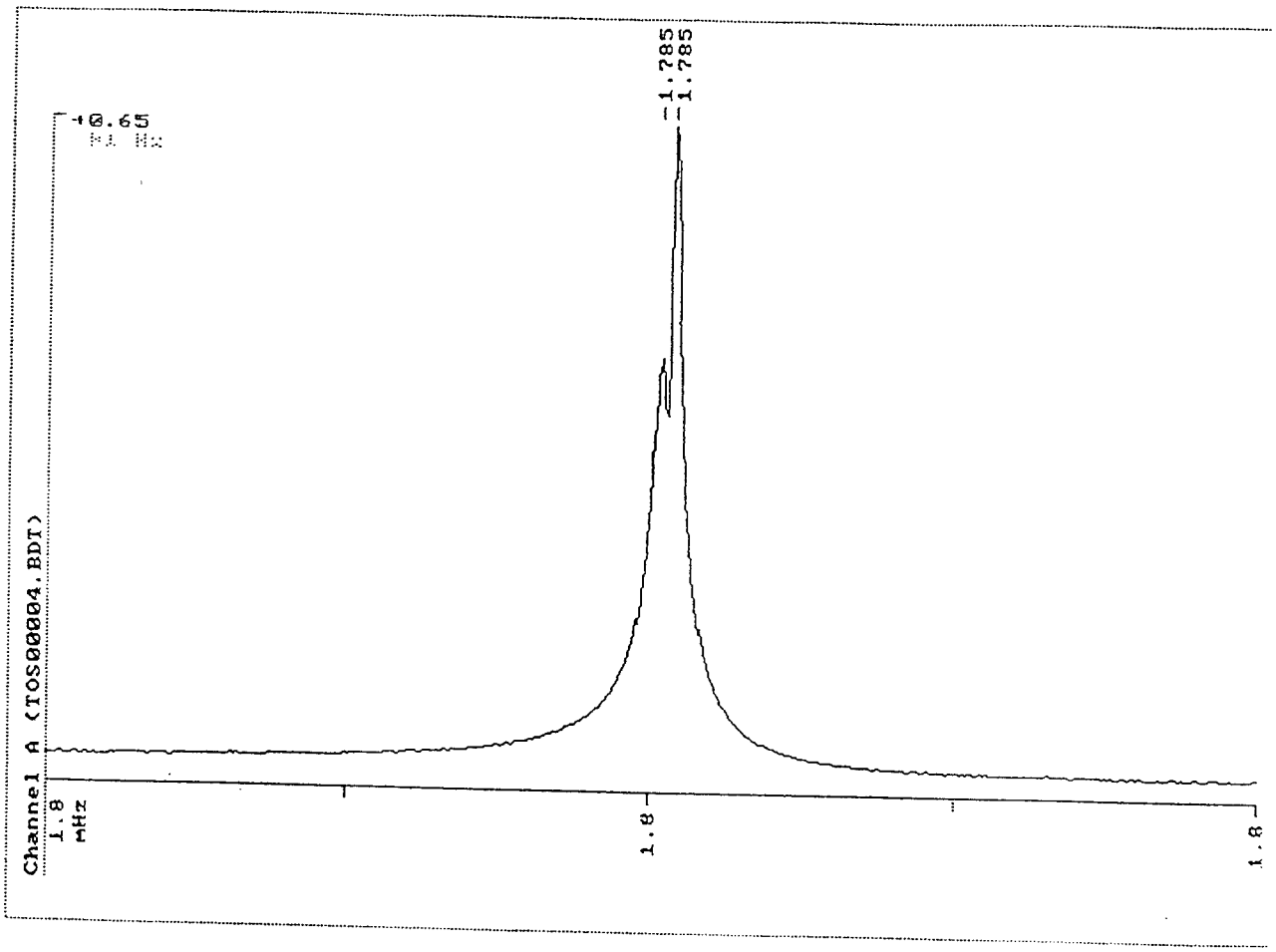

01/04/94 10:53am Filename: <TOS00005.BDT>
Frequency 1780.000000 - 1790.000000 kHz, Amplitude 1.000000 volt
Data point density: 400 Stepwidth: 25.062657 Hz.

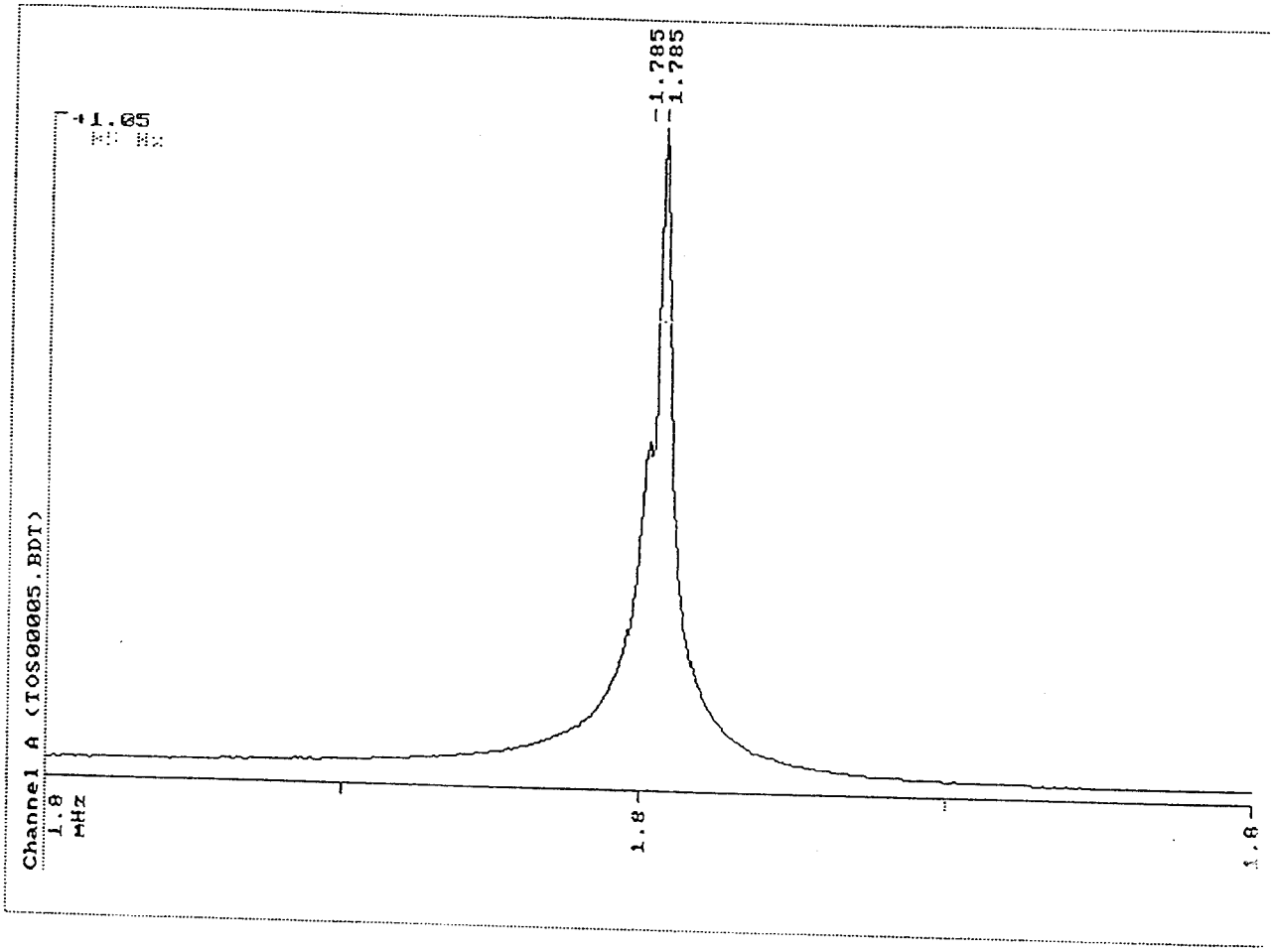

01/04/94 10:56am Filename: <TOS00006.BDT>
Frequency 1780.000000 - 1790.000000 kHz, Amplitude 1.000000 volt
Data point density: 400 Stepwidth: 25.062657 Hz.

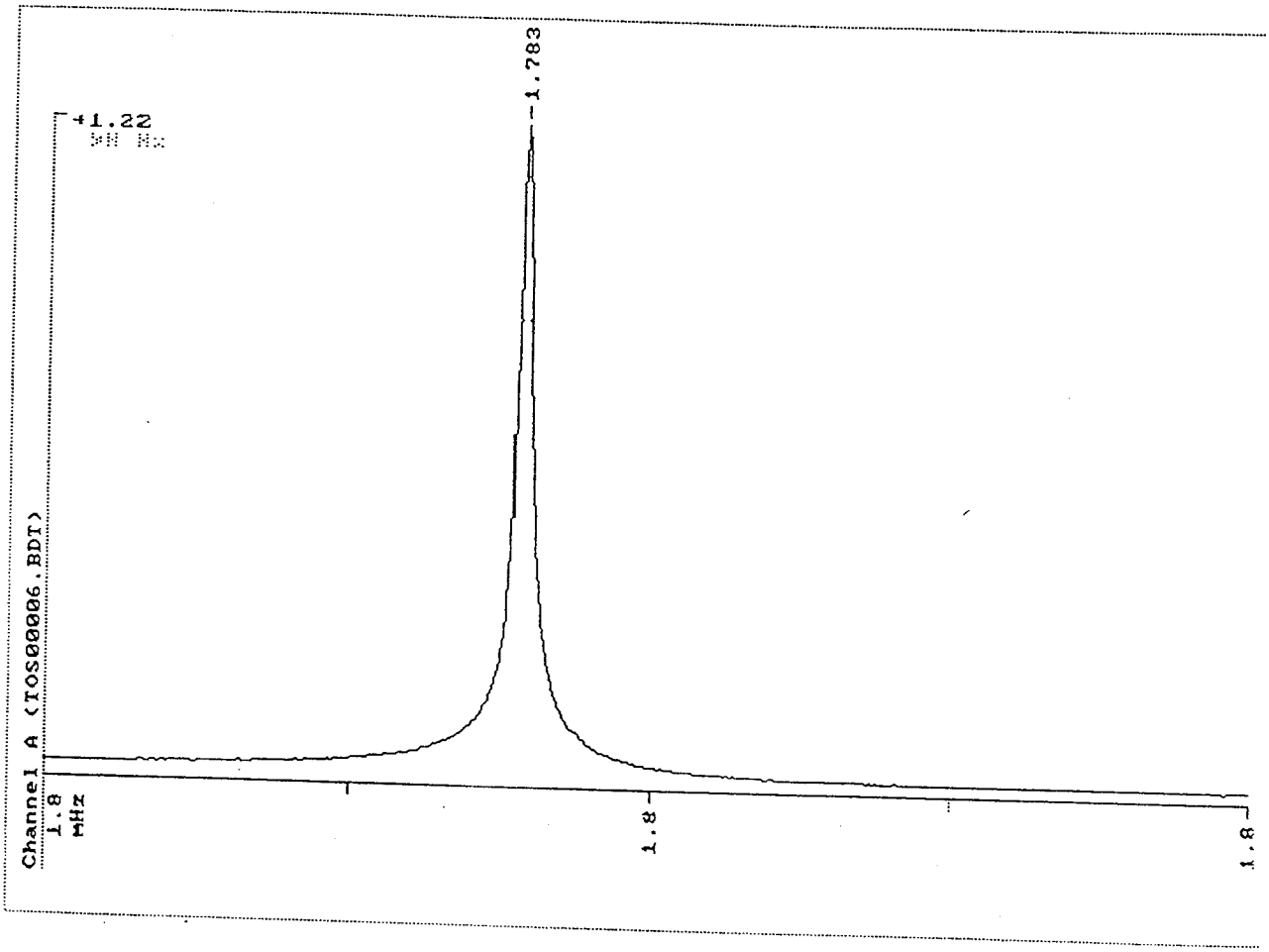

01/04/94 10:57am Filename: <TOS00007.BDT>
Frequency 1780.000000 - 1790.000000 kHz, Amplitude 1.000000 volt
Data point density: 400 Stepwidth: 25.062657 Hz.

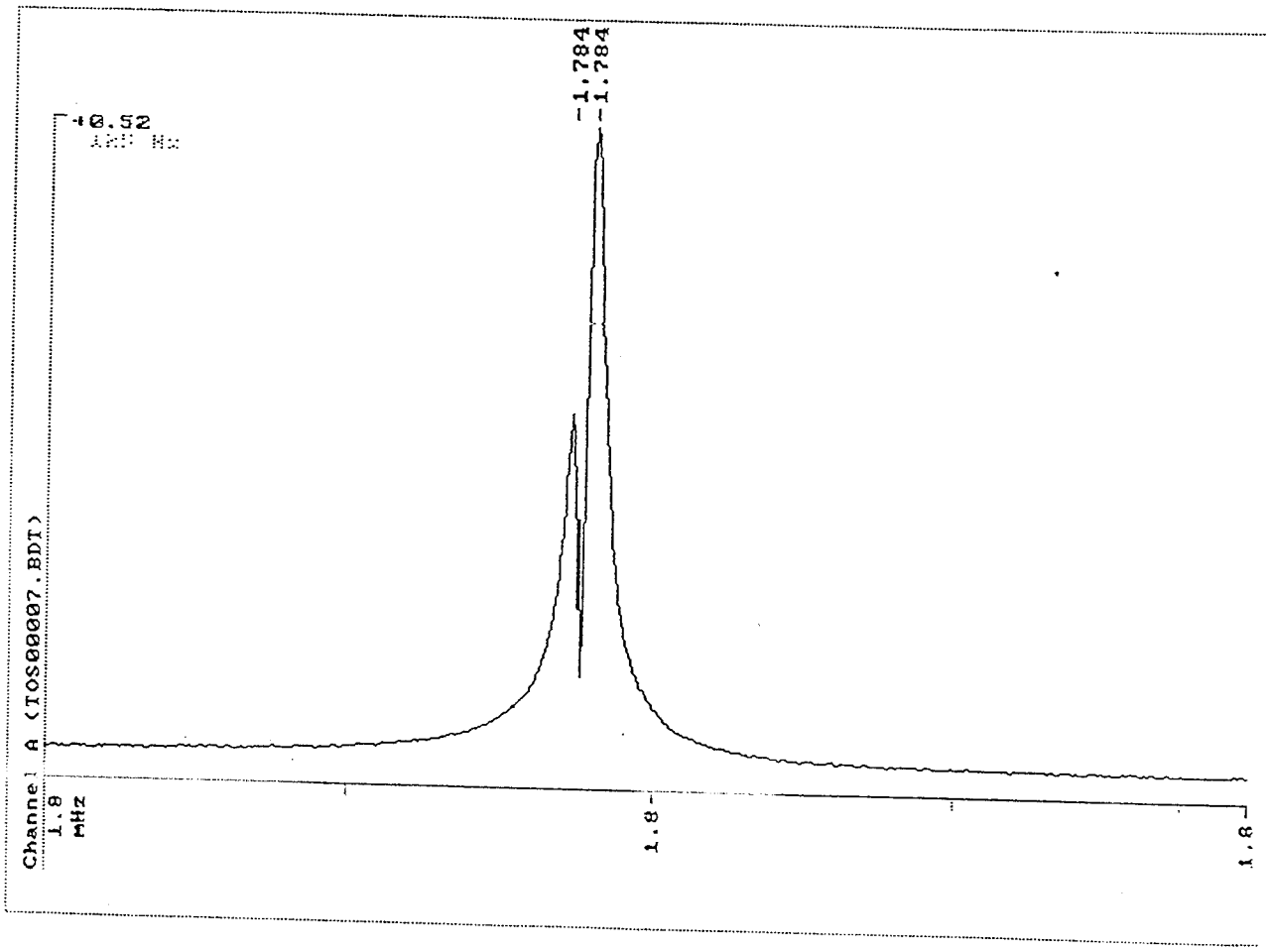

$\delta f/f = .0105$

01/04/94 10:59am Filename: <TOS00008.BDT>
Frequency 1780.000000 - 1790.000000 kHz, Amplitude 1.000000 volt
Data point density: 400 Stepwidth: 25.062657 Hz.

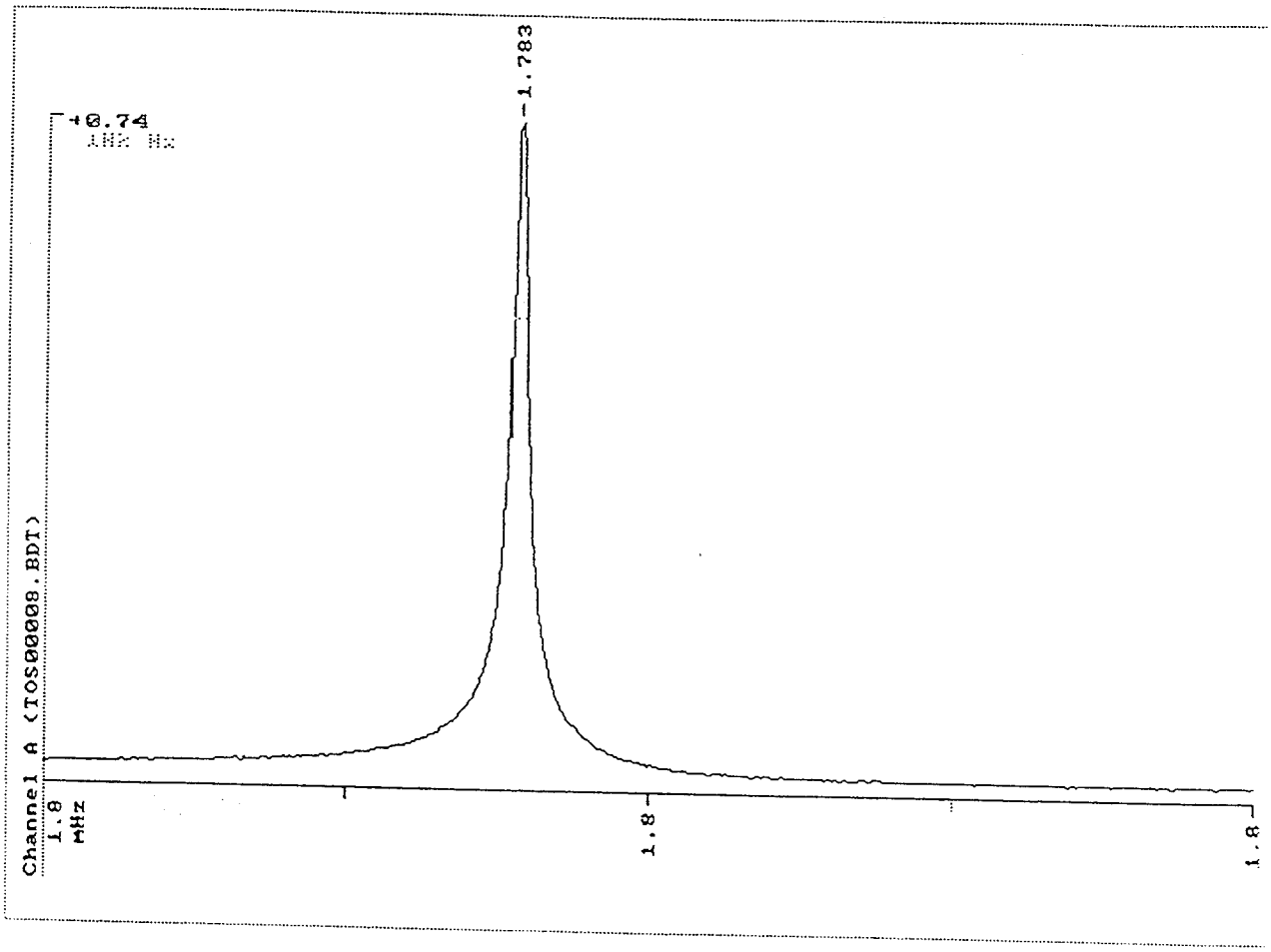

01/04/94 11:02am Filename: <TOS00009.BDT>
Frequency 1780.000000 - 1790.000000 kHz, Amplitude 1.000000 volt
Data point density: 400 Stepwidth: 25.062657 Hz.

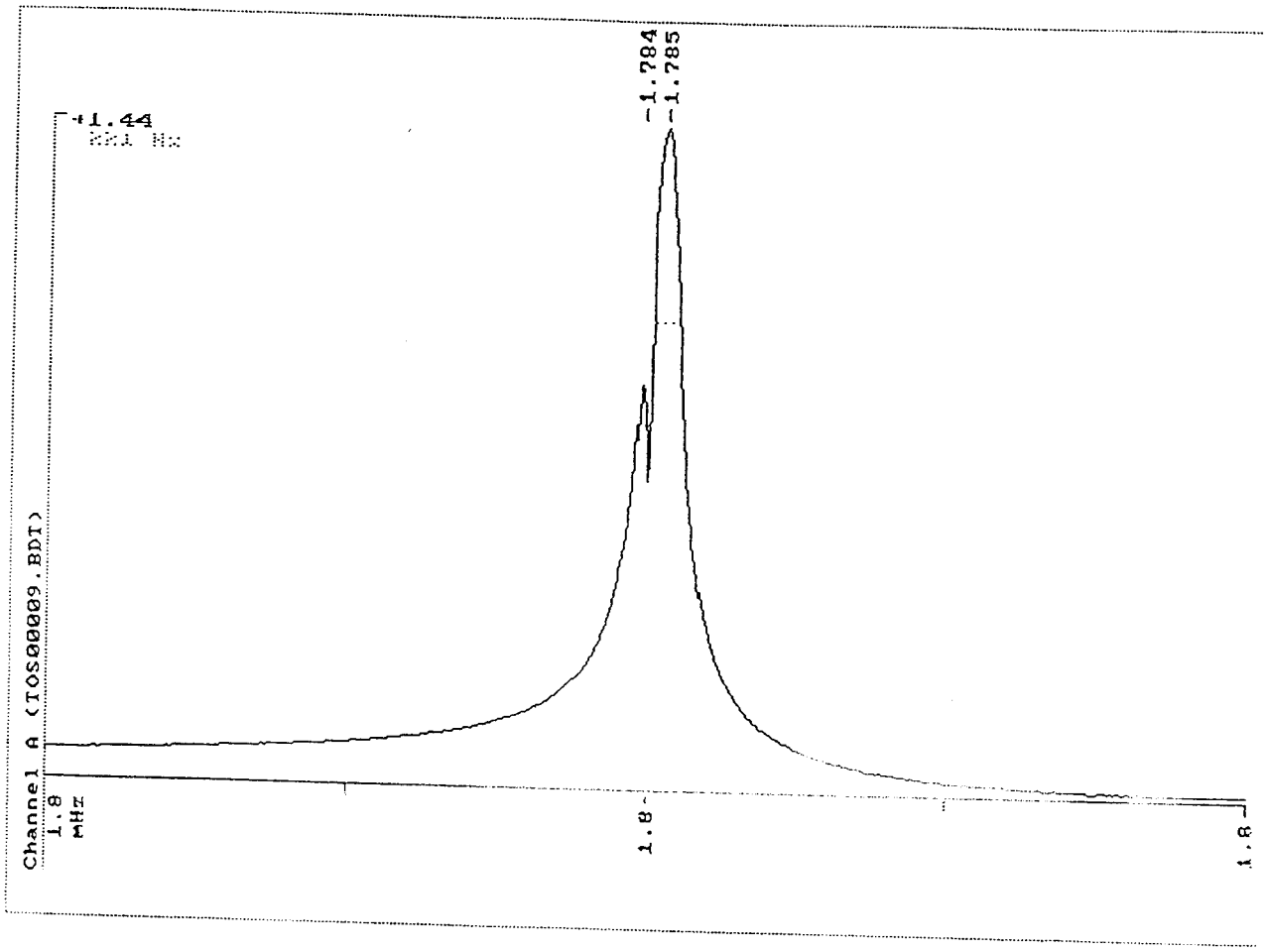

01/04/94 11:04am Filename: <TOS00010.BDT>
Frequency 1780.000000 - 1790.000000 kHz, Amplitude 1.000000 volt
Data point density: 400 Stepwidth: 25.062657 Hz.

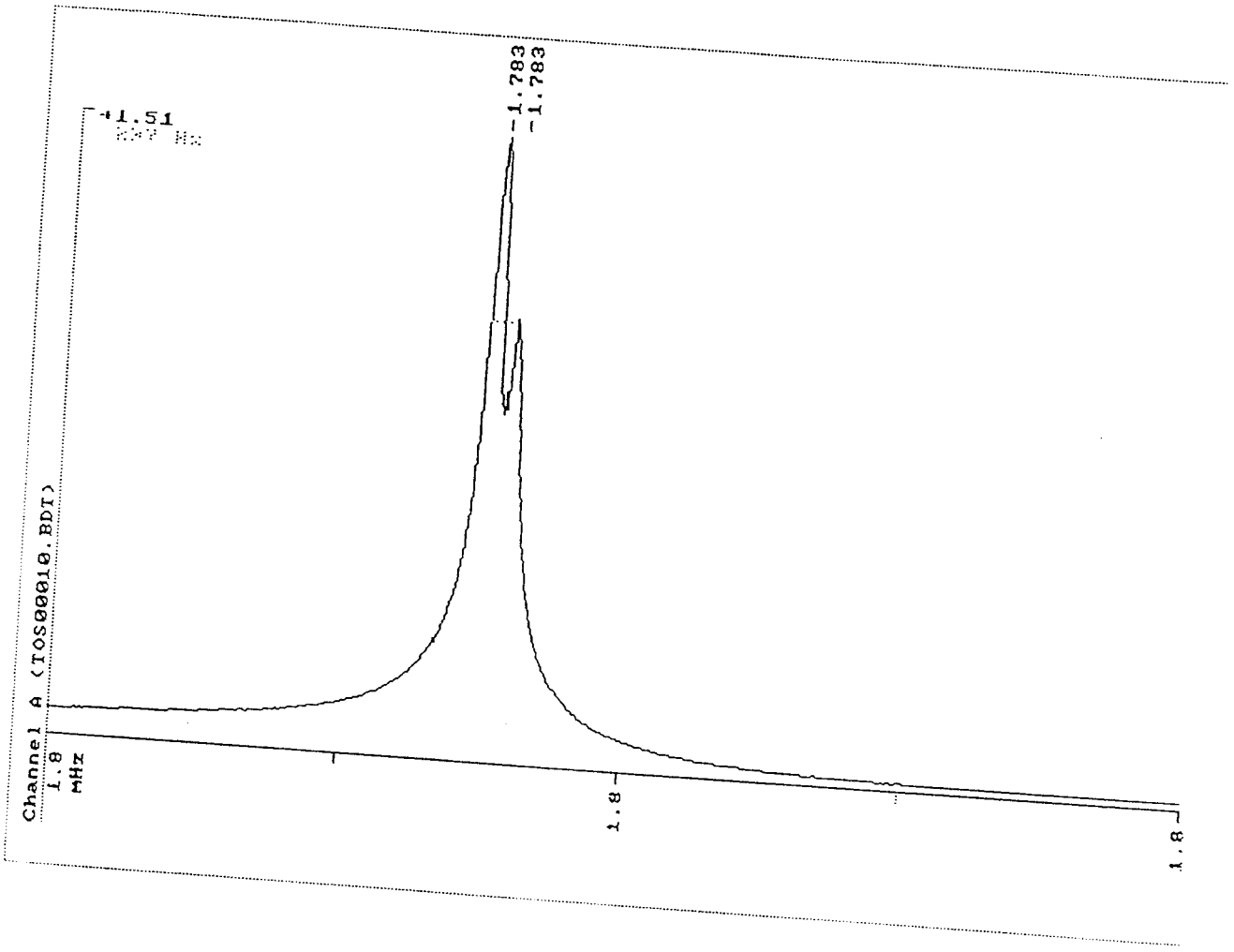

01/04/94 12:44pm Filename: <TOS00001.BDT>
Frequency 787.000000 - 791.000000 kHz, Amplitude 0.100000 volt
Data point density: 400 Stepwidth: 10.025063 Hz.

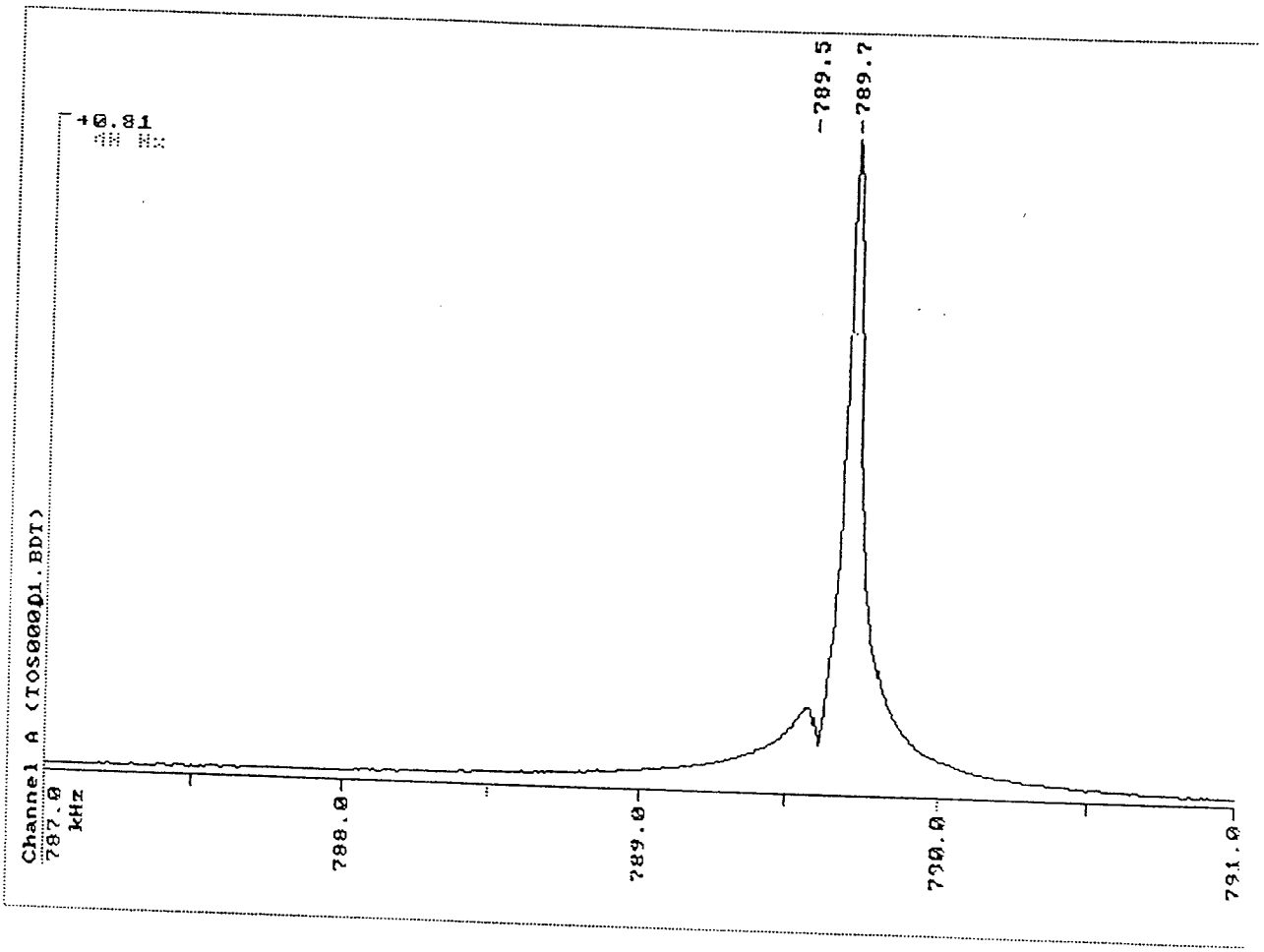

$\Gamma H/_F = .0177$

01/04/94 12:47pm Filename: <TOS00002.BDT>
Frequency 787.000000 - 791.000000 kHz, Amplitude 0.100000 volt
Data point density: 400 Stepwidth: 10.025063 Hz.

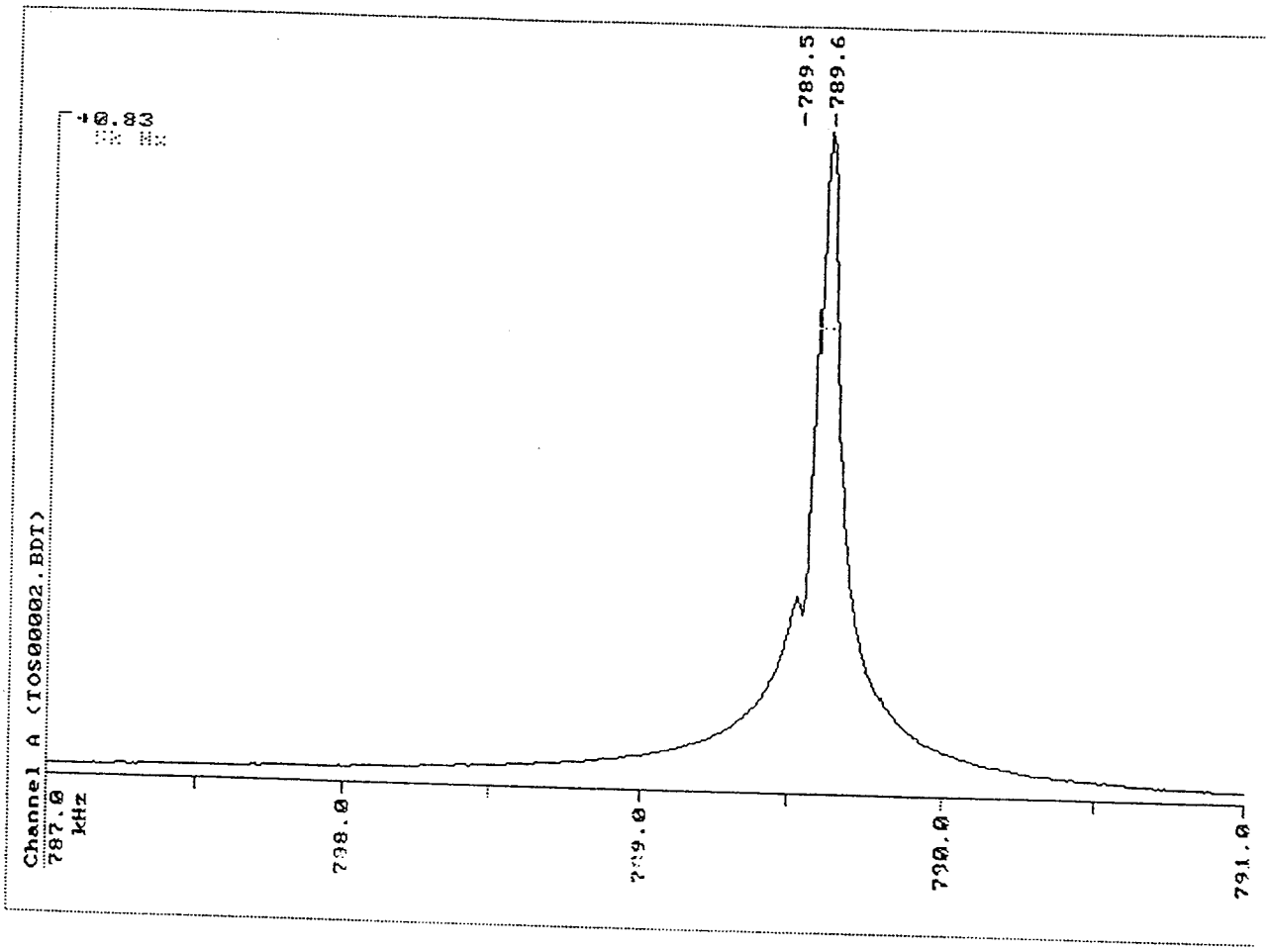

01/04/94 12:51pm Filename: <TOS00003.BDT>
Frequency 787.000000 - 791.000000 kHz, Amplitude 0.100000 volt
Data point density: 400 Stepwidth: 10.025063 Hz.

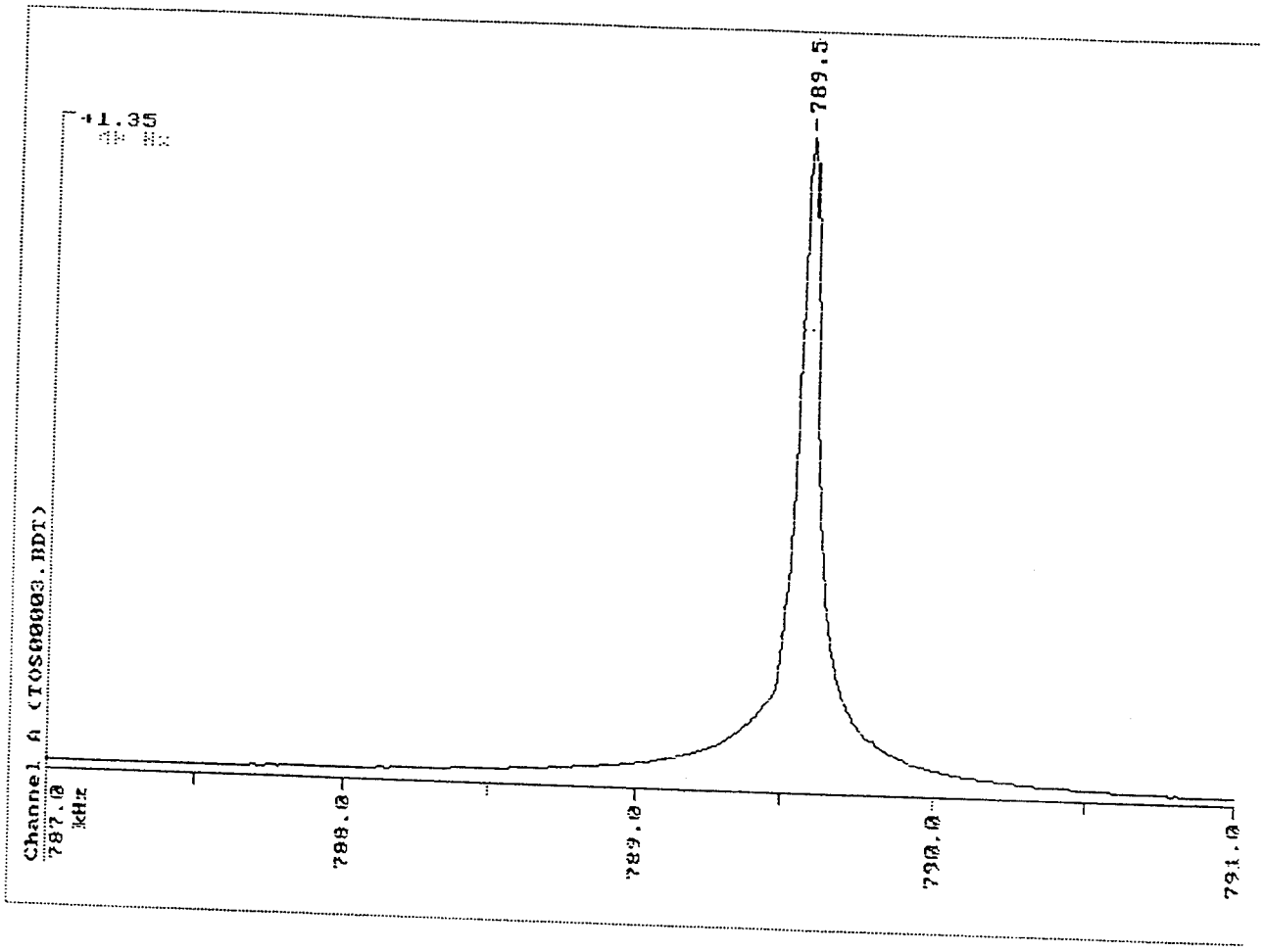

01/04/94 12:52pm Filename: <TOS00004.BDT>
Frequency 787.000000 - 791.000000 kHz, Amplitude 0.100000 volt
Data point density: 400 Stepwidth: 10.025063 Hz.

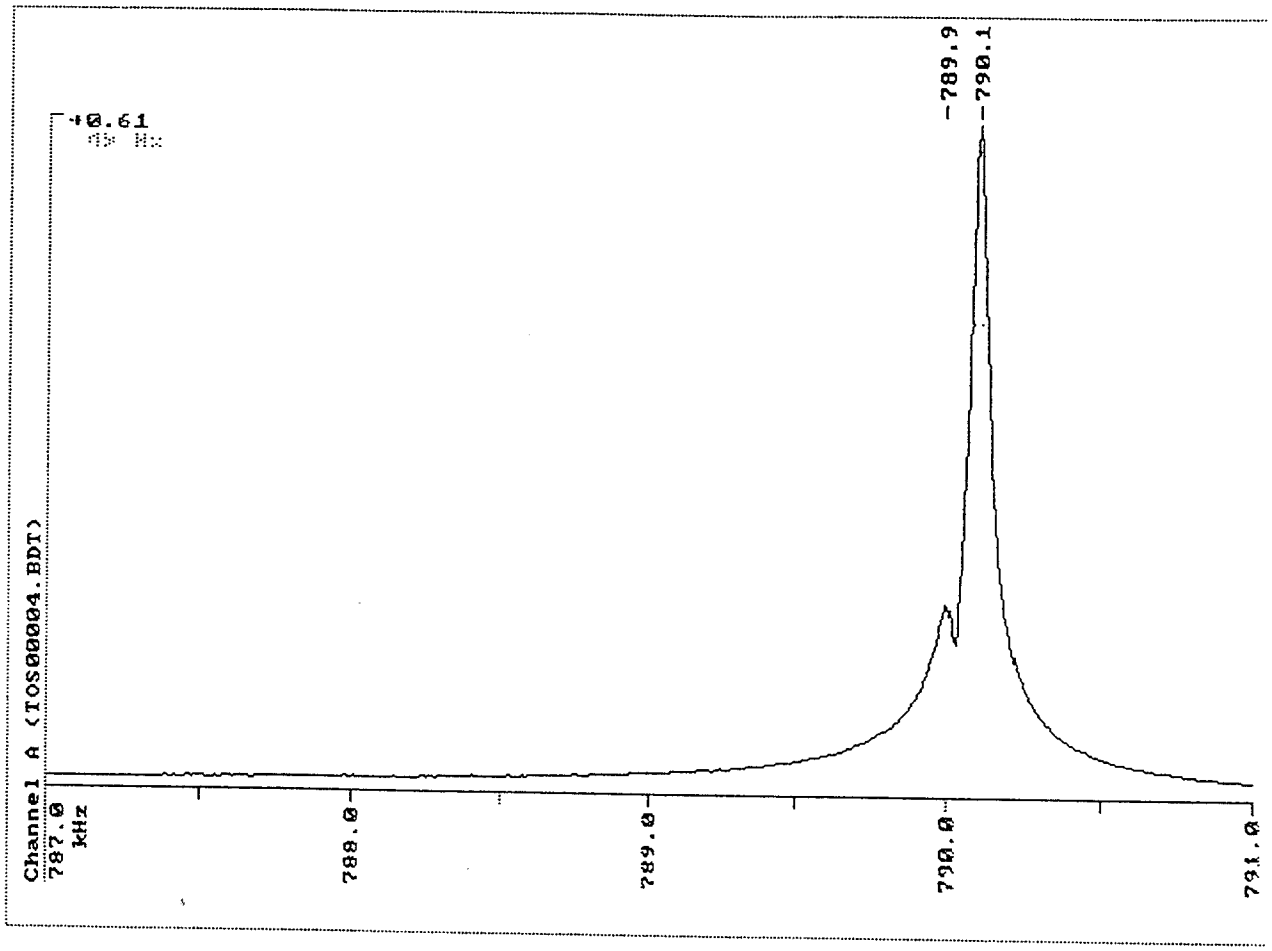

01/04/94 1:01pm Filename: <TOS00005.BDT>
Frequency 787.000000 - 791.000000 kHz, Amplitude 0.100000 volt
Data point density: 400 Stepwidth: 10.025063 Hz.

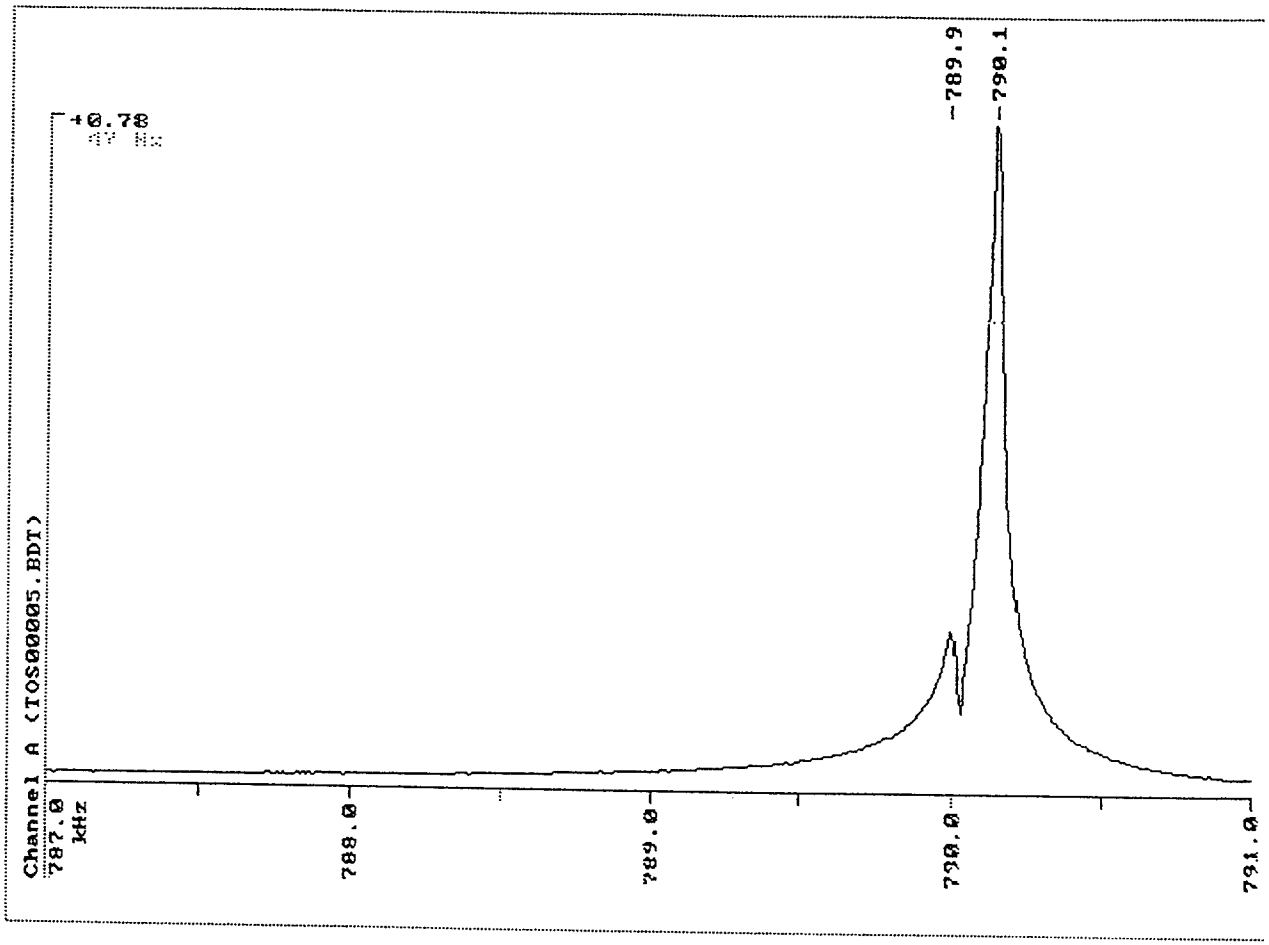

$\Delta f/f = .0198$

01/04/94 1:18pm Filename: <TOS00006.BDT>
Frequency 787.000000 - 791.000000 kHz, Amplitude 0.100000 volt
Data point density: 400 Stepwidth: 10.025063 Hz.

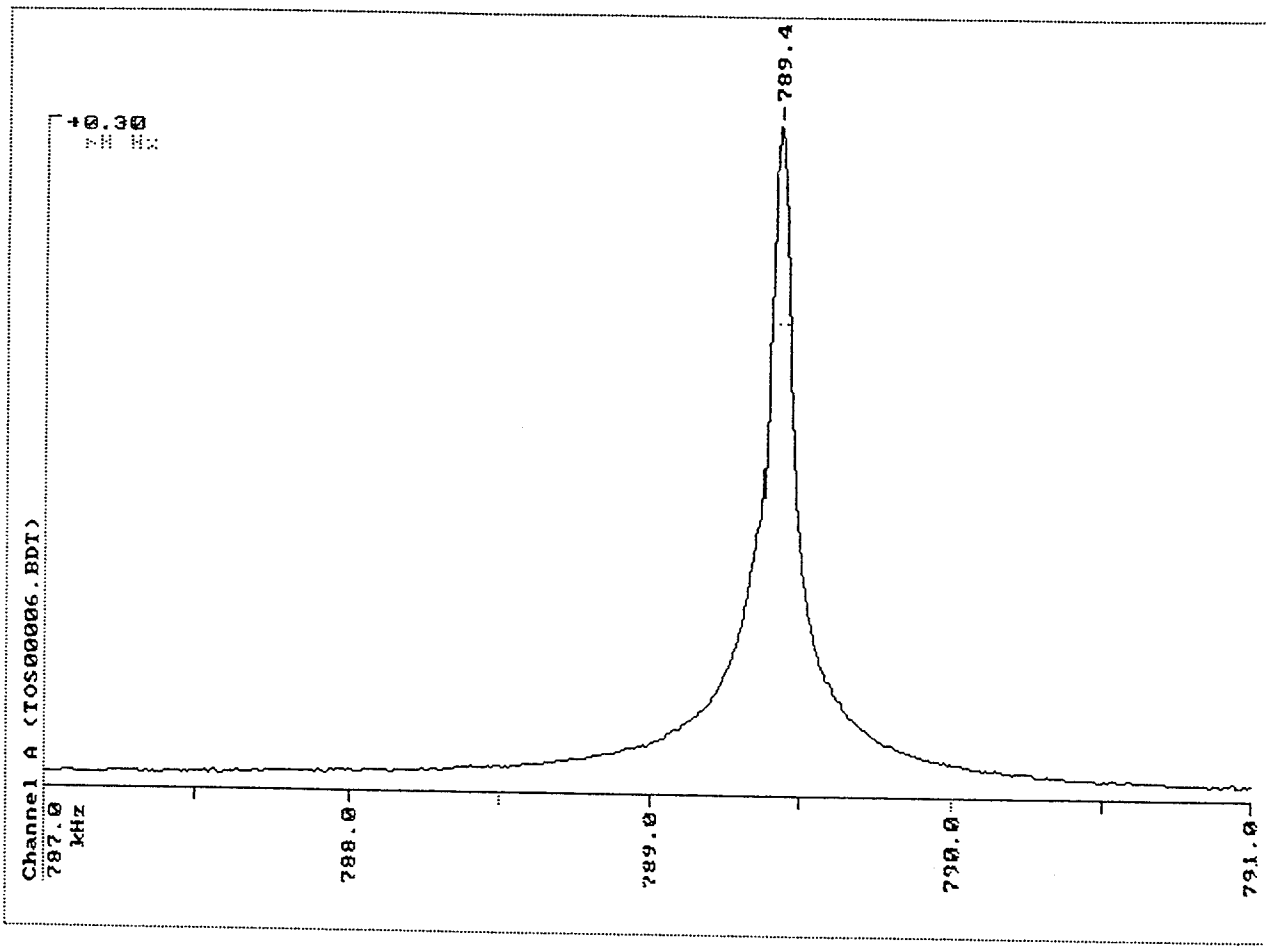

01/04/94 1:21pm Filename: <TOS00007.BDT>
Frequency 787.000000 - 791.000000 kHz, Amplitude 0.100000 volt
Data point density: 400 Stepwidth: 10.025063 Hz.

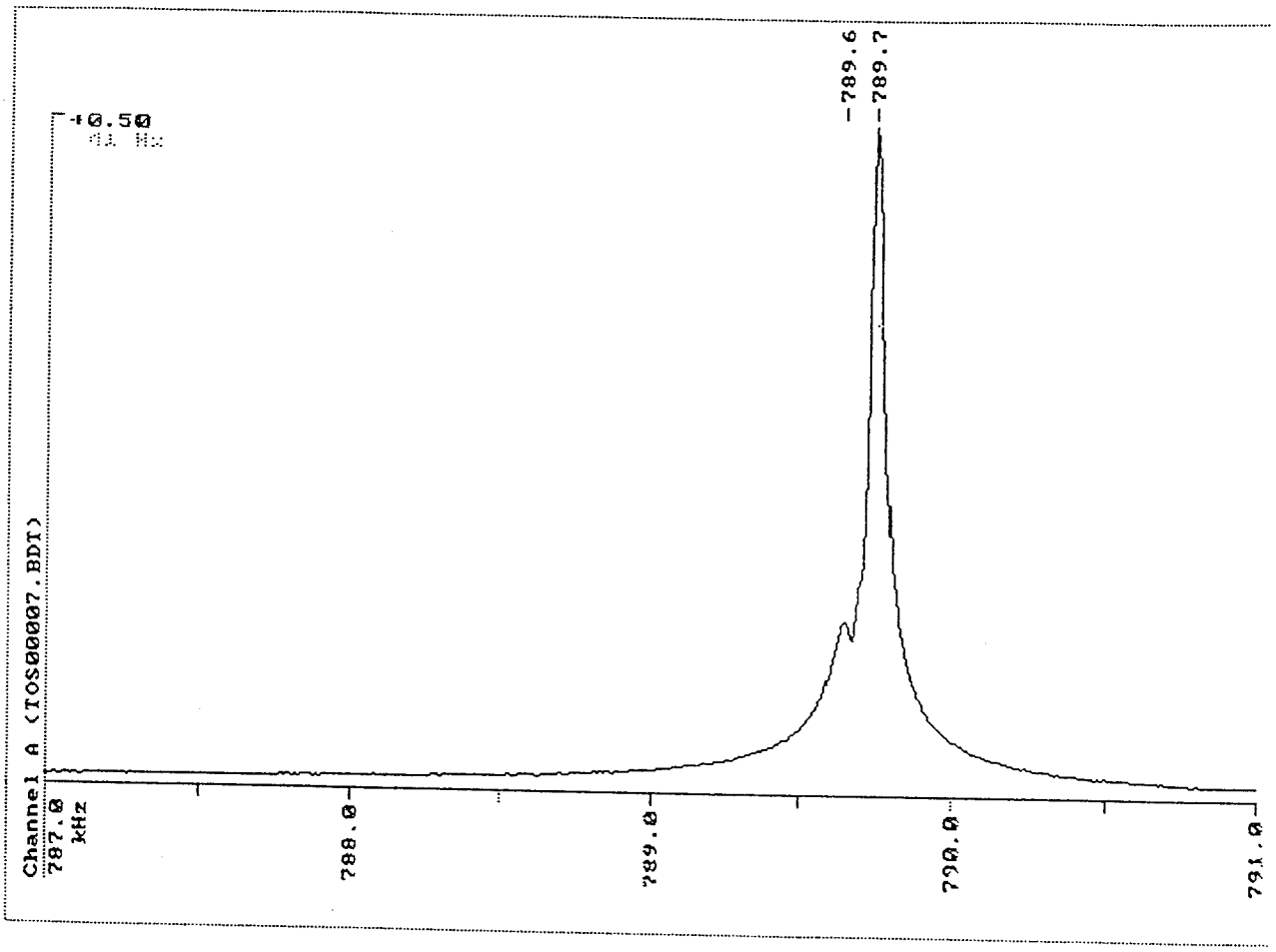

01/04/94 1:23pm Filename: <TOS00008.BDT>
Frequency 787.000000 - 791.000000 kHz, Amplitude 0.100000 volt
Data point density: 400 Stepwidth: 10.025063 Hz.

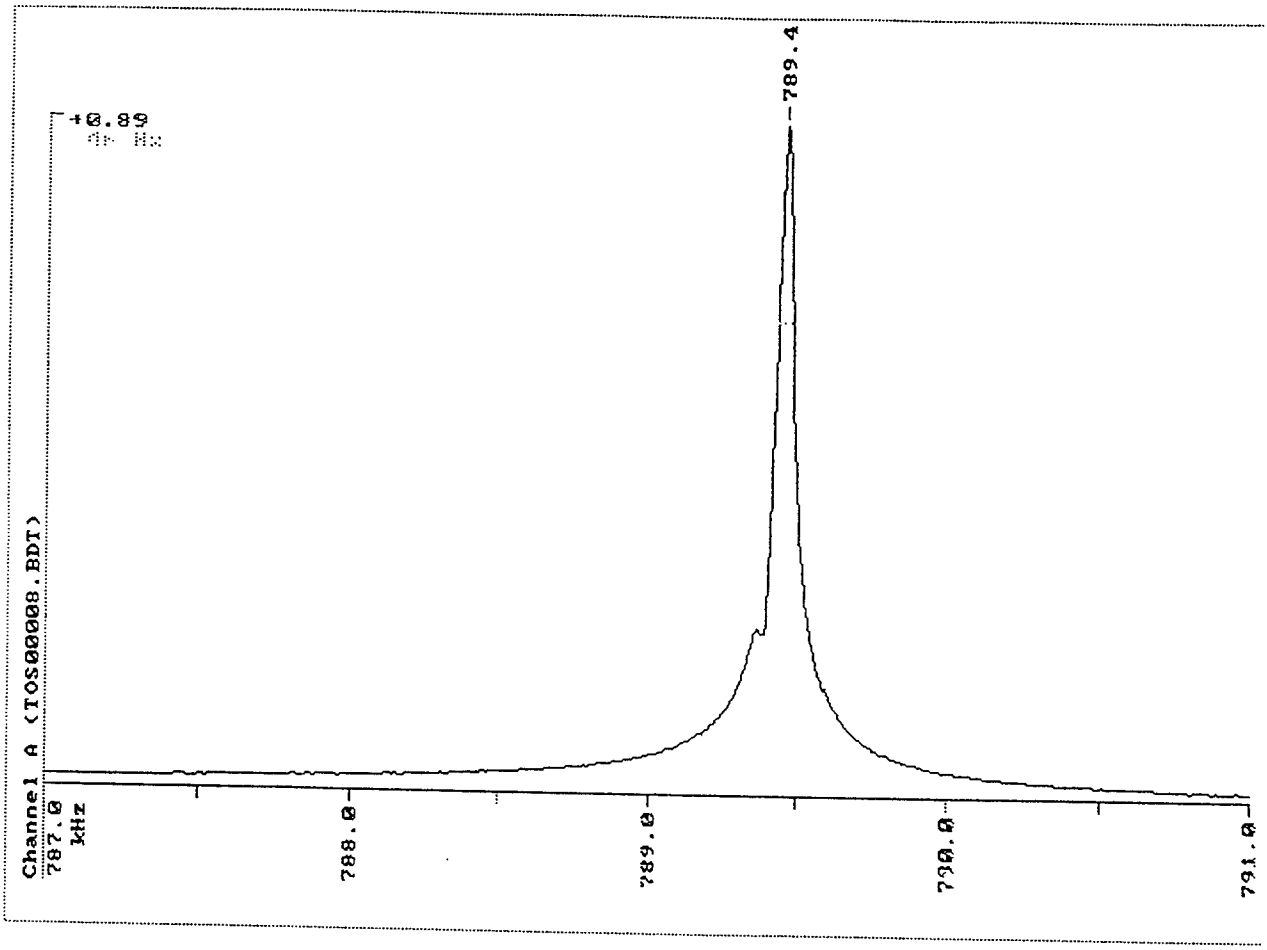

01/04/94 10:19am Filename: <TOS00001.BDT>
Frequency 3115.000000 - 3125.000000 kHz, Amplitude 1.000000 volt
Data point density: 400 Stepwidth: 25.062657 Hz.

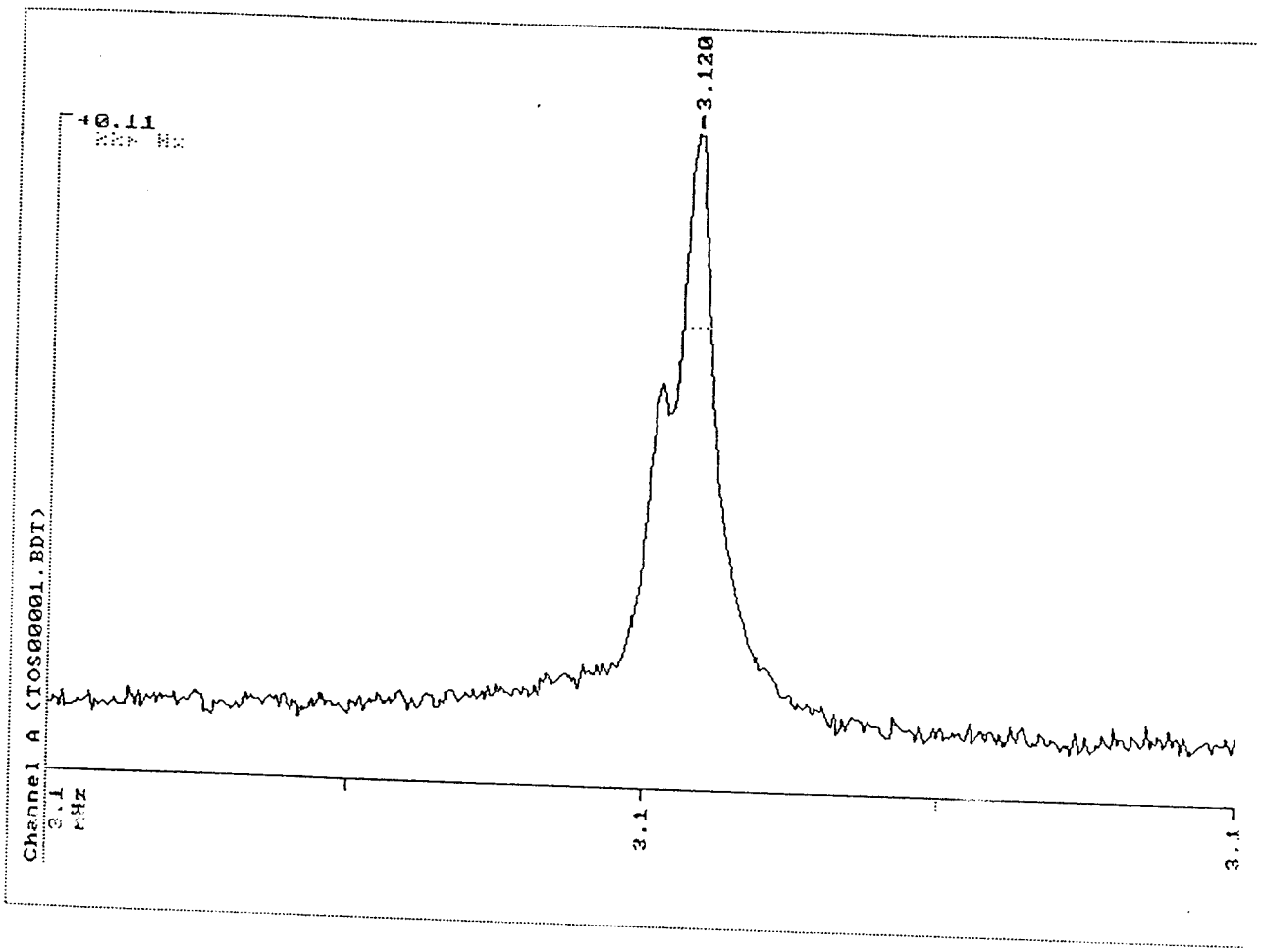

01/04/94 10:15am Filename: <TOS00002.BDT>
Frequency 3120.000000 - 3130.000000 kHz, Amplitude 0.100000 volt
Data point density: 400 Stepwidth: 25.062657 Hz.

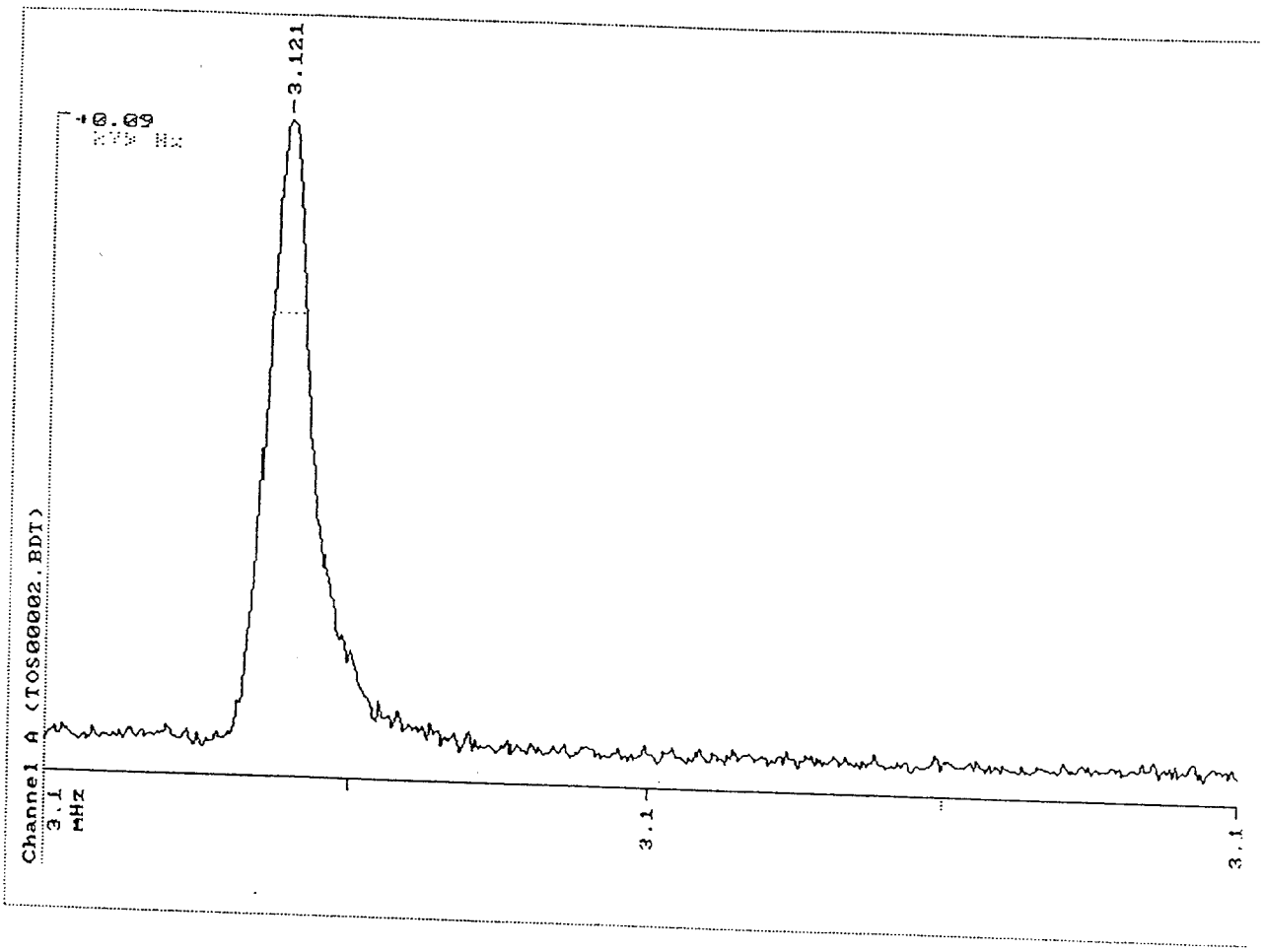

01/04/94 10:19am Filename: <TOS00001.BDT>
Frequency 3115.000000 - 3125.000000 kHz, Amplitude 1.000000 volt
Data point density: 400 Stepwidth: 25.062657 Hz.

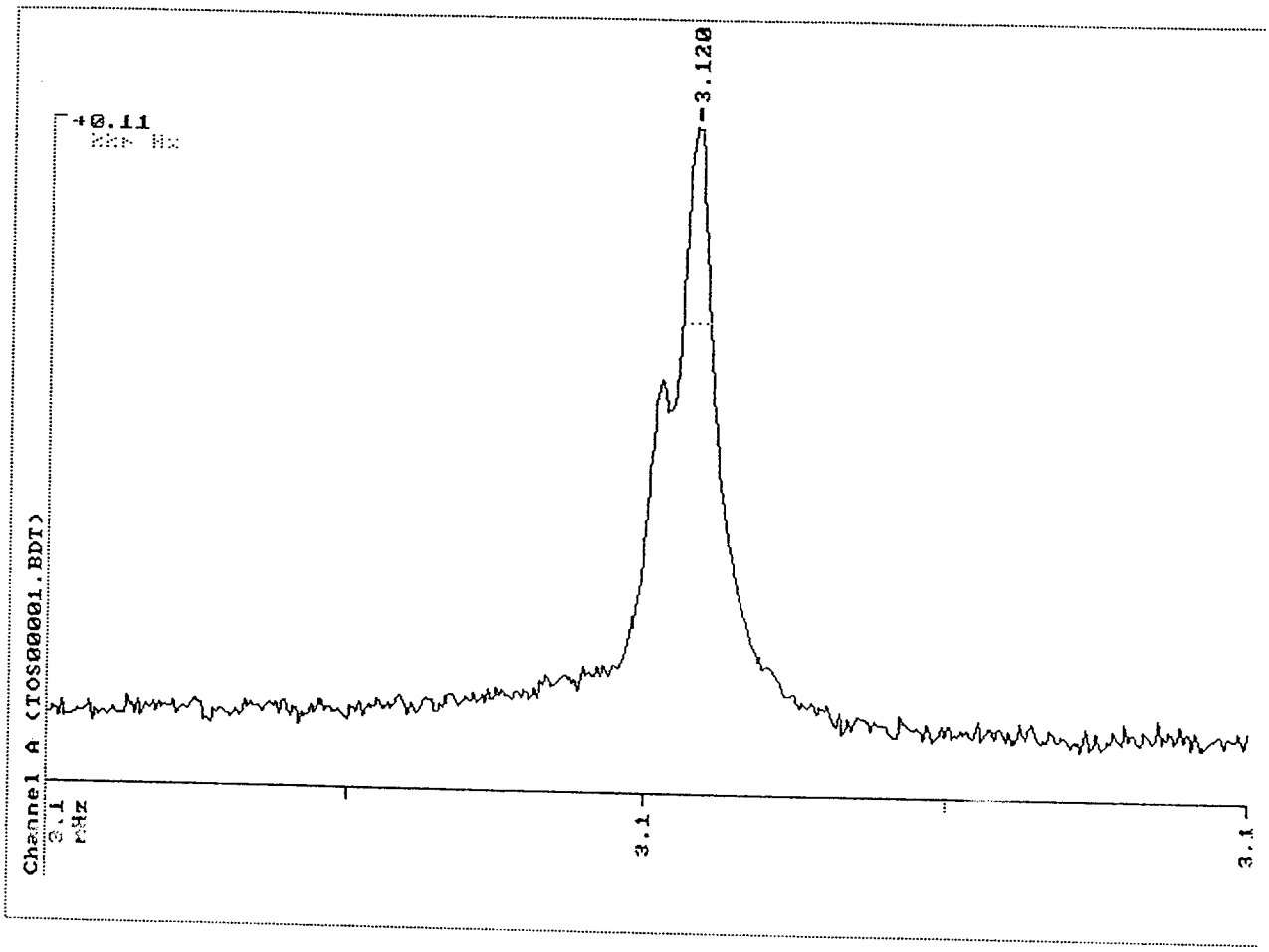

01/04/94 10:15am Filename: <TOS00002.BDT>
Frequency 3120.000000 - 3130.000000 kHz, Amplitude 0.100000 volt
Data point density: 400 Stepwidth: 25.062657 Hz.

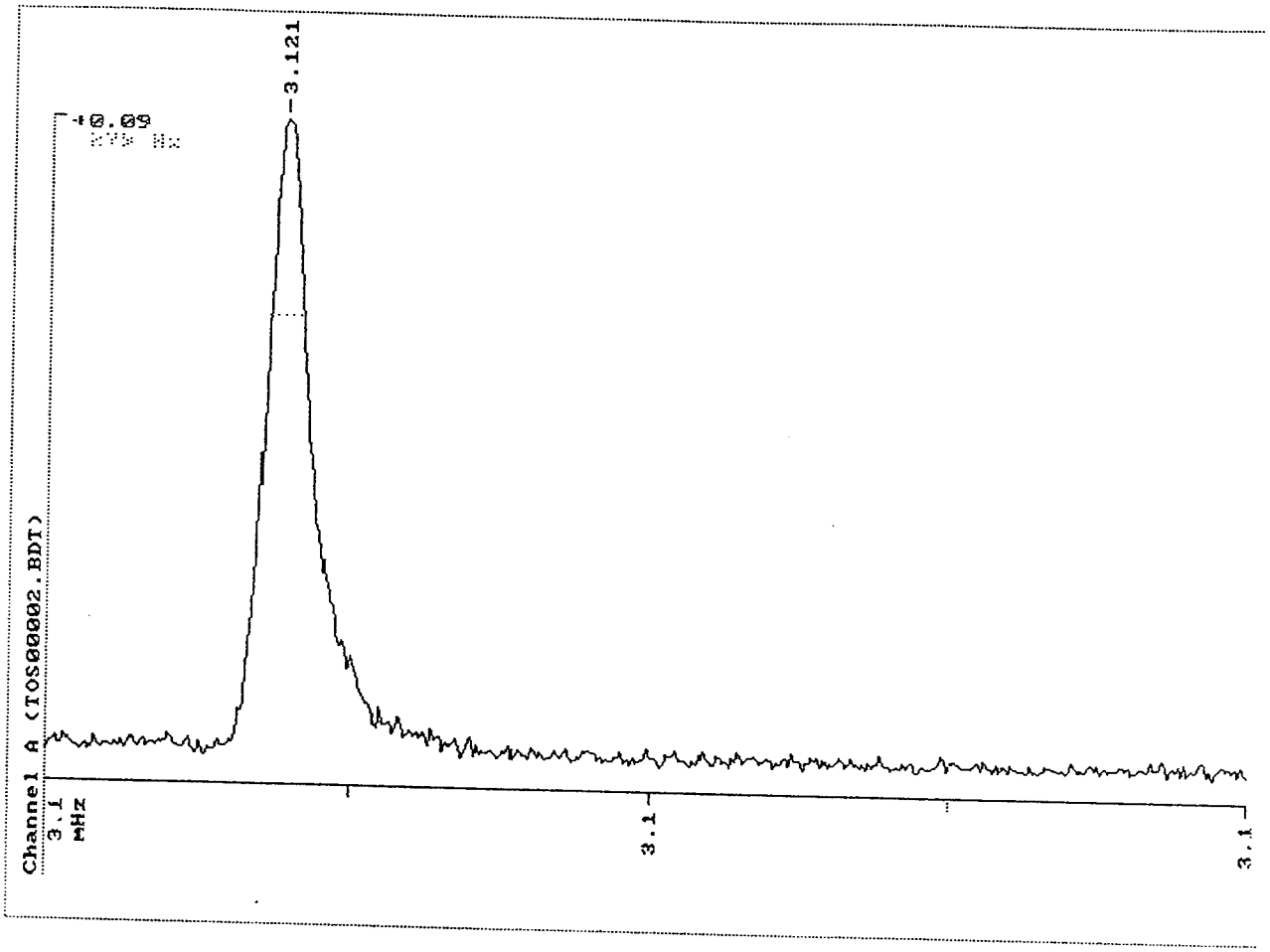

01/04/94 10:21am Filename: <TOS00003.BDT>
Frequency 3115.000000 - 3125.000000 kHz, Amplitude 1.000000 volt
Data point density: 400 Stepwidth: 25.062657 Hz.

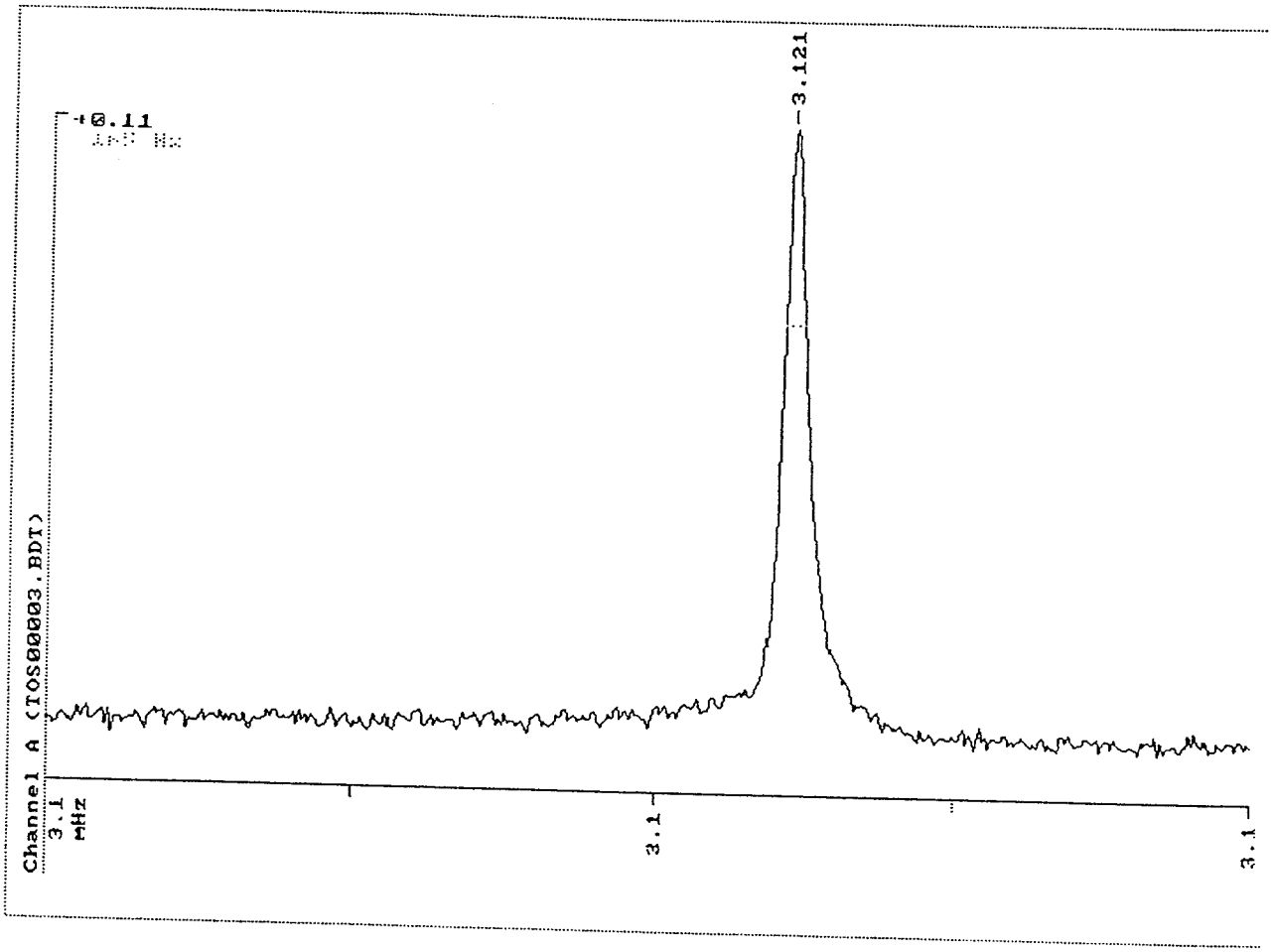

01/04/94 10:12am Filename: <TOS00004.BDT>
Frequency 3120.000000 - 3130.000000 kHz, Amplitude 0.100000 volt
Data point density: 400 Stepwidth: 25.062657 Hz.

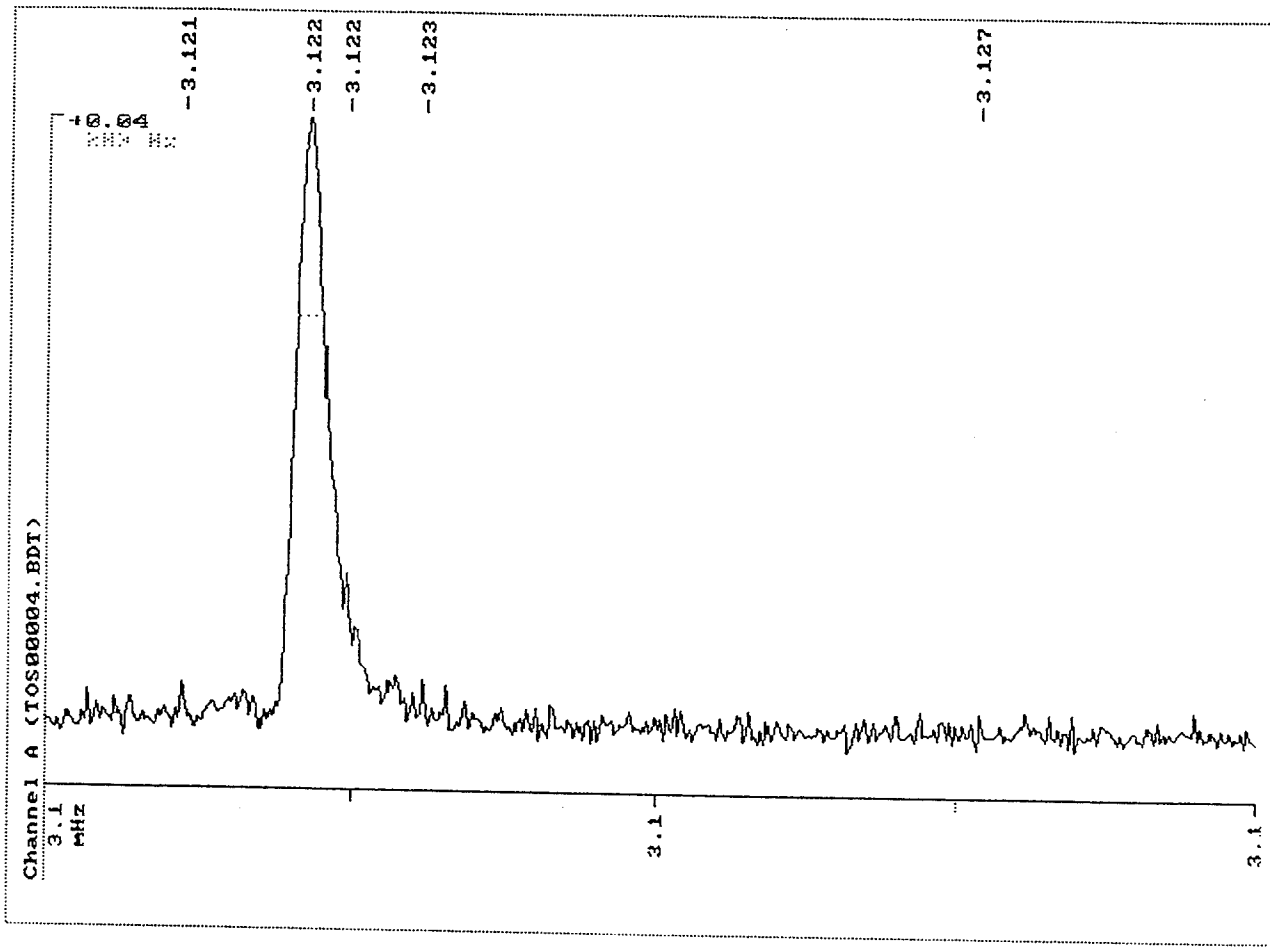

01/04/94 10:23am Filename: <TOS00005.BDT>
Frequency 3115.000000 - 3125.000000 kHz, Amplitude 1.000000 volt
Data point density: 400 Stepwidth: 25.062657 Hz.

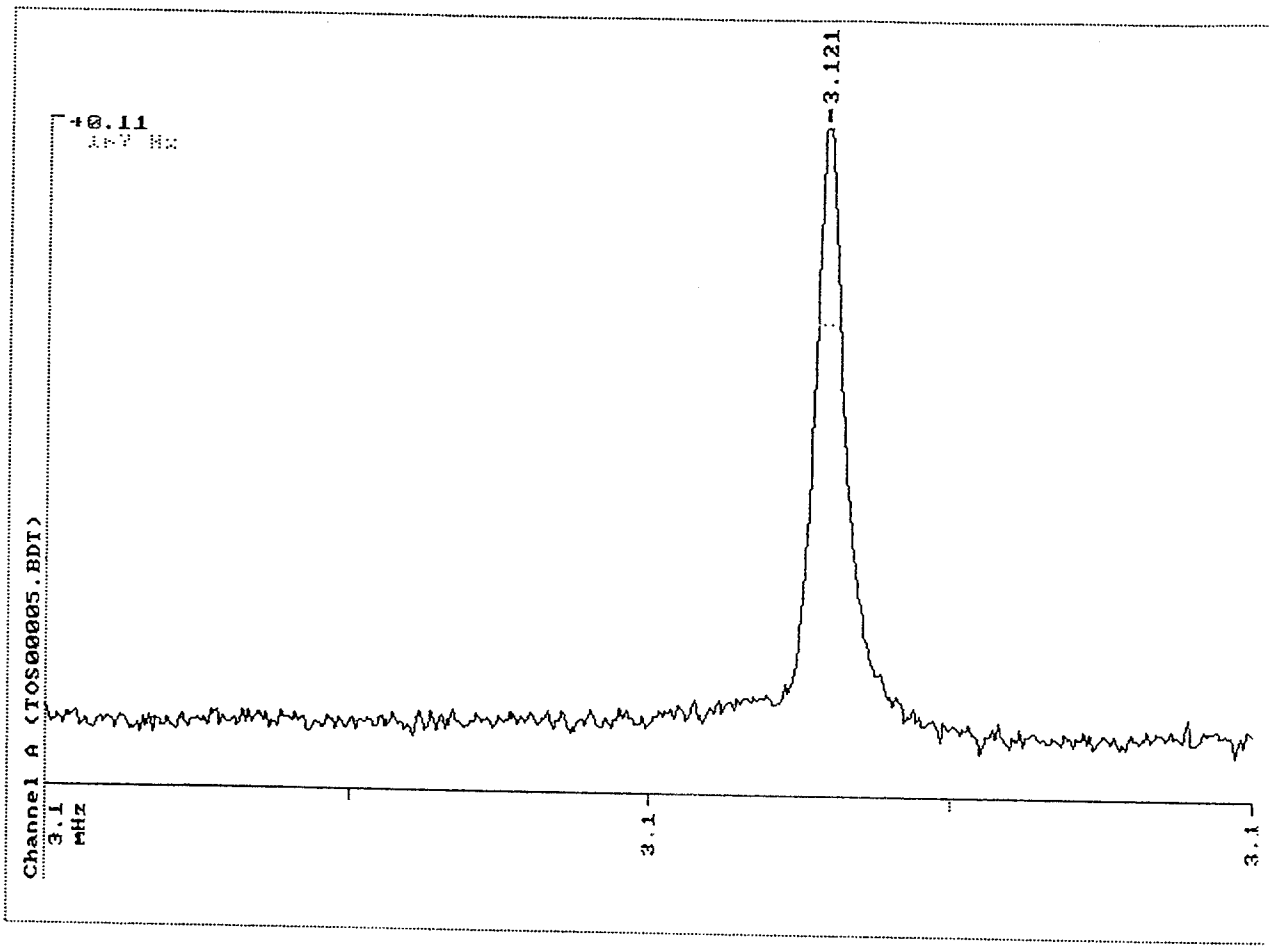

01/04/94 10:24am Filename: <TOS00006.BDT>
Frequency 3115.000000 - 3125.000000 kHz, Amplitude 1.000000 volt
Data point density: 400 Stepwidth: 25.062657 Hz.

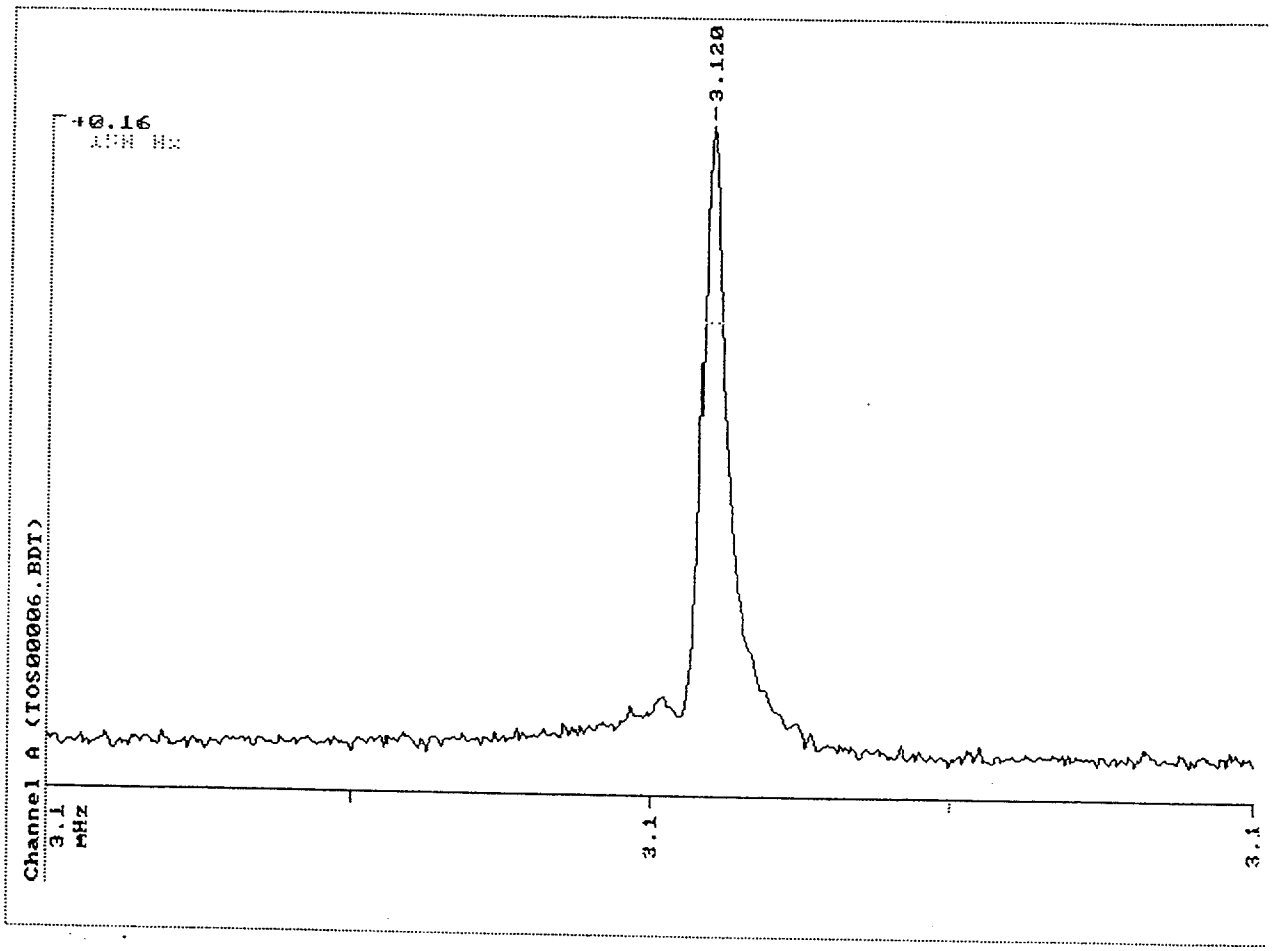

01/04/94 10:26am Filename: <TOS00007.BDT>
Frequency 3115.000000 - 3125.000000 kHz, Amplitude 1.000000 volt
Data point density: 400 Stepwidth: 25.062657 Hz.

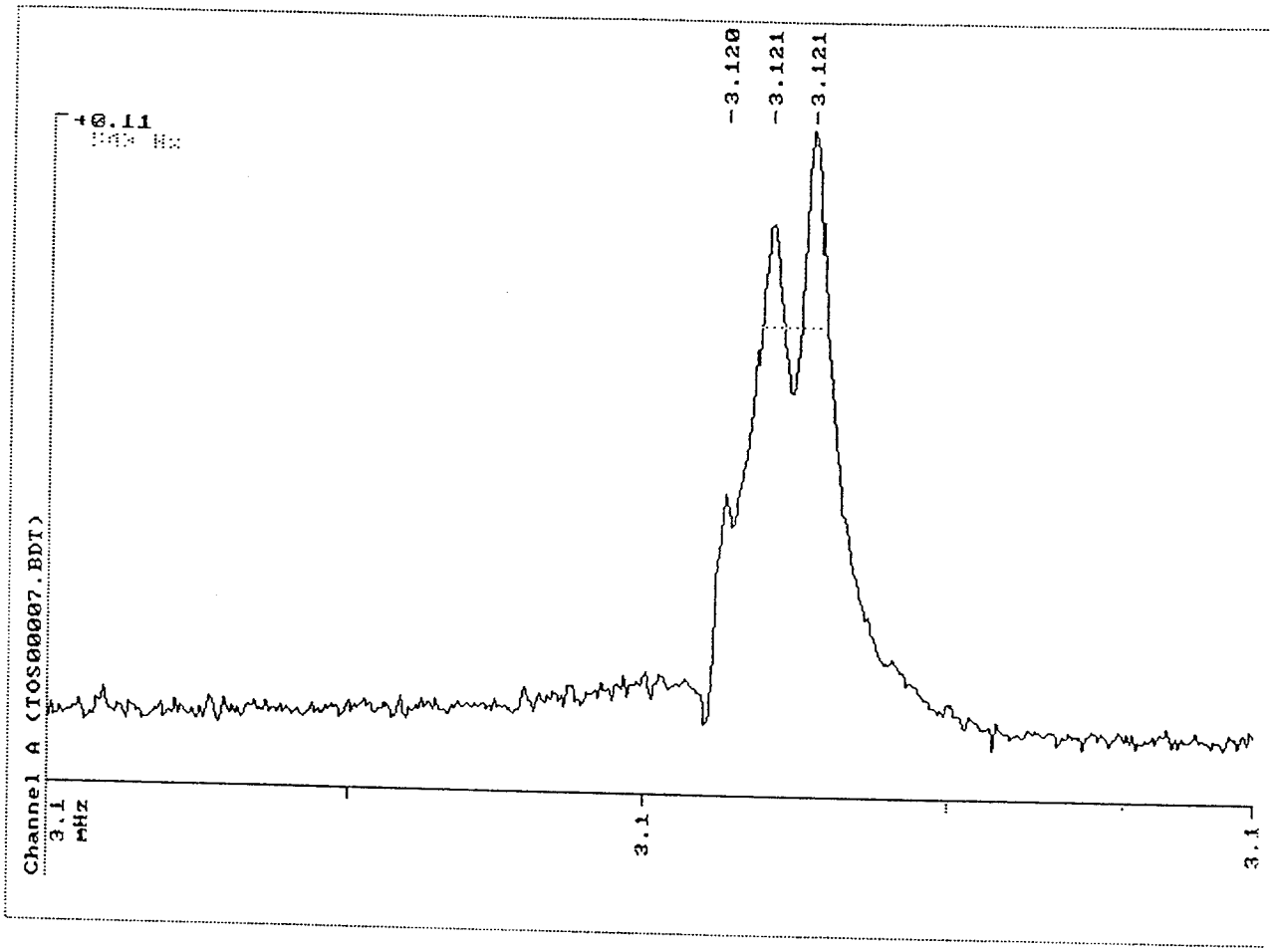

01/04/94 10:31am Filename: <TOS00008.BDT>
Frequency 3115.000000 - 3125.000000 kHz, Amplitude 1.000000 volt
Data point density: 400 Stepwidth: 25.062657 Hz.

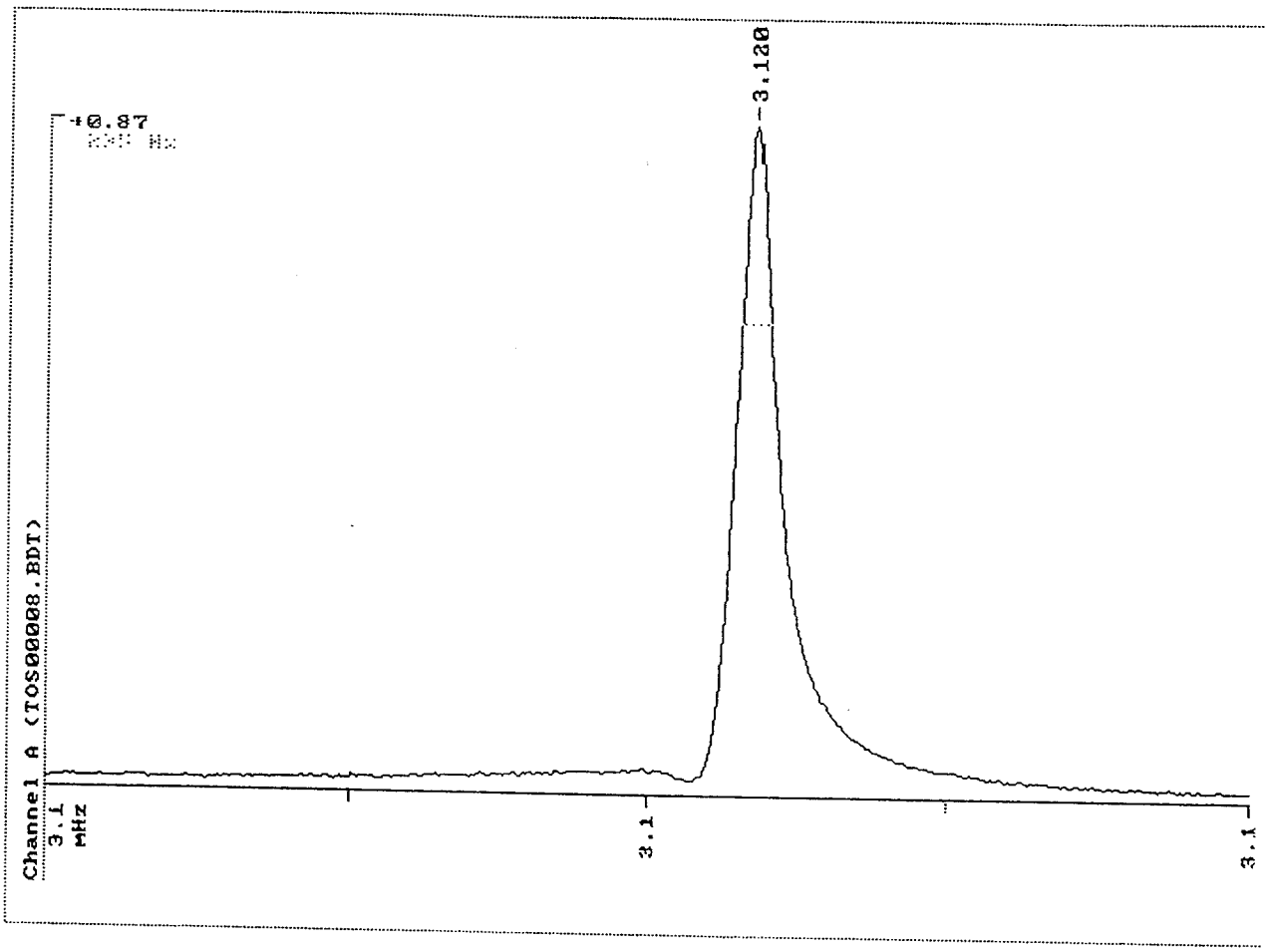

01/04/94 10:34am Filename: <TOS00009.BDT>
Frequency 3115.000000 - 3125.000000 kHz, Amplitude 1.000000 volt
Data point density: 400 Stepwidth: 25.062657 Hz.

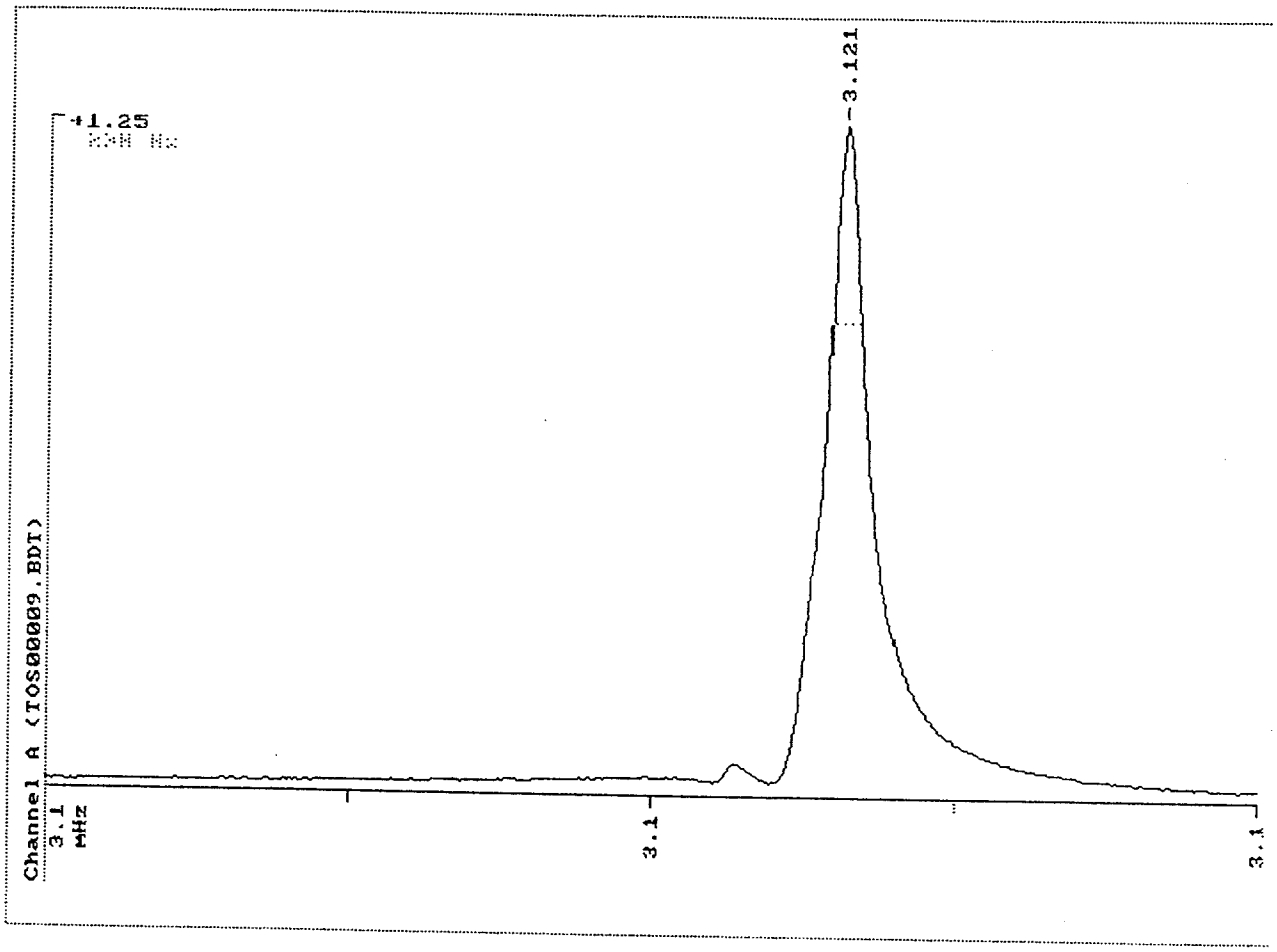

01/04/94 10:36am Filename: <TOS00010.BDT>
Frequency 3115.000000 - 3125.000000 kHz, Amplitude 1.000000 volt
Data point density: 400 Stepwidth: 25.062657 Hz.

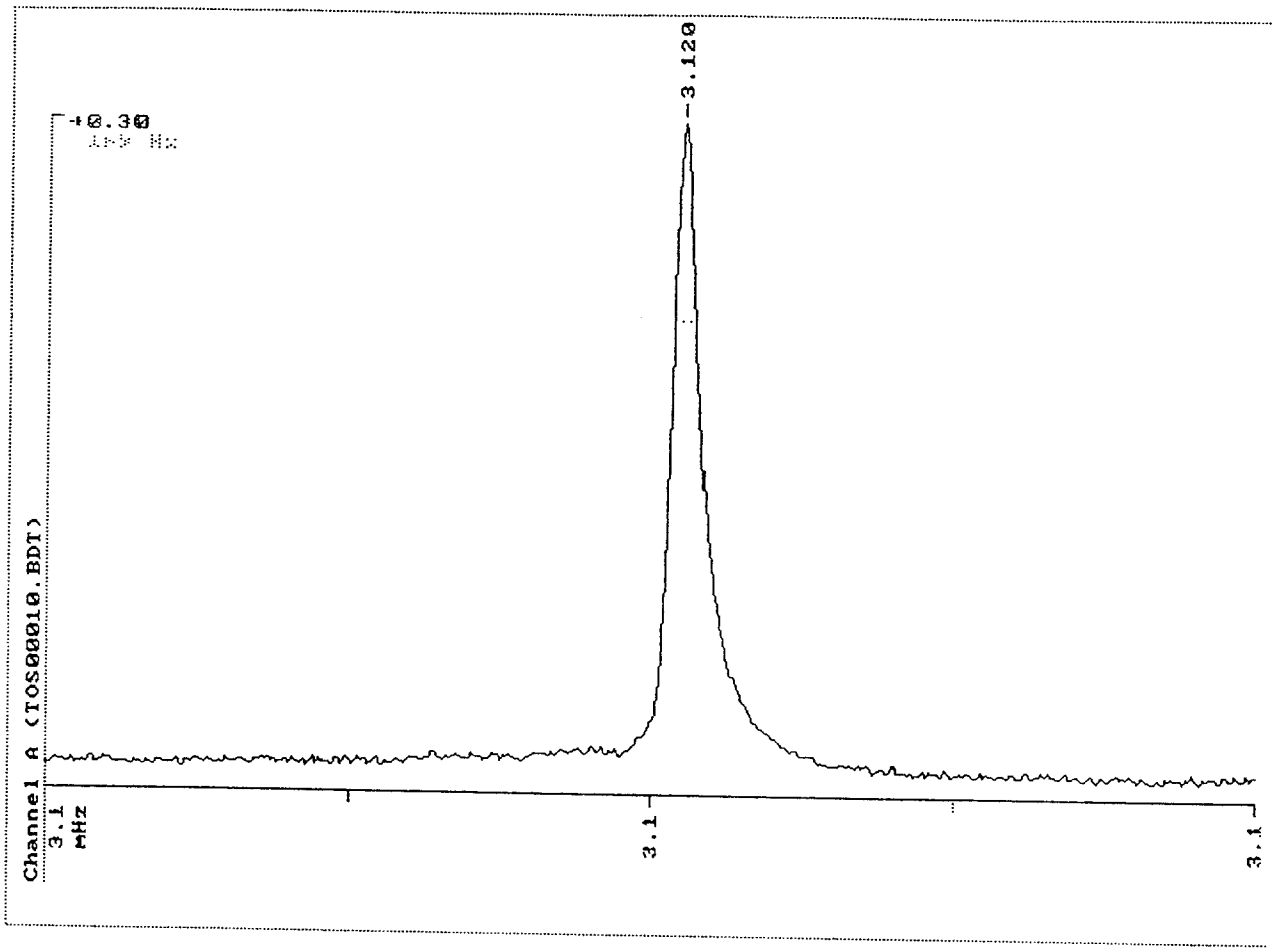

09/01/93 9:46am Data not saved as file. Printout 1
Frequency 309.000000 - 311.000000 kHz, Amplitude 0.900000 volt
Data point density: 500 Stepwidth: 4.008016 Hz.

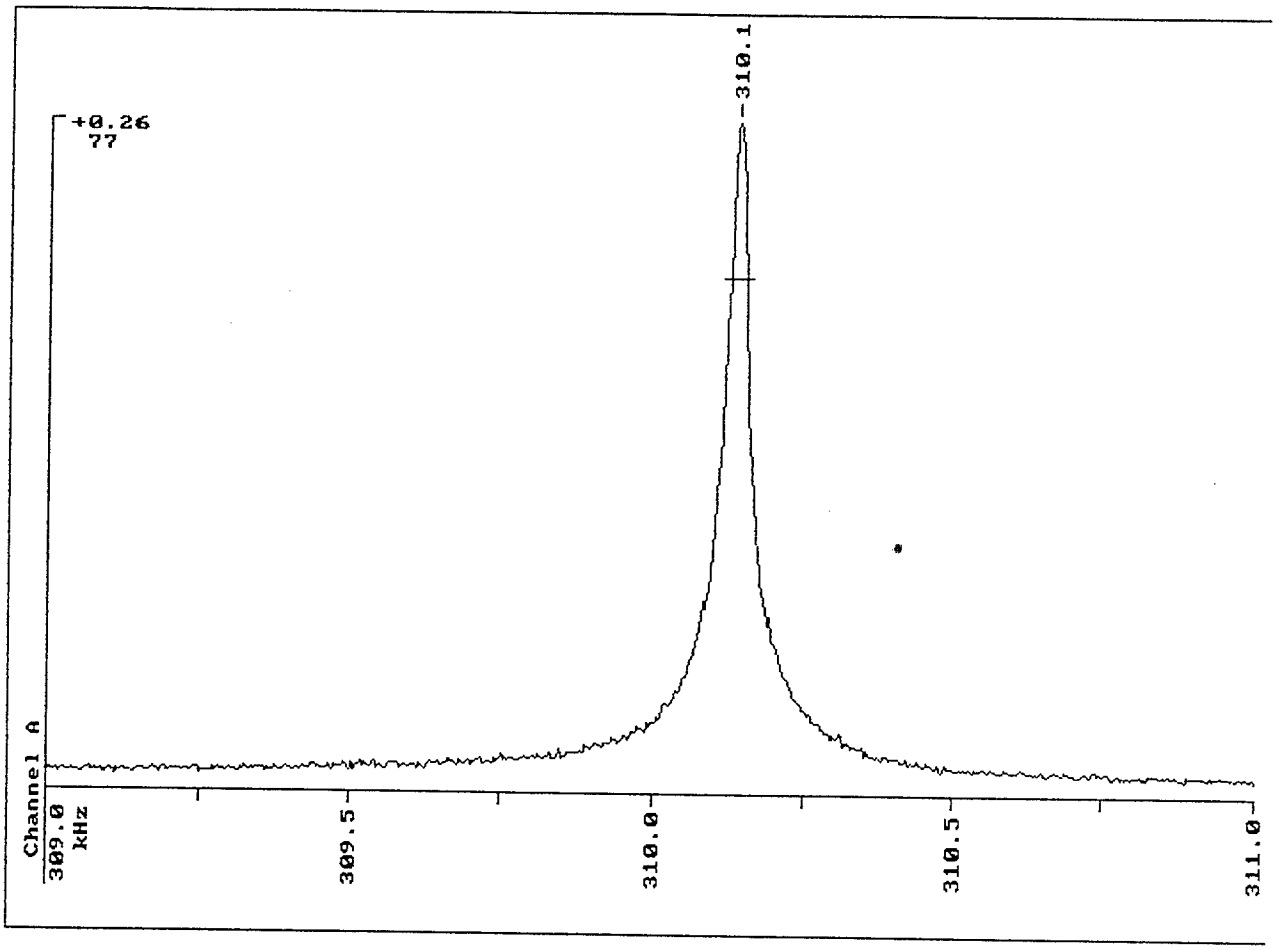

CeK 10

P&W Cerbec 7/8
good bulk qualities

09/01/93 9:32am Data not saved as file. Printout 7
Frequency 2050.000000 - 2070.000000 kHz, Amplitude 0.900000 volt
Data point density: 500 Stepwidth: 40.080160 Hz.

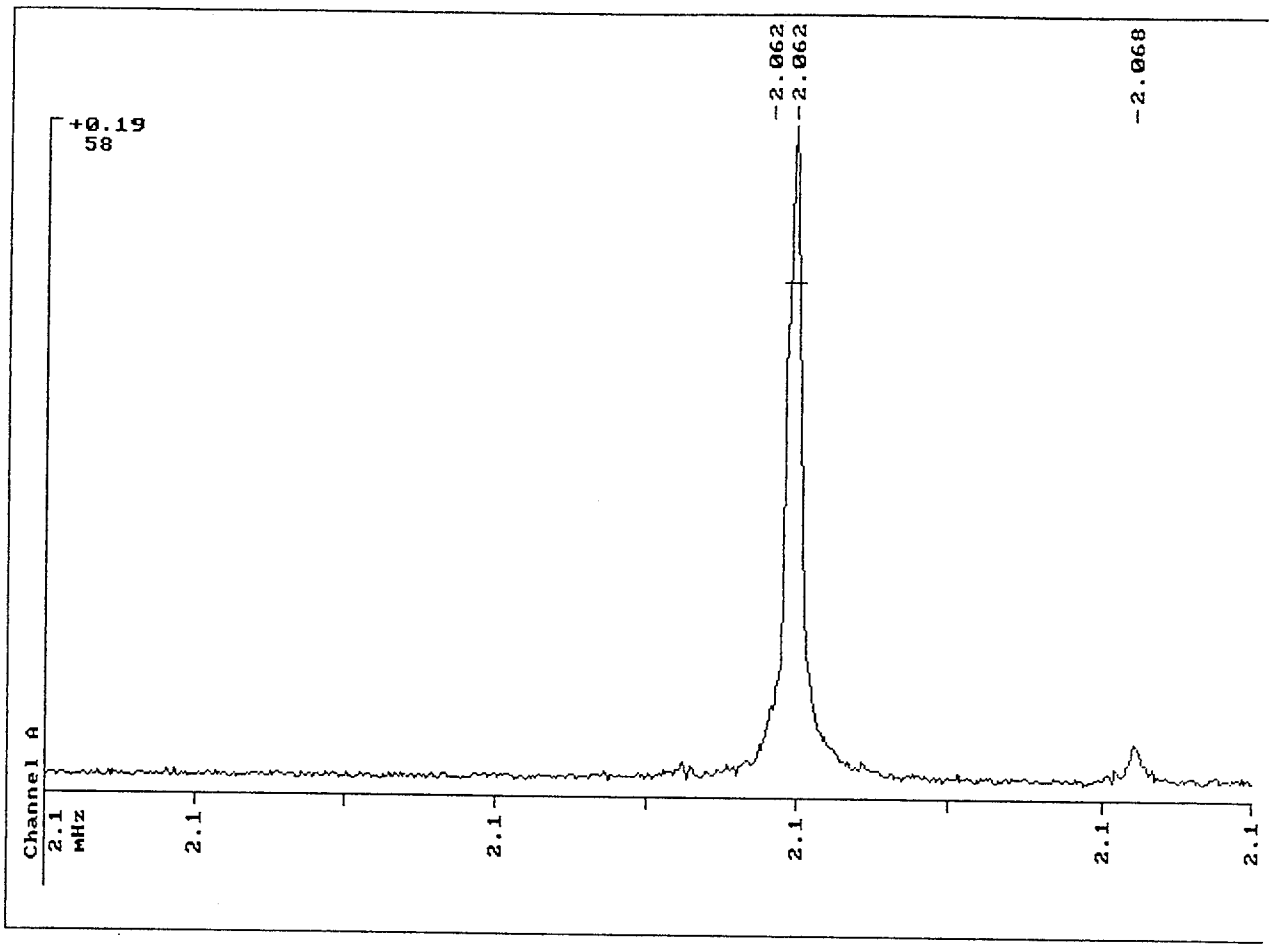

Cel 10

P&W Cerbec 7/8
near perfect surface

09/01/93 9:50am Data not saved as file. Printout 2
Frequency 309.000000 - 311.000000 kHz, Amplitude 0.900000 volt
Data point density: 500 Stepwidth: 4.008016 Hz.

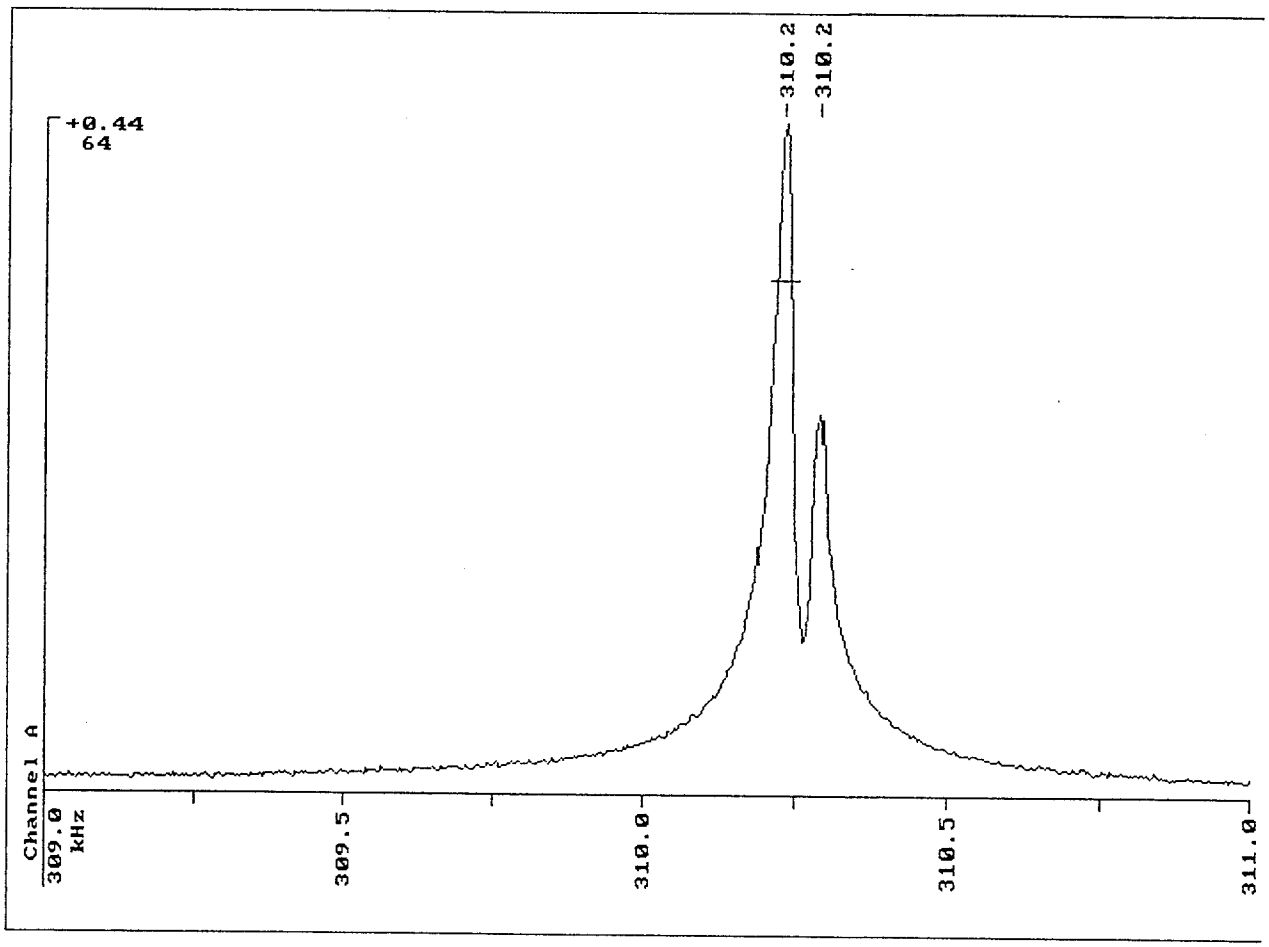

CER 18

P&W small crack at pt of P&W x-ray .015"

09/01/93 9:30am Data not saved as file. Printout 5
Frequency 2050.000000 - 2070.000000 kHz, Amplitude 0.900000 volt
Data point density: 500 Stepwidth: 40.080160 Hz.

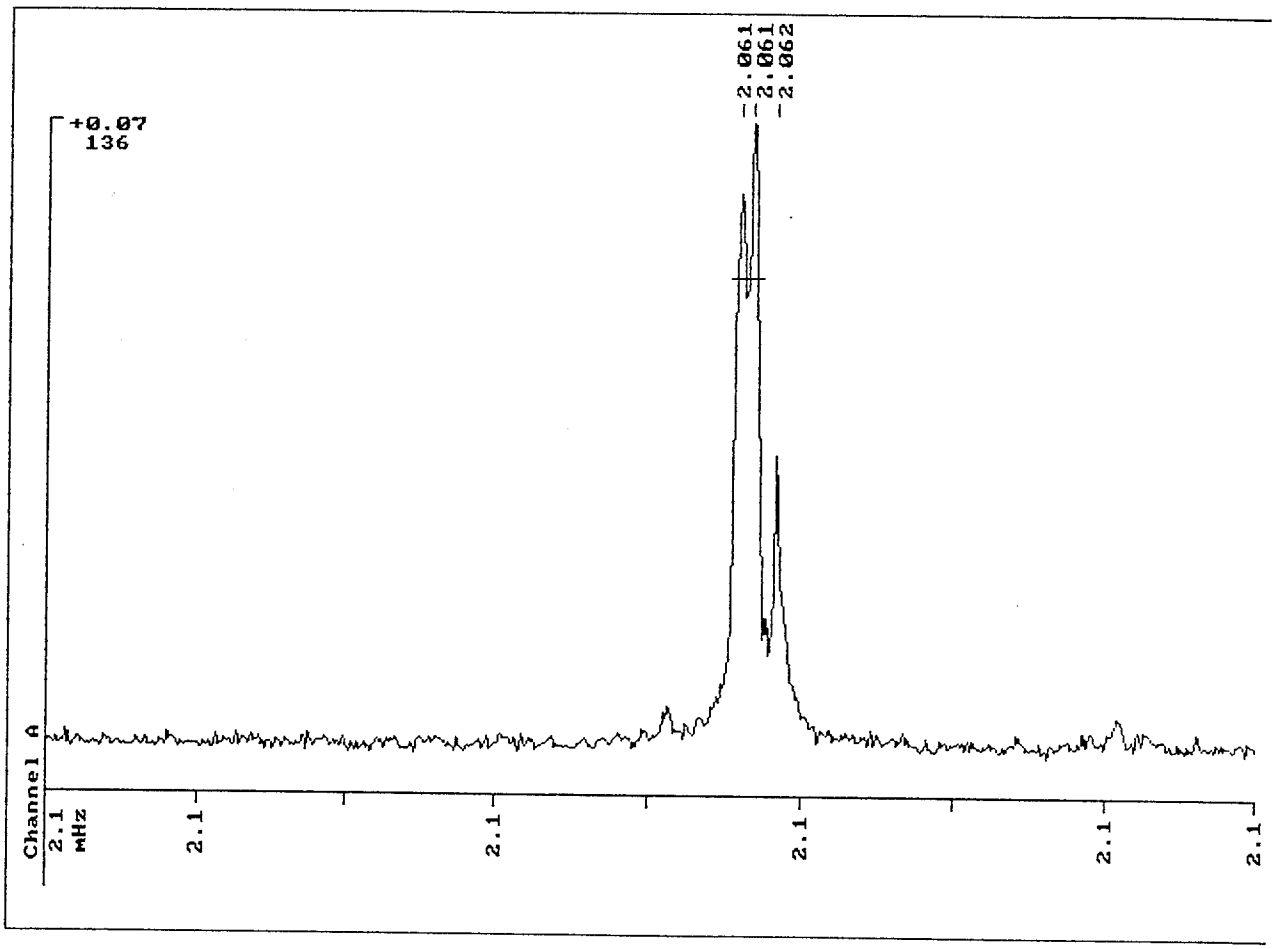

Cor 18

P&W
surface pit or crack

01/28/94 10:08am Filename: <GE000008.BDT>
Multi-scan: for frequency, amplitude data see <SAMPLE.SCT>.
Overall Data point density: 1200

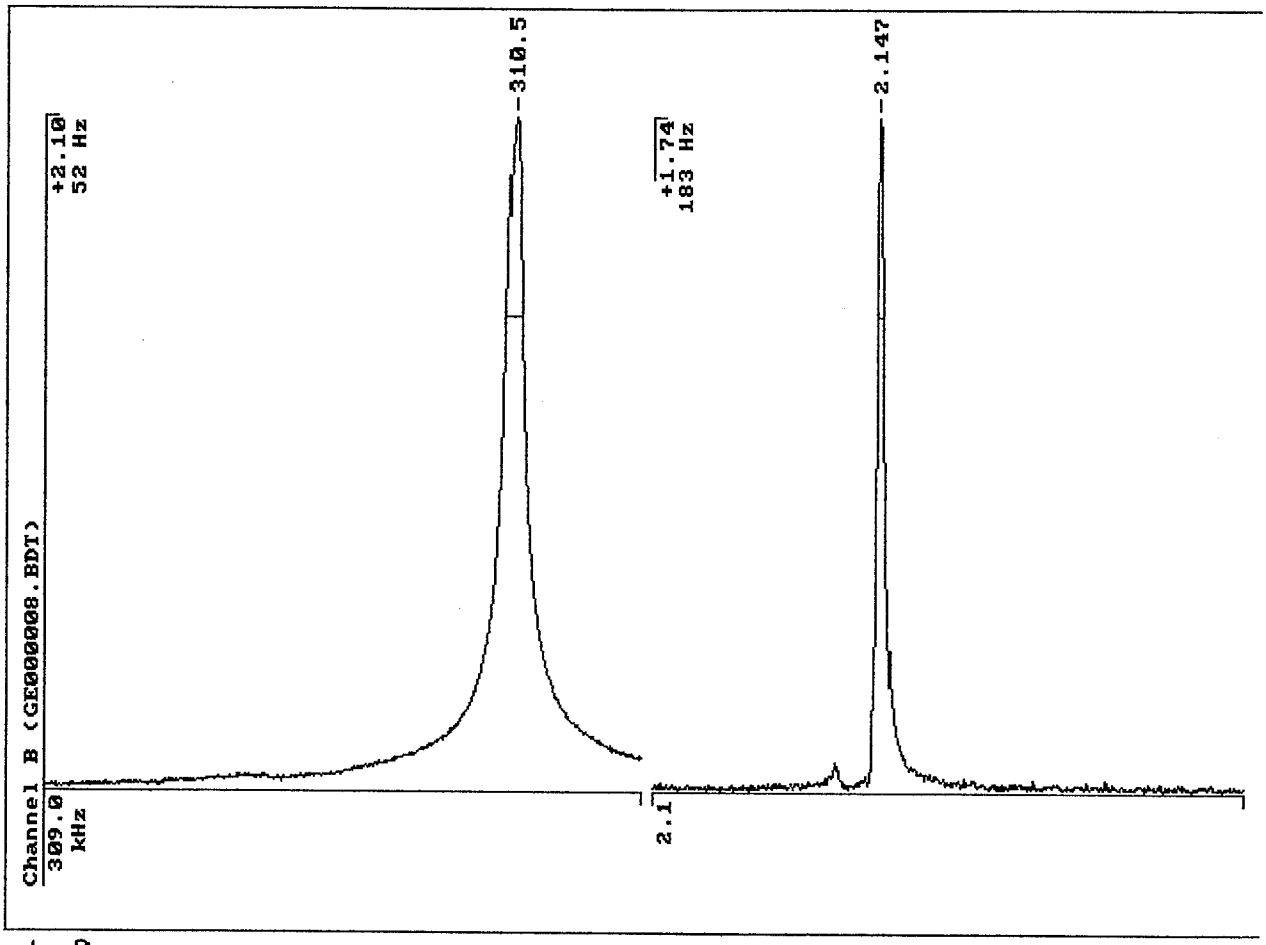

1-8

GE 7/8 NBD 200
no damage

01/28/94 10:09am Filename: <GE000009.BDT>
Multi-scan: for frequency, amplitude data see <SAMPLE.SCT>.
Overall Data point density: 1200

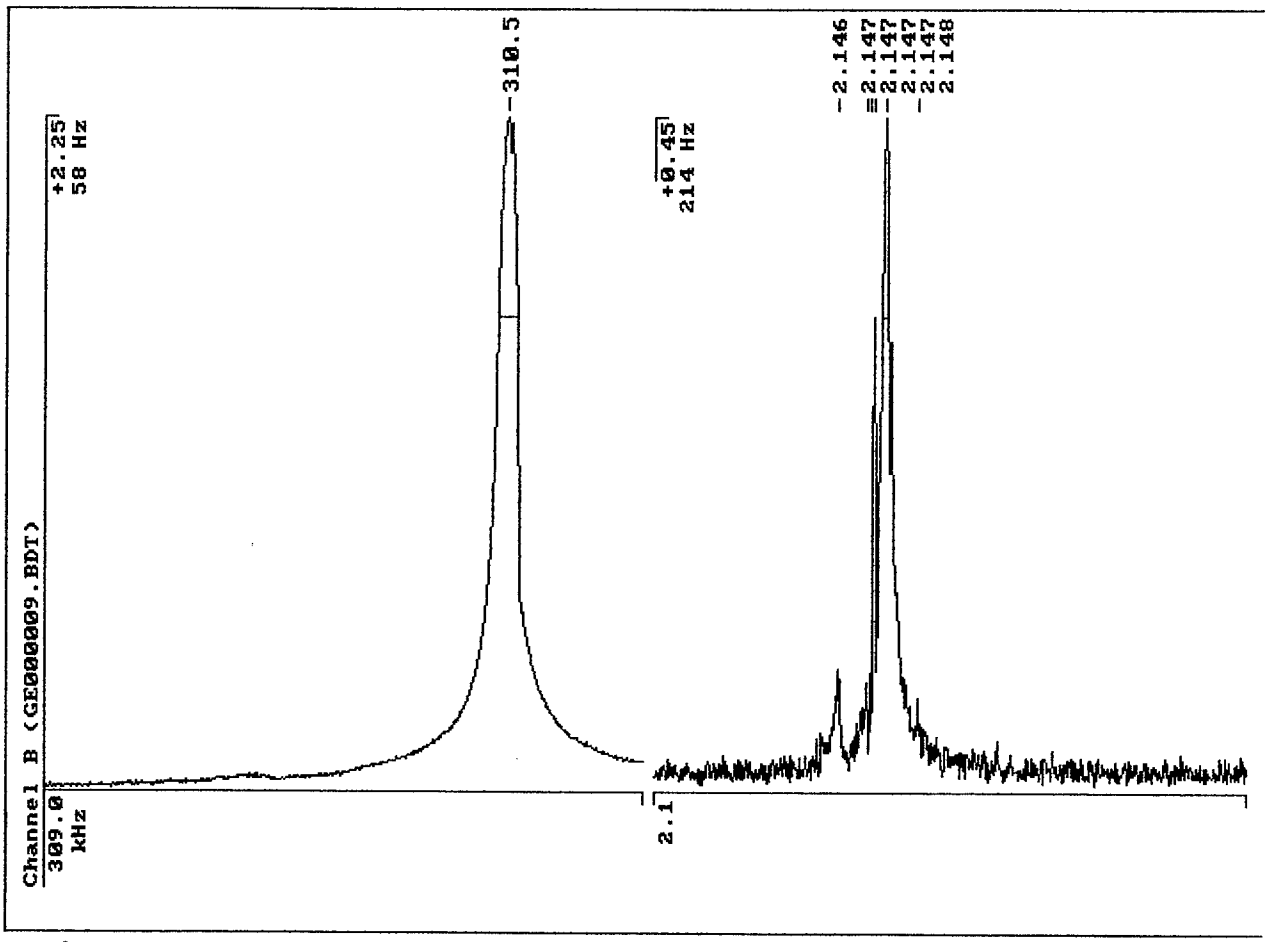

1-9

66
Slight surface damage

01/28/94 10:20am Filename: <GE000014.BDT>
Multi-scan: for frequency, amplitude data see <SAMPLE.SCT>.
Overall Data point density: 1200

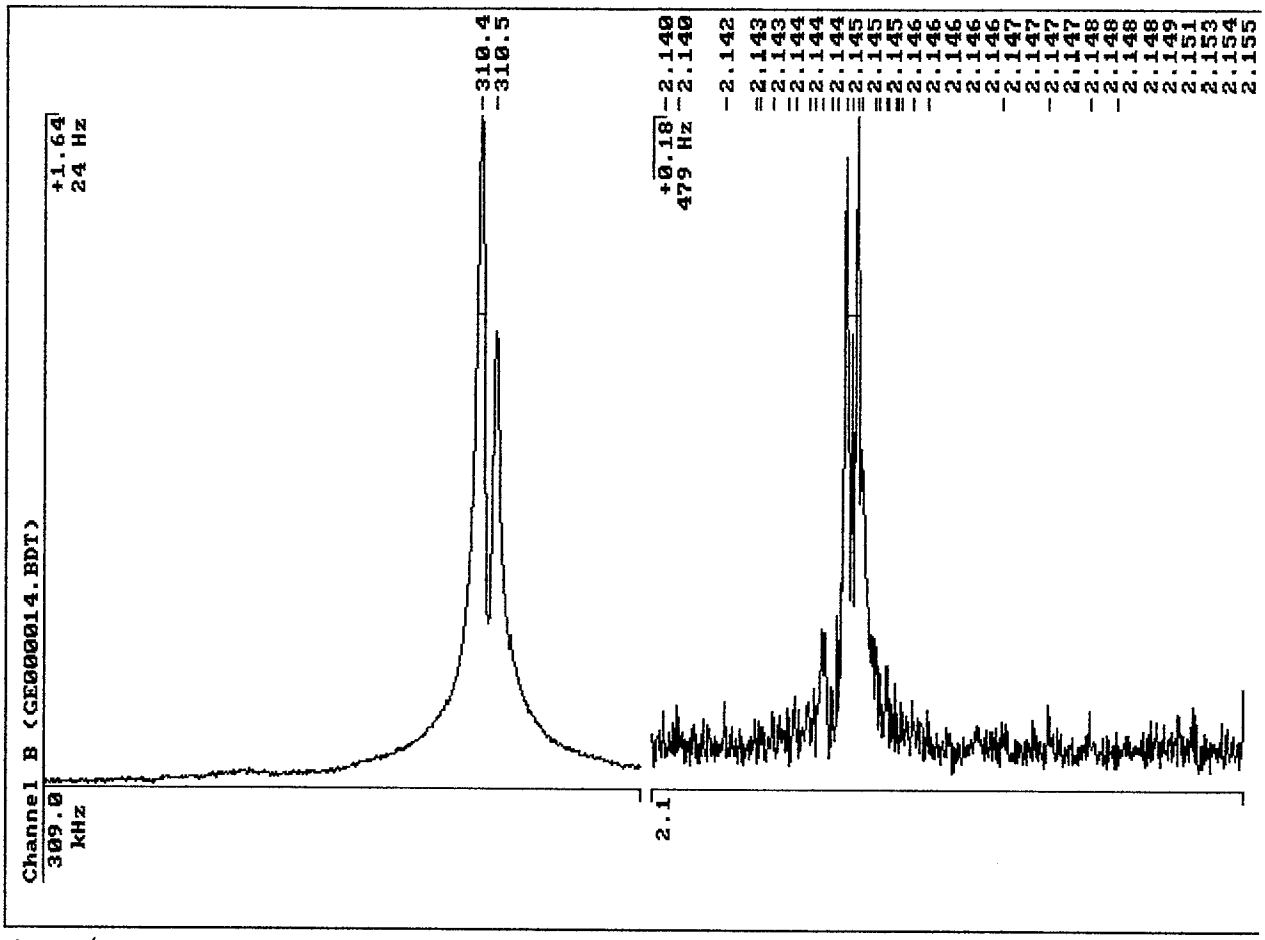

1-14

68
Surface & bulk flow

01/28/94 11:18am Filename: <GE000040.BDT>
Multi-scan: for frequency, amplitude data see <SAMPLE.SCT>.
Overall Data point density: 1200

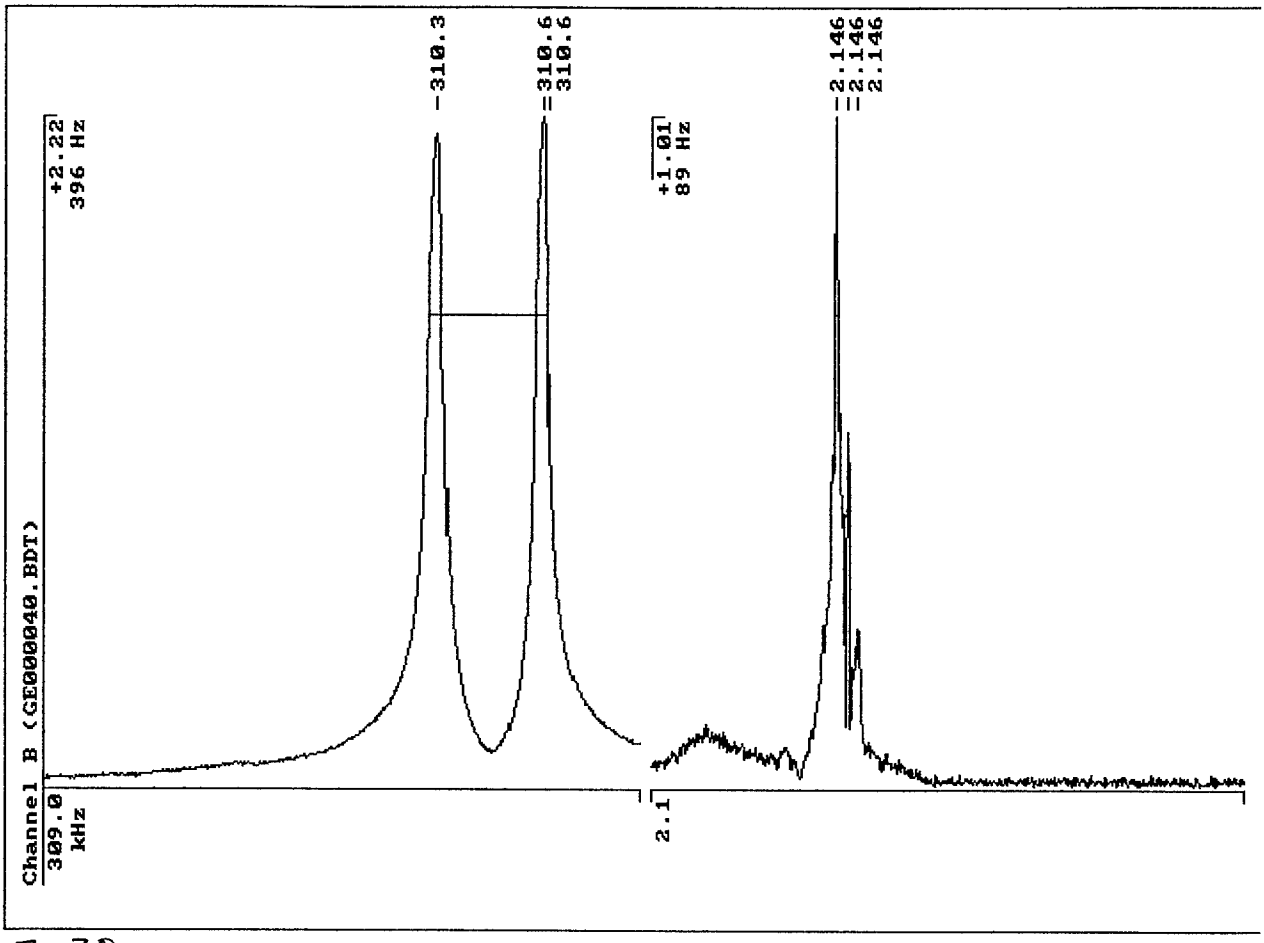

Z-20

66
Visible flaw

01/28/94 12:24pm Filename: <GE000060.BDT>
Multi-scan: for frequency, amplitude data see <SAMPLE.SCT>.
Overall Data point density: 1200

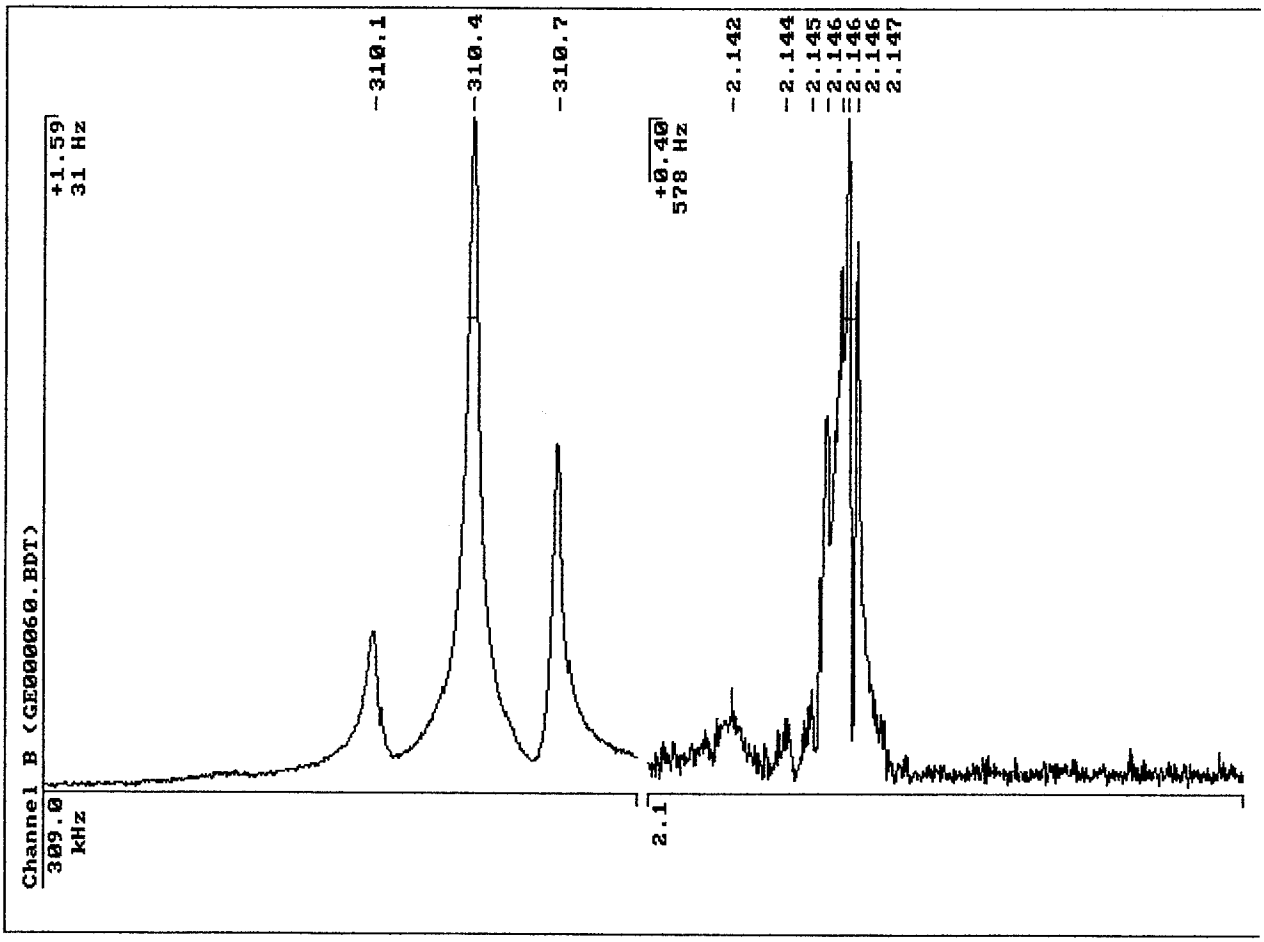

3-20

65
2 visible flows